

**UNCLASSIFIED**

**AD 419057**

**DEFENSE DOCUMENTATION CENTER**

**FOR**

**SCIENTIFIC AND TECHNICAL INFORMATION**

**CAMERON STATION, ALEXANDRIA, VIRGINIA**



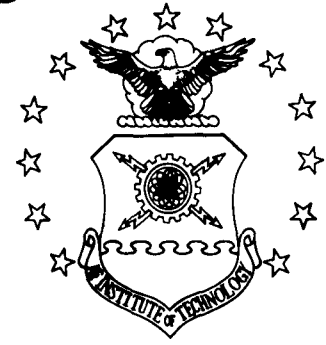
**UNCLASSIFIED**

NOTICE: When government or other drawings, specifications or other data are used for any purpose other than in connection with a definitely related government procurement operation, the U. S. Government thereby incurs no responsibility, nor any obligation whatsoever; and the fact that the Government may have formulated, furnished, or in any way supplied the said drawings, specifications, or other data is not to be regarded by implication or otherwise as in any manner licensing the holder or any other person or corporation, or conveying any rights or permission to manufacture, use or sell any patented invention that may in any way be related thereto.

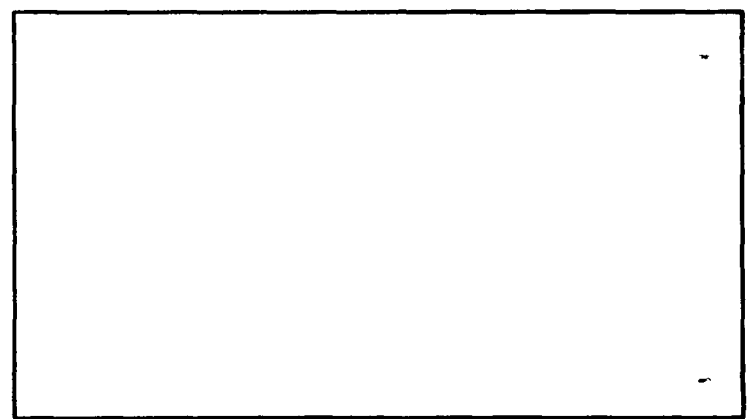
64-5

CATALOGED BY DDC  
AS AD No. 419057

# AIR FORCE INSTITUTE OF TECHNOLOGY



AIR UNIVERSITY  
UNITED STATES AIR FORCE



419057

## SCHOOL OF ENGINEERING

WRIGHT-PATTERSON AIR FORCE BASE, OHIO

THE ELECTRICAL CHARACTERISTICS  
OF AN ELECTROHYDRODYNAMIC GENERATOR  
FOR AN  
ALTERNATING INPUT

F/L J. Paul Sutherland  
F/L John W. Storr

GA/Phys/63-11, 12

**THE ELECTRICAL CHARACTERISTIC OF AN  
ELECTROHYDRODYNAMIC GENERATOR FOR AN ALTERNATING INPUT**

**THESIS**

**Presented to the Faculty of the School of Engineering of  
the Air Force Institute of Technology**

**Air University**

**in Partial Fulfillment of the  
Requirements for the Degree of  
Master of Science**

**By**

**John Paul Sutherland, B.Sc.**

**F/L**

**RCAF**

**and**

**John Wilson Storr, msc, B.Eng.**

**F/L**

**RCAF**

**Graduate Astronautics**

**August 1963**

Preface

This investigation was carried out at the Aeronautical Research Laboratory under the sponsorship of Dr. Hans Von Ohain. His enthusiasm and guidance served to further our interest and render enjoyable our work in the field of electro-fluid dynamic energy conversion.

The electrohydrodynamic generator used in this study was designed and built by the ARL for the purpose of preliminary studies in this subject. The DC characteristics of the generator were previously investigated by Lauritsen and Wheeler and since our work was primarily experimental their reports were extremely valuable in helping us to understand and use the generator. The operation of this device as an alternating current generator had not been done before, nor, to our knowledge, had any theoretical or experimental work with AC been attempted in the field of MHD power generation. The uniqueness of this study coupled with the fact that this generator was never intended as a practical device precludes the use of our numerical results for anything other than an indication of trends. Our data should therefore not be examined out of context.

We wish to acknowledge with gratitude the guidance and assistance given us throughout this study by our thesis advisor Maj. Richard C. Wingerson. His interest and helpful co-operation lightened our task considerably. Further we are indebted to Capt. Matthew Kabrisky for his advice in electronic matters and in particular for his help during the design of the high-voltage alternating power source. Our appreciation goes also to Mr. Michael Hawes and a great many others of the ARL whose co-operation and assistance proved invaluable.

Contents

	Page
Preface . . . . .	ii
List of Figures . . . . .	vi
List of Tables. . . . .	x
List of Symbols . . . . .	xi
Abstract. . . . .	xiv
I. Introduction. . . . .	1
Background. . . . .	1
Principle of Operation of the Electrohydrodynamic Generator . . . . .	2
Purpose and Scope of the Investigation. . . . .	5
II. Description of the Apparatus. . . . .	9
The Electrohydrodynamic Generator . . . . .	9
General Description. . . . .	9
Ionization Region. . . . .	9
Transport Region. . . . .	10
Neutralization Region. . . . .	10
Other Equipment. . . . .	10
High-Voltage Alternating Power Source. . . . .	13
Load Resistance. . . . .	13
Air Supply . . . . .	13
Instrumentation. . . . .	13
III. Theoretical Considerations. . . . .	17
Assumptions . . . . .	17
Selection of Operating Parameters . . . . .	18
Needle Configuration. . . . .	18
Reservoir Pressure, $P_0$ . . . . .	18
Transport Distance, $L$ . . . . .	19
Attractor Voltage, $V_a$ . . . . .	19
Load Resistance, $R_L$ . . . . .	19
Output Voltage, $V_o$ . . . . .	19
Output Voltage Prediction . . . . .	20
Differential Equation of the Generator. . . . .	21
Sine wave Input . . . . .	21
Square Wave Input . . . . .	22
Step (Exponential) Input. . . . .	23

Contents

	Page
Ion Transport Phenomena. . . . .	24
Turbulence in Fluid Flow. . . . .	24
Ion Diffusion . . . . .	25
Interface Mixing. . . . .	25
Ion Current Build-up Time . . . . .	25
Maximum Operating Frequency of the Generator . . . . .	26
Maximum Frequency from Ion Flow . . . . .	26
Maximum Frequency from Output Capacitance . . . . .	28
Self-Sustained Oscillation . . . . .	28
<b>IV. Experimental Scope and Procedure . . . . .</b>	<b>31</b>
Direct Current Characteristics . . . . .	31
Scope . . . . .	31
Procedure . . . . .	32
Peak Output Voltage Characteristics. . . . .	32
Scope . . . . .	32
Procedure . . . . .	32
RMS Output Voltage Characteristics . . . . .	33
Scope . . . . .	33
Procedure . . . . .	34
Output Voltage for Step Input. . . . .	34
Scope . . . . .	34
Procedure . . . . .	35
Output Voltage for Biased Alternating Input. . . . .	35
Scope . . . . .	35
Procedure . . . . .	36
<b>V. Results and Discussion . . . . .</b>	<b>37</b>
Experimental Error . . . . .	37
Direct Current Characteristics . . . . .	38
Spread of Data. . . . .	38
Comparison with Previous Experiment . . . . .	42
Peak Output Voltage Characteristics. . . . .	43
Comparison with DC Results. . . . .	43
Effect of Load Resistance . . . . .	47
Effect of Frequency . . . . .	47
RMS Output Voltage Characteristics . . . . .	47
Comparison with Peak Output Voltage Results . . . . .	58
Effect of Load Resistance . . . . .	60
Effect of Frequency . . . . .	60
Comparison of Square and Sine Wave Results. . . . .	61
Output Power Characteristics . . . . .	62
Effect of Load Resistance . . . . .	62
Effect of Frequency . . . . .	67

Contents

	Page
Comparison of Square and Sine Wave Powers. . . . .	67
Output Power Characteristics. . . . .	67
Input Power Ratio . . . . .	69
Output Power Ratio. . . . .	70
Output Wave Shape. . . . .	70
Comparison of Actual and Predicted Sine Wave Outputs. . . . .	75
Comparison of Actual and Predicted Square Wave Outputs. . . . .	78
Comparison of Actual and Predicted Step Function Outputs . . . . .	80
Unusual Wave Shapes . . . . .	84
Output Voltage for Step Input. . . . .	84
Determination of Input and Output Time Constants and Output Capacitance. . . . .	84
Effect of Exponential Input . . . . .	86
Time to Reach Ionization Potential. . . . .	86
Transit Time. . . . .	88
Output Voltage for Biased Alternating Inputs . . . . .	88
Determination of Output Capacitance and Roll-off Frequency . . . . .	88
Comparison of Frequency and Wave Shape with Unbiased Input. . . . .	90
VI. Conclusions. . . . .	93
VII. Recommendations. . . . .	96
Bibliography . . . . .	98
Appendix A: High-Voltage Alternating Power Source Specifications and Design. . . . .	99
Appendix B: Prediction of Output Voltages for Selected Input Voltages. . . . .	102
Appendix C: Flow Parameters in the Transport Region . . . . .	115
Appendix D: Generator Self-Sustained Oscillation Calculations . . . . .	118
Appendix E: Sine Wave:Square Wave Power Calculations. . . . .	120
Appendix F: Original Experimental Data. . . . .	123
Appendix G: Complete Engineering Drawings of the MID Generator. . . . .	133
Vitas. . . . .	139

List of Figures

Figure		Page
1	The MHD Power Generation Process. . . . .	4
2	The MHD Generator. . . . .	7
3	Full Size Sectional Side View of the MHD Generator . . . . .	8
4	The Experimental Apparatus . . . . .	11
5	Schematic of the Experimental Apparatus. . . . .	12
6	The Load Resistance. . . . .	14
7	The Load Resistances . . . . .	15
8	Schematic of the Electrical Model of the MHD Generator. . . . .	21
9	Negative Ion Direct Current Characteristic . . . . .	39
10	Positive Ion Direct Current Characteristic . . . . .	40
11	Average Direct Current Characteristics. . . . .	41
12	Peak Voltage Characteristics ( $R_L = 50$ megohms) . . . . .	44
13	Peak Voltage Characteristics ( $R_L = 100$ megohms). . . . .	45
14	Peak Voltage Characteristics ( $R_L = 200$ megohms) . . . . .	46
15	RMS Voltage Characteristics for Sine Wave Input ( $R_L = 50$ megohms). . . . .	48
16	RMS Voltage Characteristics for Sine Wave Input ( $R_L = 100$ megohms) . . . . .	49
17	RMS Voltage Characteristics for Sine Wave Input ( $R_L = 200$ megohms) . . . . .	50
18	RMS Voltage Characteristics for Square Wave Input ( $R_L = 50$ megohms). . . . .	51

GA/Phys/63-11, 12

19	RMS Voltage Characteristics for Square Wave Input ( $R_L = 100$ megohms) . . . . .	52
20	RMS Voltage Characteristics for Square Wave Input ( $R_L = 200$ megohms) . . . . .	53
21	Effect of Frequency on Output Voltage for Sine Wave Input. . . . .	54
22	Effect of Load Resistance on Output Voltage for Sine Wave Input . . . . .	55
23	Effect of Frequency on Output Voltage for Square Wave Input. . . . .	56
24	Effect of Load Resistance on Output Voltage for Square Wave Input . . . . .	57
25	DC Characteristics Showing Range of $V_a$ for Kink in Sinusoidal Voltage Characteristics. . . . .	59
26	Output Power Characteristics for Sine Wave Input. . . . .	63
27	Output Power Characteristics for Square Wave Input. . . . .	64
28	Effect of Load Resistance on Output Power for Sine Wave Input. . . . .	65
29	Effect of Load Resistance on Output Power for Square Wave Input. . . . .	66
30	Comparison of Output Powers for Sine and Square Wave Inputs. . . . .	68
31	Oscilloscope Photographs Showing Change of Output Wave Shape with Frequency-Sine Wave Input. . . . .	71
32	Oscilloscope Photographs Showing Change of Output Wave Shape with Frequency-Square Wave Input. . . . .	72

GA/Phys/63-11, 12

33	Oscilloscope Photographs Showing Change of Output Wave Shape with Attractor Voltage-Sine Wave Input. . . . .	73
34	Oscilloscope Photographs Showing Change of Output Wave Shape with Attractor Voltage-Square Wave Input. . . . .	74
35	Oscilloscope Photographs Showing Output Wave Shapes Used for Comparison with Predicted Output Wave Shapes .	76
36	Output Wave Shape for Sine Wave Input . . . . .	77
37	Output Wave Shape for Square Wave Input . . . . .	79
38	Oscilloscope Photographs-Step Input . . . . .	81
39	Output Wave Shape for Step (Exponential) Input. . . . .	82
40	Oscilloscope Photographs Showing Unusual Output Wave Shapes for Square Wave Input. . . . .	83
41	Variation of Attractor and Output Voltages with Time for Step Input. . . . .	85
42	Effect of Exponential Input on Output Voltage . . . . .	87
43	Attenuation of Output Voltage with Frequency for Fixed Biased Input. . . . .	89
44	Oscilloscope Photographs Showing Variation of Output Wave Shape with Frequency for Biased Sine Wave Input. .	91
45	Comparison of Output Wave Shapes for Biased and Unbiased Sine Wave Inputs. . . . .	92
A1	The High-Voltage Power Source . . . . .	100
A2	The High-Voltage Power Source with Plexiglass Cover in Place. . . . .	101
D1	Schematic of Self-Sustained Oscillation Circuit . . . . .	118

GA/Phys/63-11, 12

II	Theoretical Calculation of Ratio of Sine Wave Output Power to Square Wave Output Power. . . . .	122
----	--	-----

GA/Phys/63-11, 12

List of Tables

Table		Page
I	$I_0$ Coefficients for Output Voltage Prediction for Sine Wave Input . . . . .	107
II	Computer Data-Predicted Output Voltage for Values of Phase Angle for Sine Wave Input . . . . .	108
III	Predicted Output Voltage for Square Wave Input. . . . .	111
IV	Predicted Output Voltage for Step Input . . . . .	114
V	Peak-to-Peak Output Voltage Data for a Sine Wave Input.	124
VI	Direct Current Characteristic Data ( $R_L = 100$ megohms)...	125
VII	Output Voltage Data for Step Input . . . . .	127
VIII	Output Voltage for Biased Sine Wave Input. . . . .	128
IX	RMS Output Voltage Data for a Sine Wave Input. . . . .	129
X	RMS Output Voltage Data for a Square Wave Input. . . . .	130
XI	Power Calculations. . . . .	131

List of Symbols

Symbol		Units
$C_0$	Generator output capacitance	farads or $\mu\text{mf}$
$C_t$	Tank circuit capacitance	farads or $\mu\text{f}$
$E$	Electric field strength	volts/m
$E_x$	Electric field strength at x	volts/m
$\tilde{E}_x$	Electric field strength at x	non-dimensional
$I_0$	Ion or output current	amps or $\mu\text{a}$
$\tilde{J}$	Current density	non-dimensional
$K$	Ion mobility at STP	$\text{m}^2/\text{volt}\cdot\text{sec}$
$L$	Length of transport region	m or in.
$L_t$	Inductance of tank coil	henries
$M$	Mach number	
$P$	Air pressure	psia
$P_L$	Output power	watts
$P_0$	Stagnation air pressure	psia or psig
$Q$	Efficiency of inductor	
$R$	Gas constant	$\text{lb}\cdot\text{ft}/\text{lb}\cdot\text{m}^{\circ}\text{R}$
$R_L$	Load resistance	ohms or megohms
$R_1 C_1$	Generator input time constant	sec or msec
$R_t$	Resonant resistance	ohms or megohms
$T$	Air temperature	$^{\circ}\text{F}$ or $^{\circ}\text{R}$
$T_0$	Stagnation air temperature	$^{\circ}\text{F}$ or $^{\circ}\text{R}$
$V_a$	Attractor voltage	volts or kv

GA/Phys/63-11, 12

$V_f$	Fluid velocity	m/sec or fps
$V_o$	Output voltage	volts or kv
$V_T$	Ion transit velocity	m/sec or fps
$c$	Velocity of sound	m/sec or fps
$f$	Frequency	cps or ko/s
$f_L$	Limiting frequency	cps
$f_R$	Roll-off frequency	cps
$k$	Ion mobility	$m^2/volt-sec$
$t$	Time	sec
$t_r$	Ion transit time	sec or msec
$u$	Ion drift velocity	m/sec or fps
$x$	Distance along transport region	m or in.
$\tilde{x}$	Distance along transport region	non-dimensional
$\gamma$	Ratio of specific heats	
$\rho$	Air density	$lbm/ft^3$
$\rho_o$	Stagnation air density	$lbm/ft^3$
$\rho_o^1$	Air density at STP	$lbm/ft^3$
$\omega$	Angular frequency	

Subscripts

L	Load or limiting
R	Rolloff
T	Transit
a	Attractor
f	Fluid

GA/Phys/63-11, 12

i	Input
o	Output or stagnation
max	Maximum
r	Transit
t	Tank circuit
x	Arbitrary station in transport region

Abstract

The electrohydrodynamic generator investigated transforms kinetic energy from a high velocity airstream into recoverable electrical energy by transporting corona discharge ions against an electric field. Theoretical and experimental investigations of the electrical characteristics of the generator were conducted for alternating inputs. The feasibility of alternating current power generation was demonstrated, optimum input wave shape and ranges of load resistance and frequency determined, and self-sustained oscillation hypothesized. The output capacitance of the generator proved to be the limiting factor in the experimentation. Further investigation, particularly with a biased alternating input, on a generator designed specifically for alternating current operation is recommended.

GA/Phys/63-11, 12

THE ELECTRICAL CHARACTERISTICS OF AN  
ELECTROHYDRODYNAMIC GENERATOR FOR AN ALTERNATING INPUT

I. Introduction

Background

The idea of a means of electrical power generation by direct energy conversion is a most attractive one. In a direct energy conversion process, electrical energy is obtained directly from the primary source with no intervening mechanical apparatus. With such a process, one would expect to be able to increase the efficiency and reliability and reduce the weight and cost compared with conventional power generation processes. Electro-fluid dynamic energy conversion, which extracts electrical energy directly from the energy of a flowing fluid, offers these advantages.

These advantages would be especially significant in a space application of electro-fluid dynamic energy conversion where fluid dynamic energy is available from a thermodynamic cycle (Ref 3:4). This type of process, however, has received very little study to date. Considerably more effort has been expended on investigations of magnetohydrodynamic power generation, since it appears that high efficiencies can be achieved much more readily than with electrohydrodynamic (or EHD) power generation.

AA/Phys/63-11, 12

The Aeronautical Research Laboratory, recognizing the need for a study of the possibilities of MHD power generation, published, in 1961, a report by Lawson, Von Ohain, and Wattendorf (Ref 3), which pointed out the performance potentialities of MHD energy conversion and outlined specific areas requiring research.

The MHD generator used in this and previous studies was designed by Von Ohain in 1960. Wheeler and Lauritsen (Refs 7 and 2) established the feasibility of power generation with this generator and arrived at a number of conclusions regarding its optimum operation. They also determined that power can be generated using either positive or negative ions. This fact immediately suggested that the generation of alternating current power should be attempted. The study described in this report grew out of the findings and recommendations of Wheeler (Ref 7:75), Lauritsen (Ref 2:34), and Lawson, Von Ohain and Wattendorf (Ref 3:13) and is one phase of the Aeronautical Research Laboratory program on electro-fluid dynamic energy conversion.

#### The Principle of Operation of the Electrohydrodynamic Generator

The operation of an MHD generator is analagous to that of a Van de Graaff generator except that, in lieu of charges being moved by an endless belt, they are transported by a flowing fluid. The charges move with a velocity less than that of the fluid, whereas, in the Van de Graaff machine, the charges move with the same velocity as the belt. The MHD generator converts the energy of the flowing fluid into electrical energy in three steps:

1. Ions or charged particles are injected into the fluid.

GA/Phys/63-11, 12

2. Kinetic energy is transferred from the neutral molecules in the flow to the ions or charged particles.
3. The kinetic energy of the ions or charged particles is recovered as electrical energy.

The process is illustrated in Figure 1.

Charge separation or ion production may be accomplished in a variety of ways:

1. Corona discharge.
2. Ionizing radiation.
3. Thermal radiation.
4. Direct injection of charged particles.

In the generator used in the study, ions are produced by corona discharge, the action of a high electric field at the point of ionization. The ions are then swept downstream, through the insulating channel by the neutral fluid particles.

The transfer of energy to the charged particles may be accomplished in two ways (Ref 3:9):

1. By transporting them, through viscous interaction with neutral fluid molecules, against the electric field between the planes of ionization and neutralization.
2. By transforming the fluid energy into kinetic energy of high speed particles of suitable mass which are then forced along a ballistic path against an electrostatic field.

The generator studied makes use of the former method with air as a working fluid. The ions gain momentum and energy through collisions with neutral molecules and tend to move downstream with the flow through the transport region.

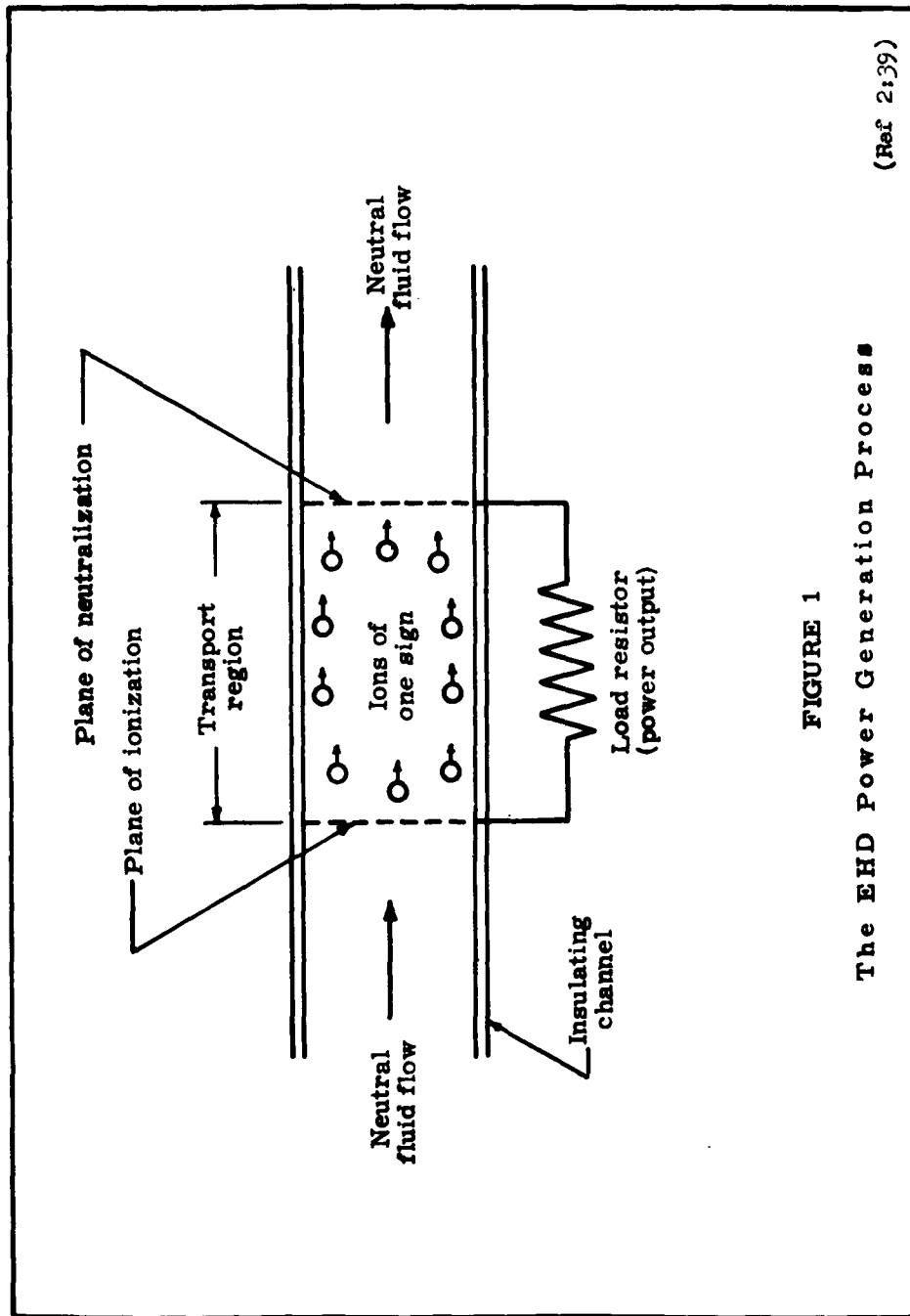


FIGURE 1  
The EHD Power Generation Process

(Ref 2:39)

GA/Phys/63-11, 12

The ions are deposited on a collector or electrode which is electrically connected to ground through a load resistance. This defines the plane of neutralization. The build-up of charges on the collector creates a potential difference across the load resistance causing a neutralizing current to flow through it.

In order to realize a net electrical power gain, it is necessary for energy to be transferred from the large number of neutral particles in the flow to the smaller number of charged particles (Ref 3:8). The potential on the collector and the space charge of the ions themselves in the transport region result in an electric field against which the ions are forced to move. The action of the electric field on the ions results in a slippage or difference in velocity between the charged and neutral particles in the flow. Obviously, in order to achieve an electrical output, the slippage or drift velocity between the ions and molecules must be less than the flow velocity of the uncharged molecules.

The power output of the generator, which is realized by the flow of neutralization current through the load resistance, is equal to the rate at which the fluid does work in transporting the ions downstream against the electric field in the transport region (Ref 5:1).

#### Purpose and Scope of the Investigation

The purpose of the study was to examine the behaviour of an EHD generator, whose DC characteristics were known, in the generation of alternating current power and to determine the feasibility of self-sustained oscillation, voltage transformation and amplification with the generator.

The generator used in the study was a prototype model, built under

GA/Phys/63-11, 12

Project No. 7116-03 of the Aeronautical Research Laboratory of the Office of Aerospace Research, USAF. As pointed out in the preface, the generator is a research model and the results presented in the report are significant only in so far as they indicate trends.

The meanings of the terms self-sustained oscillation, voltage transformation and amplification are analogous to their meanings in a conventional electronic sense. Oscillation implies the feed-back of a portion of the electrical output to the input so that the generator will operate continuously with no external source of energy other than that of the working fluid. Transformation implies the use of a transformer to step down the output voltage of the generator to a more useable level with a minimum of losses. Amplification implies modulation of the electrical input to the generator with an electrical signal and detection of the amplified signal at the generator output.

The study incorporates both theoretical and experimental aspects and, where possible, experiment has been correlated with theory. From a theoretical point of view, output voltages are predicted, for specified operating conditions, for sine wave, square wave and step inputs, transit time and critical frequencies are determined; and a method for self-sustained oscillation is postulated. Experimentally, the feasibility of AC power generation was demonstrated, output voltage and power characteristics were obtained for sine wave and square wave inputs at certain frequencies and using certain values of load resistance, and the input and output time constants of the generator were determined. Further, certain transient phenomena in the generator were examined, and a cursory investigation of the operation of the generator with a combined DC and AC input was carried out.

GA/Phys/63-11.12

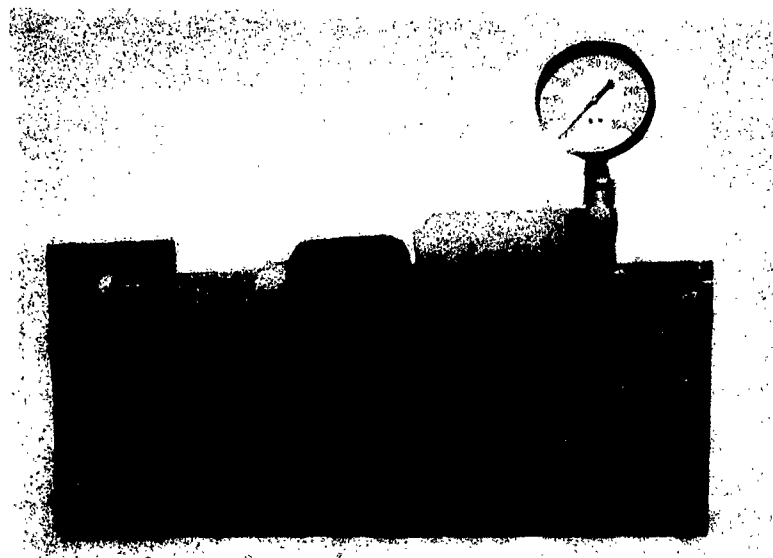


FIGURE 2

The EHD Generator

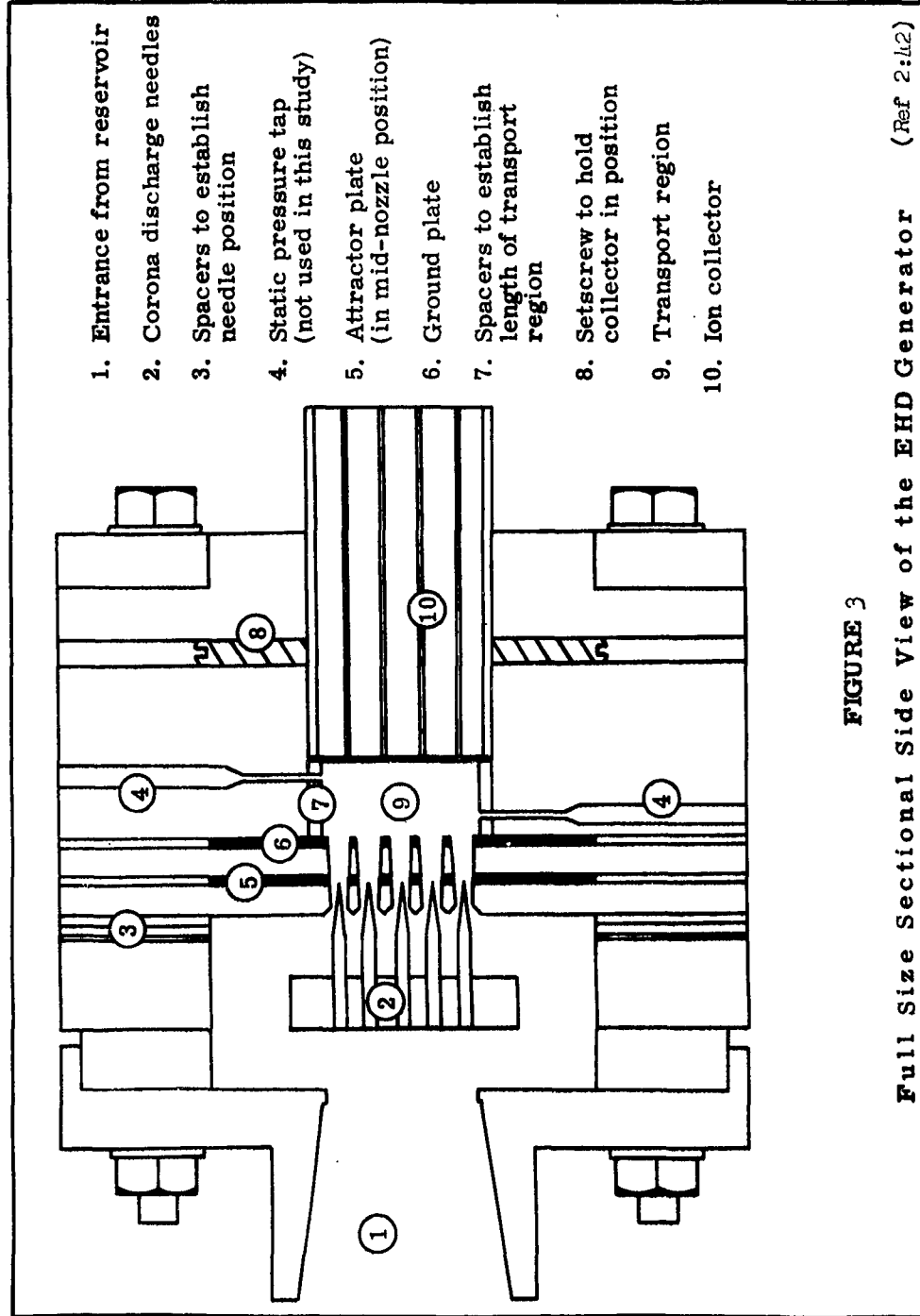


FIGURE 3

Full Size Sectional Side View of the EHD Generator (Ref 2:42)

## II. Description of the Apparatus

The experimental apparatus used in this study consisted of an EHD generator, a high-voltage alternating power source, load resistances, a high pressure air supply, and the necessary instrumentation for recording data. Each of these is described below.

### The Electrohydrodynamic Generator

The basic principle of operation of an EHD generator is discussed in Chapter I. The following is a detailed description of the generator which was used in this investigation.

General Description. As can be seen in Figure 2, the generator is of cylindrical cross-section with the working fluid (air) flowing axially through it. It is made of plexiglass and steel with an outside diameter of  $4\frac{1}{2}$  inches and a length of 5 inches. A full size sectional side view is shown in Figure 3, and a complete set of engineering drawings is given in Appendix G. For the purpose of its description the generator may be conveniently divided into three principle regions; the ionization region, the transport region, and the neutralization region.

Ionization Region. Air enters the generator under pressure from the reservoir and flows through a square array of 25 holes cut through a multi-layered disc. The disc is composed of two thin layers of steel, which serve as the attractor and ground plate electrodes, separated by layers of plexiglass. The holes in the disc are machined in the shape of convergent-divergent nozzles and, since the mass flow of air is sufficiently high, the flow through the nozzles is supersonic. A square array of 25 steel, corona discharge needles is mounted such that each needle is centered in one of the nozzles, its tip being in the same plane as the attrac-

GA/Phys/63-11, 12

tor electrode. A high voltage input signal applied to the attractor causes high intensity electric fields to form at the points of the grounded needles. Corona discharge occurs and the ions thus formed are swept downstream by the air flow into the transport region. At the entrance to the transport region, the ions pass through the ground plate electrode. This grounded electrode serves to shield the attractor and the needles from the electric fields in the transport region and, at the same time, provides an end point for the electric field lines in that region.

Transport Region. The transport region is a one-inch-square plexiglass channel, one-half inch in length, bounded on the upstream end by the ground plate electrode and on the downstream end by the collector electrode. It is in this region that energy is extracted from the air flow as it transports the ions against the electric field.

Neutralization Region. As the ions leave the transport region they pass through a fine steel screen fastened to the upstream end of a square steel tube  $2\frac{1}{4}$  inches long with internal neutralizing surfaces. These surfaces consist of eight steel strips running longitudinally in the tube and intersecting each other at right angles. They provide 25 flow channels, each of which has an approximate length to diameter ratio of 10. This tube serves as the collector and is grounded through a load resistance. As each ion contacts the collector, it gives up its charge to become a neutral air molecule. These charges accumulate to give an output voltage on the collector.

#### Other Equipment

A photograph of the apparatus is shown in Figure 4, and a schematic of the electrical connections is given in Figure 5.

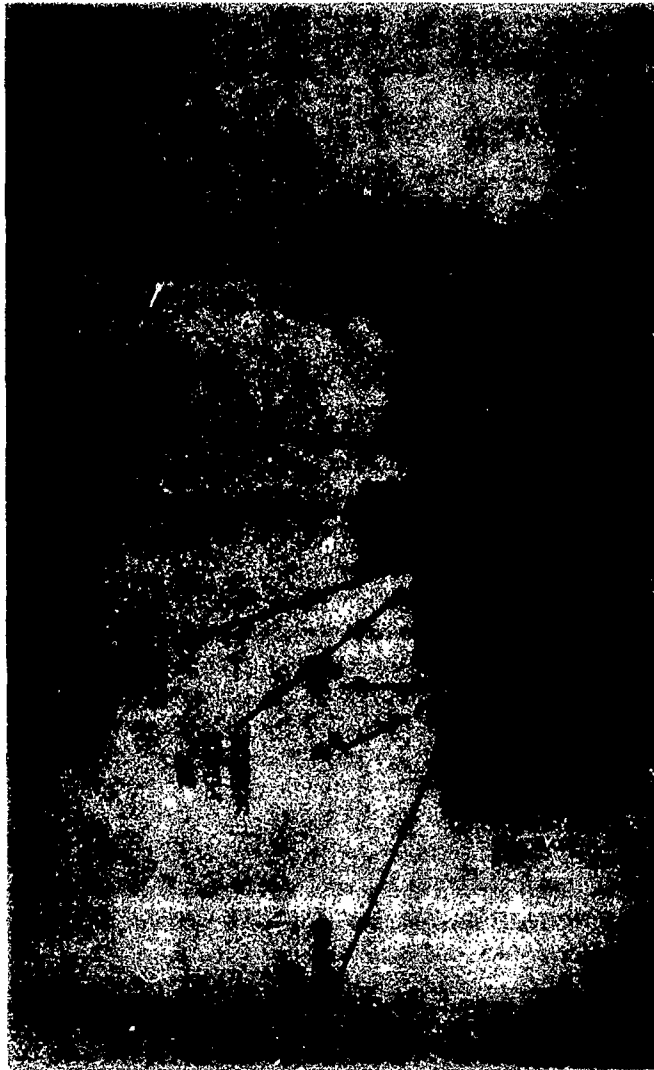


FIGURE 4  
The Experimental Apparatus

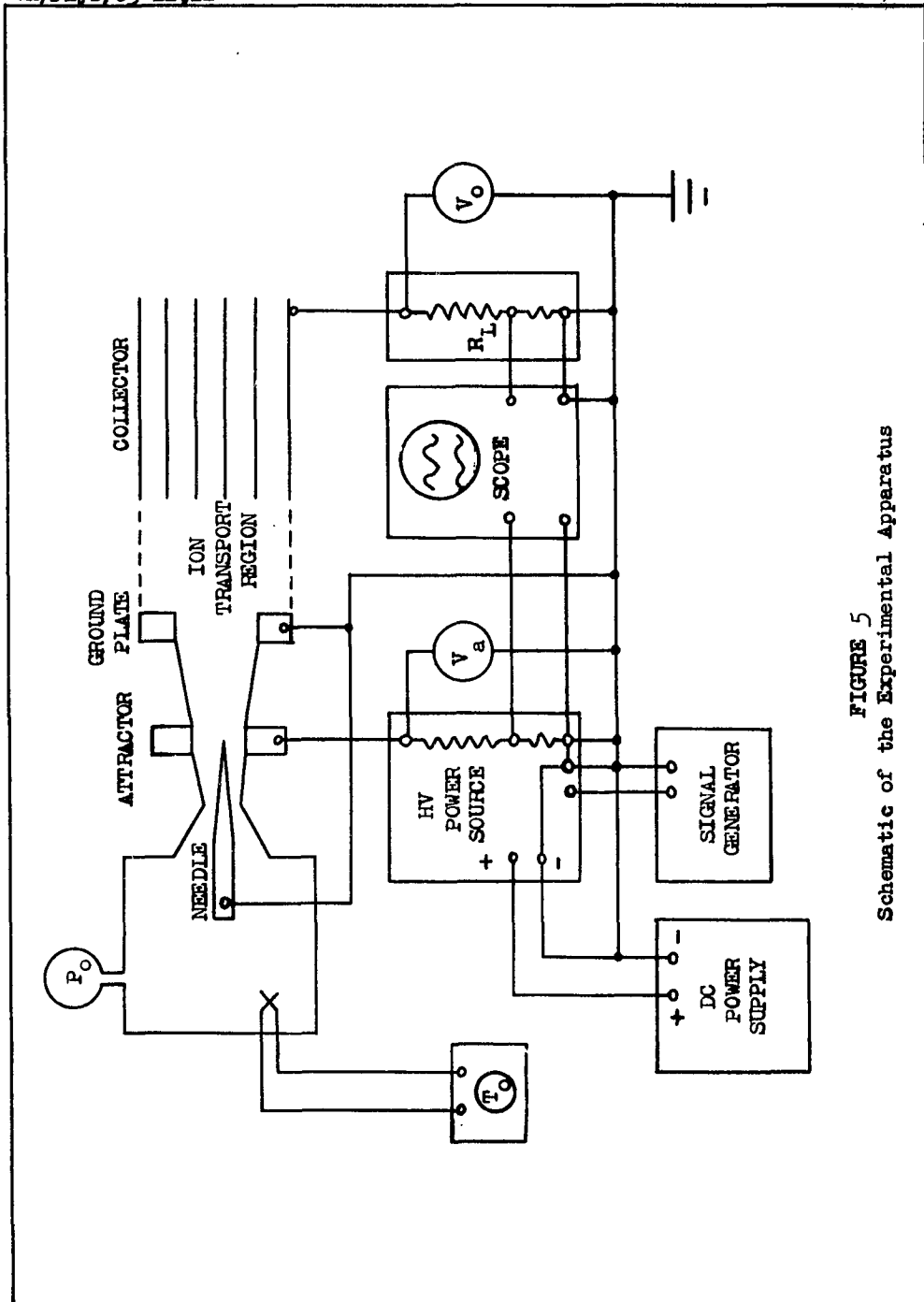


FIGURE 5  
Schematic of the Experimental Apparatus

GA/Phys/63-11, 12

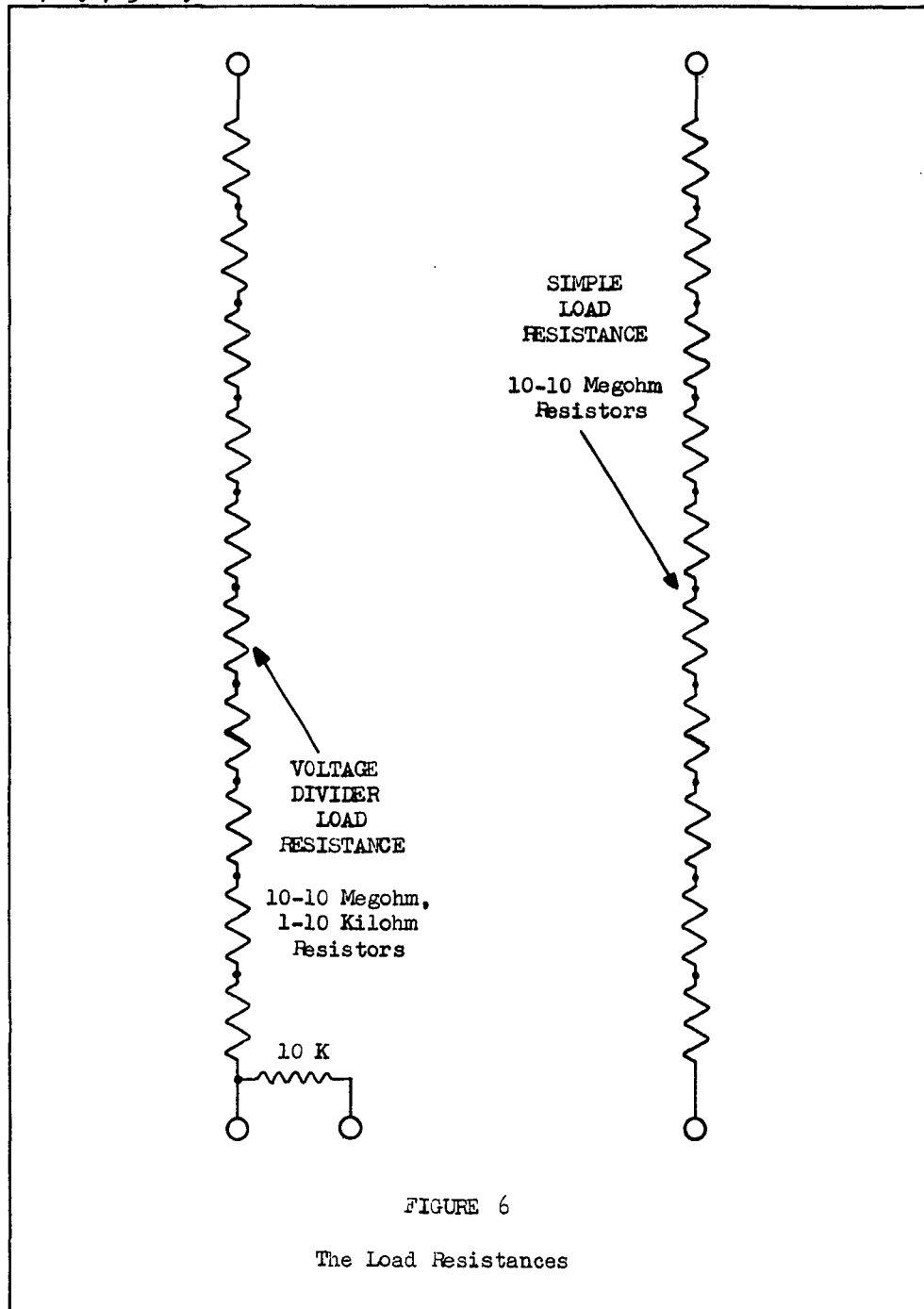
High-Voltage Alternating Power Source. Before any work could be done on the MHD generator, it was necessary to design and build a high-voltage AC power source. Several designs were postulated until one which could be built within the time and funds available was finally chosen. The power source which was used consisted of a single-stage, high-gain amplifier, powered by a 30 kv-10 ma DC power supply and driven by low voltage square and sine wave generators. The output wave shape had a satisfactorily small amount of distortion in the frequency range from 10 to 100 cps. The complete design and specifications for the power source are given in Appendix A.

Load Resistance. Since the maximum output voltage was expected to be around 30,000 volts, it was necessary to design and build a special load resistance which would contain this voltage. The load served also as a voltage divider for the oscilloscope input and so had to be calibrated. Consequently, load networks using 10 megohm precision resistors were built in the configuration shown in Figure 6. By connecting the two banks in parallel or series it was possible to obtain output loads of 50, 100, and 200 megohms. Figure 7, is a photograph of the load resistances.

Air Supply. The air supply consisted of a one-inch, 3000 psi supply line. The air was dried to  $-65^{\circ}\text{F}$ .

Instrumentation. A Tektronix Type 555 Dual-Beam Oscilloscope was used to measure and record input and output peak-to-peak voltages and wave shapes. The scope was calibrated within an accuracy of  $\frac{3}{4}\%$ .

A Tektronix Oscilloscope Camera Model C-12 was used with 3000 speed Polaroid film. The probable accuracy of the voltage measurement from the photographs was  $\pm 0.05\text{cm}$ .



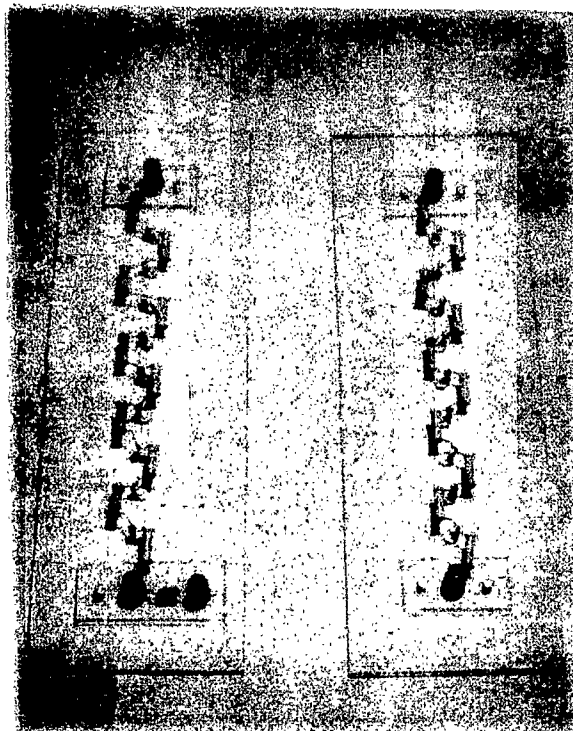


FIGURE 7

The Load Resistances

GA/Phys/63-11, 12

The EMS input and output voltages were read on two Sensitive Research Model ESH Electrostatic Voltmeters. The output voltmeter had the following ranges and probable errors: 0-5,000; 1%; 0-10,000, 1%; 0-20,000, 1%; 0-30,000, 1%. The input voltmeter had the following ranges and probable errors: 0-5,000, 1%; 0-15,000, 3%; 0-30,000, 1%.

The total temperature was measured with an Iron-Constantin Thermocouple, Type Y, and read directly on a Sim-Ply-Trol Pyrometer, Assembly Products, Inc. The range was -75 to +225°F and the probable error was  $\pm 2^{\circ}$ .

Total pressure was measured with a Bourdon Tube Pressure Gauge, Jas. P. Marsh Corp. The range was 0-300 psig and the probable error was  $\pm 1$ psi.

A Freed Radio Co. High Voltage Power Supply, 0-30 kv, 10 ma, was used as the positive DC power supply for the input amplifier.

A Beta Series 201 Portable High Voltage DC Power Supply, 0-30 kv, 1 ma, was used as the negative DC power supply.

The input signal to the amplifier was provided by a Hewlett-Packard Test Oscillator Model 650A and a Measurements Corp. Model 71 Square Wave Generator. The frequency was read from the dials of the generators and cross-calibrated with the oscilloscope time scale. The probable error was  $\pm 0.5$ cps.

### III. Theoretical Considerations

In this chapter, several distinct problems are examined from a theoretical point of view. The general assumptions which are applicable throughout the investigation are listed and the selection of certain operating parameters for the generator is then outlined. The following specific problems are considered:

1. The prediction of the generator output voltage for typical input voltages.
2. Ion transport phenomena.
3. Maximum operating frequency of the generator.
4. The design of a circuit for self-sustained oscillation of the generator.

#### Assumptions

The theoretical and experimental investigations described in this report were predicated on several basic assumptions. These assumptions, which are listed below, are applicable throughout the study:

1. The HED generator is capable of generating a measureable amount of power while operating with an alternating input voltage.
2. The operating parameters of the generator which were found by previous experiment to give optimum performance with a steady input will also give optimum performance with an alternating input.
3. The frequencies being examined are sufficiently low that the operation of the generator may be considered to be quasi-static. That is, the DC characteristics of the generator

GA/Phys/63-11, 12

are still valid when the generator is operated with an alternating input.

4. Small variations in the temperature and moisture content of the air will not affect the electrical performance of the generator.
5. The flow through the nozzles and transport region of the generator is isentropic and one-dimensional (axial).
6. The energy extracted from the flow is much less than the total energy of the flow. Therefore, the velocity and density of the air are considered constant throughout the transport region.

In addition to those listed above, certain other assumptions were required for particular areas of investigation. These are specified throughout the report as they apply. The validity of the assumptions is discussed in later chapters.

#### Selection of Operating Parameters

Before experimental work could begin, it was necessary to fix some of the operating parameters of the generator. These parameters governed the generator geometry, the air flow and the electrical circuitry requirements. The decisions regarding the operating parameters were made somewhat arbitrarily, based on the results of Wheeler (Ref 7) and Lauritsen (Ref 2).

Needle Configuration. The needle tips were centered in the plane of the attractor electrode. Lauritsen obtained optimum ion production with this needle configuration (Configuration VII) (Ref 2:32).

Reservoir Pressure,  $P_0$ . The reservoir pressure was held at 150 psig during all experimental runs. Lauritsen found that for this pressure the

GA/Phys/63-11, 12

collector current was almost the same for positive ions as it was for negative ions (Ref 2:63, 96-97). It was hypothesized that this condition would yield the most symmetrical output wave shape for an alternating input.

Transport Distance, L. A transport distance of 0.5 inch was used exclusively by Lauritsen and to some extent by Wheeler. Wheeler obtained a reasonable (although not maximum) power output with this transport distance (Ref 7:63). To allow a better correlation between the AC results and Lauritsen's and Wheeler's DC results, the transport distance was fixed at 0.5 inch for this study.

Attractor Voltage,  $V_a$ . According to Lauritsen, for  $P_0 = 150$  psig,  $L = 0.5$  inch and both positive and negative ions, ionization occurred when the attractor voltage reached 5 to 6 kv and breakdown occurred when the attractor voltage reached 8 to 10 kv (Ref 2:63). Therefore, the range of attractor voltages selected for this investigation extended up to 10 kv 0-p.

Load Resistance,  $R_L$ . Wheeler obtained a maximum power output with a load resistance in the vicinity of 100 to 150 megohms (Ref 7:63). It was considered that two 100 megohm loads, which would provide values of resistance of 50, 100 and 200 megohms depending on the manner in which they were connected, would adequately cover the range of load resistances desired.

Output Voltage,  $V_o$ . An estimate of output voltage was obtained from some of Wheeler's data. At  $P_0 = 150$  psig,  $L = 0.5$  in. and  $R_L = 100$  megohms,  $P_L$  is found to be 3.9 watts (Ref 7:63). This corresponds to an output voltage of 19.75 kv. Therefore, a maximum voltage of the order of 20 kv was anticipated across the 100 megohm load.

GA/Phys/63-11, 12

Output Voltage Prediction

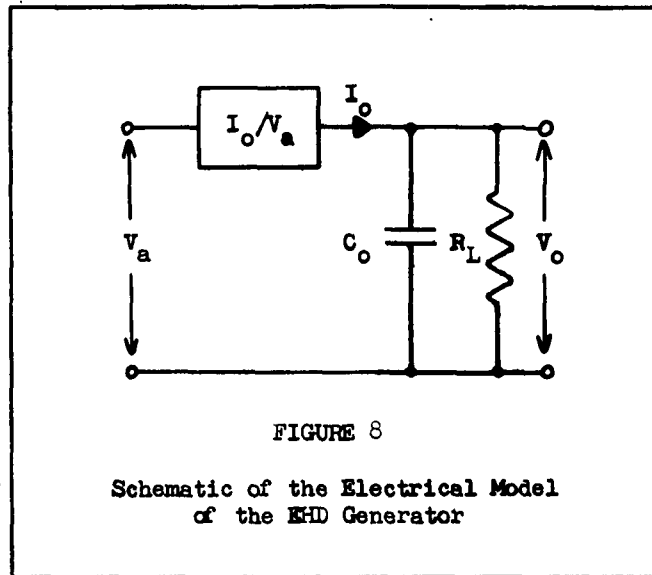
If an electrical model can be postulated for the MHD generator, then, for a given set of operating conditions and a given input voltage, it should be possible to predict the output voltage. The following analysis represents an attempt to predict the output voltage for three typical inputs.

Two assumptions which are used in this analysis but are not listed under the general assumptions are:

1. The output capacitance of the MHD generator is the dominant factor in the shaping of the output voltage.
2. The value of the output capacitance, as determined from the step input data (Figure 41) is 55.6 micromicro-farads.

Since quasi-steady operation of the generator is assumed, an instantaneous value of output current may be obtained from the DC characteristic (Figure 11) for any instantaneous value of attractor voltage. In other words, if the attractor voltage is known as a function of time, then the output current is also known as a function of time.

Since the output capacitance and the DC characteristic are the only effects considered in this analysis, the electrical model of the generator consists of an active element with a parallel resistance-capacitance output circuit. The capacitance is the output capacitance of the generator,  $C_0$ ; the resistance is the load resistance,  $R_L$ , connected across the generator output; the attractor voltage is  $V_A$ ; the current flowing through the circuit is the ion current, designated as the output current,  $I_0$ ; and the voltage developed across the circuit is the output voltage,  $V_0$ . A schematic of the model is shown in Figure 8.



Differential Equation of the Generator. For a parallel R-C circuit, the following equation, relating the voltage developed across the circuit to the current flowing through it, may be written:

$$I_o = \frac{V_o}{R_L} + C_o \frac{dV_o}{dt}$$

or

$$\frac{dV_o}{dt} + \frac{1}{R_L C_o} V_o - \frac{I_o}{C_o} = 0 \quad (1)$$

If we solve this equation for  $V_o$  (see Appendix B) we obtain

$$V_o(t) = \frac{e^{-t/R_L C_o}}{C_o} \int_0^t e^{t/R_L C_o} I_o(t) dt \quad (2)$$

where  $I_o(t)$  is a function of time and  $V_o(0) = 0$ .

Sine Wave Input. In order to predict  $V_o$  for a sinusoidal input, an expression was found for  $I_o$  as a function of time and the differential equation of the generator was solved to give  $V_o$  as a function of time.

GA/Phys/63-11, 12

This is carried out in detail in Appendix B according to the following steps:

1. From the DC characteristic (Figure 11),  $I_0$  is tabulated against  $\omega t$  for the sinusoidal input  $V_a(t)$ .
2. An expression for  $I_0(t)$  is found by means of Fourier Analysis.
3. The expression for  $I_0(t)$  is substituted into (2) and integrated to give  $V_o(t)$ .

The operating conditions selected were:

$$f = 10 \text{ cps}$$

$$V_a = 17.1 \text{ kv p-p}$$

$$R_L = 100 \text{ megohms}$$

For these conditions,

$$\begin{aligned} V_o(\omega t) = 10^2 & \left[ -16.83 - 49.4 \{ \sin \omega t \right. \\ & - 0.3493 \cos \omega t \} + 13.34 \{ \sin 3\omega t \\ & - 1.047 \cos 3\omega t \} - 0.1358 \{ \sin 5\omega t \\ & - 1.745 \cos 5\omega t \} + 6.16 \{ \cos 2\omega t \\ & + 0.6986 \sin 2\omega t \} - 2.085 \{ \cos 4\omega t \\ & \left. + 1.3972 \sin 4\omega t \} \right] \end{aligned} \quad (3)$$

(A plot of  $V_o$  versus  $\omega t$  is given in Figure 36.)

This is the predicted output voltage for a sine wave input for the case specified by the above operating condition.

Square Wave Input. The procedure used to predict the output voltage for a square wave input was identical to that used for a sine wave input. It is done in detail in Appendix B according to the following steps:

GA/Phys/63-11, 12

1. From the DC characteristic (Figure 11), values of  $I_0$  are found for the positive and negative half-cycles of  $V_a$ . This yields two constant values of  $I_0$  over two intervals of time.
2.  $I_0$  is substituted into (2) and integrated over the two intervals to give  $V_0(t)$ .

The operating conditions selected were:

$$f = 10 \text{ cps}$$

$$V_a = 18.4 \text{ kv p-p}$$

$$R_L = 100 \text{ megohms}$$

For these conditions, where  $B = e^{-t/0.3493}$

$$V_0(\omega t) = \begin{cases} -143 \times 10^2 (1-B) & \text{for } 0 < \omega t < \pi \\ 54 \times 10^2 (1-B) & \text{for } \pi < \omega t < 2\pi \end{cases} \quad (4)$$

A plot of  $V_0$  versus  $\omega t$  is given in Figure 37. This is the predicted output voltage for a square wave input for the case specified by the above operating conditions.

Step (Exponential) Input. The approach used in this analysis was different from that used with the sine wave and square wave inputs. Since  $V_a$  was not periodic but an exponential function which approached a step function, it would have been impossible to obtain an expression for  $I_0$  as a function of time by Fourier Analysis. Therefore, it was assumed that, above the ionization potential,  $I_0$  is a linear function of  $V_a$ . This implies that, for

$$V_a(t) = V_{a_{\max}} \left(1 - e^{-t/R_1 C_1}\right),$$

then,

$$I_0(t) = I_{0_{\max}} \left(1 - e^{-t/R_1 C_1}\right),$$

where  $R_1 C_1$  represents the time constant for the generator input. This expression for  $I_0(t)$  is then substituted into (2) and integrated to

GA/Phys/63-11, 12

give  $V_o(t)$ . The development is carried out in Appendix B.

The operating conditions selected were:

$$V_{o_{max}} = 16.2 \text{ kv}$$

$$R_L = 100 \text{ megohms}$$

$$R_1 C_1 = 1.57 \times 10^{-3} \text{ sec.}$$

For these conditions,

$$V_o(t) = 16.2 \times 10^3 \left[ 1 + 0.393 e^{-10^3 t / 1.57} - 1.393 e^{-10^3 t / 5.56} \right] (5)$$

A plot of  $V_o$  versus  $t$  is given in Figure 39. This is the predicted output voltage for a step (exponential) input for the case specified by the above operating conditions.

#### Ion Transport Phenomena

Throughout the transport region the ion flow is subjected to several phenomena which tend to distort the output wave shape and reduce the output power. Since the output capacitance of this MHD generator is large, it is possible that these phenomena will be overshadowed and difficult to observe. Their effects can therefore only be postulated with accurate verification being left for future work on a redesigned apparatus. The following four factors are considered:

1. Turbulence in the fluid flow.
2. Ion diffusion.
3. Inter-face mixing of opposite signed ions.
4. Ion current build-up time.

Turbulence in Fluid Flow. Any turbulence in the fluid flow will represent a loss in output power. Not only will there be an aerodynamic loss, but there will also be an electrical loss since less momentum in the direction of the flow will be available for transfer to the injected ions.

GA/Phys/63-11, 12

Turbulence may also cause a large percentage of the ions to go to the ground plate where they are lost. These effects will tend to distort the output wave shape and reduce the magnitude of the output voltage.

Ion Diffusion. As the ions traverse the transport region, they are subjected to random collisions mainly in the direction of air flow. Energy and momentum is transferred to these ions but not in equal amount to all ions. Consequently, all the ions in a given cross section will not be travelling with the same velocity, but their velocities will be distributed within a band. This effect will cause a distortion of the output wave shape.

Inter-face Mixing. For a perfect square wave input, ions of one sign will be followed immediately into the transport region by ions of opposite sign. At the interface, mixing of positive and negative ions will occur resulting in neutralization of some of the charges and a region of no charge. This effect represents a loss in available electrical energy and will appear as a narrowing effect on the output wave shape which will be most significant at high frequencies.

Ion Current Build-up Time. There is a possibility that some small delay exists between the time that a voltage greater than the ionization potential is applied to the attractor and full ion current is achieved. The main justification for this supposition would be the existence of a small stagnation (low velocity, high pressure) region in the immediate vicinity of the needle tip. Here a cloud of ions would form and tend to shield the tip of the needle from the applied field. Full ion current would not be realized until the cloud had grown to a size where the fluid could carry the ions downstream as fast as they were being formed. This delay would show up as a time delay or phase shift in the output voltage.

Maximum Operating Frequency of the Generator

Ideally, the maximum operating frequency of the generator is established by the velocity of the ions through the transport region. In fact, since the output capacitance of the generator is relatively large, the output will be attenuated at a much lower frequency.

Maximum Frequency from Ion Flow. In this analysis, it is assumed that the maximum frequency at which the generator will operate is limited only by the transit time (the time for the ions to travel through the transport region). In addition, all of the general assumptions made at the beginning of this chapter will apply.

The flow of ions through the transport region is governed by the velocity of the fluid flow and the ion mobility. The concept of ion mobility is best defined by the following quotation (Ref 6:2):

When an ion in a gas is in the presence of an electric field, it is subject to the usual electrostatic force laws. In the resulting motion, it frequently collides with neighboring molecules. Therefore, it cannot accelerate indefinitely but quickly reaches an average velocity analogous to the terminal velocity of a particle falling through a viscous medium under the influence of gravity. This average velocity due to the electric field is given by the product of the mobility  $k$  of the gas, and the field strength  $E$ :

$$u = kE$$

where  $k$  has the defining equation:

$$k = K \rho_0' / \rho$$

where  $\rho$  is the density of air, and  $\rho_0'$  is the density of air at 0°C and 760-mm of Hg.

The values of  $K$  for positive and negative ions in pure dry air are:

$$K = 1.6 \times 10^{-4} \quad (\text{m/sec}) / (\text{volts/m}) \quad \text{for positive ions and}$$

$$K = 2.2 \times 10^{-4} \quad (\text{m/sec}) / (\text{volts/m}) \quad \text{for negative ions (Ref 6:2).}$$

GA/Phys/63-11, 12

Where  $V_t$  = transit velocity of ions,

$V_f$  = fluid velocity,

and  $u$  = drift velocity of ions,

we can write

$$V_t = V_f + u \quad (6)$$

$$\text{But } u = kE \quad (7)$$

For the case of maximum power, the electric field in the transport region is given by Gouridine (Ref 1:2) as :

$$\tilde{E}_x = -1 - (1 - \tilde{J}(1 - \tilde{x}))^{\frac{1}{2}}$$

$$\text{where } \tilde{E}_x = \frac{E_x k}{V_f}$$

$$\tilde{x} = \frac{x}{L}$$

and for optimum operation  $\tilde{J} = 1.00$

$$\text{Hence, } E_x = (-1 + (\frac{x}{L})^{\frac{1}{2}}) \frac{V_f}{k} \quad (8)$$

Substitution of (7) and (8) into (6) and integration with respect to "t" gives a transit time,  $t_r = 0.0641$  msec. The detailed derivation is shown in Appendix C.

The theoretical analysis done by Wheeler (Ref 7:27) for the DC case shows that when a pulse of ions of one sign is just long enough to fill the transport region, the ions will be putting as much work into the flow as they will be taking out of it. Hence, the net power output will be zero. If this is taken as the limiting situation for AC operation, then the transit time is equal to one-half the period. The limiting frequency,  $f_L$ , (the frequency at which the output becomes zero) is therefore:

GA/Phys/63-11, 12

$$f_L = \frac{1}{2t_r} = 7.8 \text{ kc/s}$$

Maximum Frequency from Output Capacitance. The output capacitance of the EHD generator consists of the capacitance between the collector and ground in parallel with the stray capacitance of the load and output leads. In the design of this generator, no effort was made to minimize this output capacitance since AC operation had not been anticipated. The capacitance is therefore higher, by perhaps one order of magnitude, than it would be if it had been considered during the generator design.

From Figure 41, a plot of the step input data, it was found that, with a load resistance of 100 megohms, the RC time constant for the output of the generator was 5.56 msec, and the output capacitance therefore was 55.6  $\mu$ pf. Now, a capacitance in a RC circuit will charge up to 95% of its peak voltage in 3 time constants. Hence, the output capacitance of the generator will charge up to 95% of its maximum in  $3 \times 5.56 = 16.68$  msec. If this charging time is taken as half the period then the corresponding frequency is  $\frac{1}{2 \times 16.68} = 30$  cps. The frequency above which the output deteriorates due to output capacitance effects, then, is about 30 cps. Above this frequency, a drop in output of approximately 6 decibels per octave can be expected since the output of the generator is similar to a RC circuit.

#### Self-Sustained Oscillation

Self-sustained oscillation, as the name implies, entails feeding back part of the output to the input so that continuous operation is possible without any external excitation. For such an operation to be

GA/Phys/63-11, 12

possible the system must have power and voltage gains greater than one and the feed-back signal must be  $180^\circ$  out of phase with the input signal. The experimental EHD generator used had a power and voltage gain greater than one for low frequencies, and a phase shift of very nearly  $180^\circ$ . Self-sustained oscillation is therefore theoretically possible. The output wave shape, however, is very irregular and, because of the high ionization potential at the input, is narrower than the exciting wave shape. If this narrower wave shape is fed back to the input, a further narrowing occurs, and this process repeats itself until the gain becomes less than one and oscillation stops.

One method of obtaining a satisfactory wave shape for feed-back is to use the generator output to pulse a resonant tank circuit. At resonance, the output of the tank circuit will be a sine wave even though the pulse which is causing it to resonate is not. Part of the tank circuit output can then be fed back to the generator input to maintain oscillation, while the remainder of the output is available as AC power at a single frequency.

A tank circuit, due to its internal resistance, has electrical losses which must be overcome or it will not resonate. Hence, to maintain oscillation in the EHD generator, it is necessary to put out enough power (a) to overcome the losses of the tank circuit, and (b) to provide sufficient feed-back power to keep the loop gain greater than one. That this is theoretically possible is shown in the following analysis.

From the experimental results it was found that for this generator, a power output of 1 watt at a frequency of 10 cps was the best that could be obtained. The input power was not measured, but, on the basis of DC results (Ref 7:44), was considered negligibly small. What is required then

GA/Phys/63-11, 12

for oscillation is a tank circuit with an internal power loss of less than one watt which will resonate at 10 cps. Also the resonant impedance of the tank circuit must be of the order of 100 megohms. This is evident from Figure 22 since we must have a voltage gain greater than one. To meet these requirements, a capacitance of 0.0158  $\mu\text{f}$  and an inductance of 16,000 henries with a Q of 100 is required. These calculations are shown in Appendix D.

A capacitance of 0.0158  $\mu\text{f}$  with a 15 kv rating could be acquired. However, a transformer with a Q of 100, a primary inductance of 16,000 henries, and a voltage rating of 15 kv would be extremely difficult, if not impossible, to obtain. In practice then, this generator can never be made to oscillate without an external energy source.

A redesigned, more efficient SHD generator could possibly be made to oscillate by connecting a load resistance in series with the tank circuit. The output of the generator would thus see a large load, but the resonant resistance of the tank circuit would only be some fraction of it. If the Q of the coil is higher than that needed for resonance, then a net power output from the generator is available. This would be very desirable since this output would be sinusoidal and could readily be transformed to a lower voltage.

IV. Experimental Scope and Procedure

The investigation consisted of two basic groups of experiments. In the first group a number of runs were conducted to determine the electrical performance of the generator with various electrical inputs under different conditions. These included the determination of the direct current characteristics, the peak voltage characteristics and the RMS voltage characteristics. The second group included a series of experiments to investigate certain electrical phenomena of the generator. These included the examination of the output voltage with a step input and with a biased alternating input.

The generator was assembled with the chosen needle configuration and transport distance and these remained fixed throughout the experimental runs. The reservoir pressure was held constant at 150 psig for all runs.

Direct Current Characteristics

Scope. Average load current characteristics were determined for both positive and negative DC attractor voltages. The direct current characteristics are defined as the curves of load current,  $I_0$ , plotted against attractor voltage,  $V_a$ . The load resistance,  $R_L$ , was kept constant at 100 megohms.

A number of runs were made on different days within a three week period. There was no way of regulating the reservoir temperature,  $T_0$ , so that the data obtained was for several different values of  $T_0$  ranging from 18 to 45°F. This data was all plotted and the DC characteristics represented by average curves were drawn through the available data.

GA/Phys/63-11, 12

Procedure. The procedure followed to obtain the DC characteristics for negative ions is outlined below. The collector of the generator was connected to the 100 megohm load resistance, the needles and the ground plate were connected to ground, and the attractor was connected to the positive DC power supply through a 10 megohm series resistor. The input and output of the generator were connected through their respective voltage dividers to each channel of the oscilloscope. Flow was established through the generator at  $P_0 = 150$  psig and the attractor voltage was raised in steps from zero until voltage breakdown occurred inside the generator. Oscilloscope photographs were taken at each step, from which values of  $V_0$  and  $V_a$  were obtained.

The DC characteristic for positive ions was obtained in exactly the same way but with the negative DC power supply connected to the attractor.

#### Peak Output Voltage Characteristics

Scope. The peak output voltage characteristics were obtained for the sine wave input only since the peak and RMS output voltages for the square wave were expected to be almost identical. The peak output voltage characteristics are defined as the curves of load voltage,  $V_0$  (in kv p-p), plotted against attractor voltage,  $V_a$  (in kv zero to peak). The characteristics were determined for frequencies of 10, 20 and 30 cps and values of load resistance of 50, 100 and 200 megohms.

Procedure. The procedure followed to obtain the peak voltage characteristics is outlined below. The collector was connected to the 50 megohm load, the needles and ground plate were grounded, and the attractor was connected to the high-voltage alternating power source.

GA/Phys/63-11, 12

The power source was fed by a 10 cps signal from the sine wave signal generator. The generator input and output were connected through the voltage dividers to different channels of the oscilloscope. Flow was established through the generator and the attractor voltage was raised in increments from zero until saturation of the alternating power source was reached. Oscilloscope photographs yielded values of  $V_a$  and  $V_o$  for each step.

The same procedure was repeated with frequencies of 20 and 30 cps from the signal generator and then, with load resistances of 100 and 200 megohms, repeated again for each of the three frequencies.

#### RMS Output Voltage Characteristics

Scope. The RMS output voltage characteristics were obtained for both the sine wave and square wave inputs. The RMS output voltage characteristics are defined as the curves of load voltage,  $V_o$  (in kv RMS), plotted against attractor voltage,  $V_a$  (in kv RMS). These characteristics were determined for frequencies of 10, 25 and 40 cps and values of load resistance of 50, 100 and 200 megohms. The data for the RMS output voltage characteristics was also used to obtain the output power characteristics. These are defined as curves of output power,  $P_L$  (in watts), versus attractor voltage,  $V_a$  (in kv, RMS). The output power characteristics were determined for a frequency of 10 cps and values of load resistance of 50, 100 and 200 megohms. From the smoothed data of the RMS output voltage characteristics, a number of secondary curves were derived. These included plots of  $V_o$  versus  $f$ , with  $R_L$  as a parameter,  $V_o$  versus  $R_L$  with  $f$  as a parameter, and  $P_L$  versus  $R_L$  with  $f$  as a parameter, for fixed values of  $V_a$ .

GA/Phys/63-11, 12

Procedure. The following procedure was used to obtain the RMS output voltage characteristics. The collector was connected to the 50 megohm load resistance, the needles and ground plate were connected to ground, and the attractor was connected to the high-voltage alternating power source. The power source was fed with a 10 cps signal from the sine wave signal generator. The generator input and output were connected directly to the electrostatic voltmeters and indirectly, through the voltage dividers, to separate channels of the oscilloscope. Flow was established through the generator and the attractor voltage was raised in increments from zero until saturation of the power source was achieved. Readings of  $V_o$  and  $V_a$  were taken from the voltmeters at each step. The oscilloscope was used to monitor the generator input and output and to obtain photographs of characteristic wave shapes.

This procedure was repeated for the three frequencies at each value of load resistance for both the sine wave and square wave inputs. The upper limit of attractor voltage was established part of the time by saturation of the alternating power source and the rest of the time by voltage breakdown within the generator.

#### Output Voltage for Step Input

Scope. The relationships between the input and output voltages and time were obtained for a step input to the generator. Curves of  $(V_{a_{max}} - V_a)$  and  $(V_{o_{max}} - V_o)$  versus  $t$  were plotted for a  $V_{o_{max}}$  of 16.2 kv and a  $R_L$  of 100 megohms. From these, the input time constant,  $R_1 C_1$ , the output time constants,  $R_L C_o$ , and the output capacitance,  $C_o$ , of the generator were derived. This then permitted an examination of the effect

GA/Phys/63-11, 12

of an exponential input to the generator and of the time to reach ionization potential.

Procedure. The first step in obtaining the step input data was the modification of the high-voltage alternating power source. The blocking capacitor,  $C_3$  (Figure A1), was short circuited and a switched DC battery (22.5 volts) was connected directly to the grid of the 6BK4. When the tube was conducting, the voltage at the plate of the tube was zero. When the negative battery voltage was switched onto the grid, the tube cut off and the B+ voltage appeared at the output of the power source as a step function.

The collector was connected to the 100 megohm load resistance, the needles and ground plate were grounded as before, and the attractor was connected to the high-voltage alternating power source. The input and output of the generator were connected to separate channels of the oscilloscope. Flow was established and the attractor voltage was adjusted (with the tube cut-off) to give a reasonable output voltage ( $V_0 = 16.2$  kv). By means of the 22.5 V battery switch, the step input was applied to the generator and an oscilloscope photograph taken.

This was repeated for several different oscilloscope time scale settings. The resulting photographs gave the relationships of  $V_a$  and  $V_0$  with  $t$ .

#### Output Voltage for Biased Alternating Input

Scope. The output wave shape for the normal sine wave input shows considerable distortion since the attractor voltage only rises above the ionization potential for a portion of the cycle. If the generator operates

GA/Phys/63-11, 12

with an alternating input which is above the ionization potential for the entire cycle, then the output wave shape would be expected to show less distortion. The input voltage which satisfied this condition consisted of a sinusoidal voltage superimposed on a DC voltage such that the alternating component never dropped below the ionization potential. Runs were made at various frequencies and attractor voltages to permit examination of the output wave shape. Two variable frequency runs were made at constant  $V_a$  to obtain a relationship between  $V_o$  and  $f$ . From this, the roll-off frequency,  $f_R$ , and the output capacitance,  $C_o$ , of the generator were derived.

Procedure. These runs also required a modification of the high-voltage alternating power source. In order to allow the DC component to reach the attractor, the blocking capacitor,  $C_3$  in Figure A1, was short-circuited as in the case of the step input. The signal applied to the grid, however, was that from the sine wave generator.

The collector was connected to the 100 megohm load resistance, the needles and ground plate were connected to ground, and the attractor was connected to the alternating power source. The input and output of the generator were connected to separate channels of the oscilloscope. Flow was established and oscilloscope photographs were taken at several settings of  $V_a$  and  $f$ . Two runs were made with the AC and DC components of  $V_a$  held constant while the frequency was increased in steps and a series of oscilloscope photographs taken. From these,  $V_o$  was obtained for each frequency.

V. Results and Discussion

The results of the investigation are presented, for the most part, in graphical form and will be found throughout this chapter as they are discussed. The complete experimental data is tabulated in Appendix F.

Experimental Error

The RMS accuracy with which the voltages could be measured using the oscilloscope is determined as follows:

The accuracy of the scope was  $\pm 3\%$ .

The accuracy of the voltage measurements from the photographs was  $\pm 0.05$  cm. or, for a voltage measurement of the order of 2 cm.,  $\pm 2.5\%$ .

The accuracy of the voltage divider networks (10 -  $1\%$  10 megohm resistors in series with 1 -  $5\%$  10 kilohm resistor) is

$$\sqrt{\left[\sqrt{10 (1^2)}\right]^2 + 5^2} = 4\%$$

The total maximum experimental error of the oscilloscope voltage measurement then is

$$\sqrt{\left[\sqrt{3^2 + 2.5^2}\right]^2 + 4^2} = 5.5\%$$

In the cases where the difference of two voltages is considered, this maximum error becomes

$$\sqrt{5.5^2 + 5.5^2} = 8\%$$

For the cases where the voltages were measured with the electrostatic voltmeters, the output voltage was accurate to within  $\pm 1\%$ , and the input voltage was accurate to within  $\pm 1\%$  for voltages up to 5000 and accurate to within  $\pm 3\%$  for voltages between 5000 and 15,000. Therefore, an experimental error of  $\pm 1\%$  is assumed for the output voltage

GA/Phys/63-11, 12

and an average experimental error of  $\pm 2\%$  is assumed for the input voltage.

As indicated in Chapter II, the probable error in frequency is  $\pm 0.5$  cps, or approximately  $\pm 2\%$ , and the probable error in load resistance is approximately  $\sqrt{10 (1)^2} = 3\%$ .

#### Direct Current Characteristics

The direct current characteristics are plotted for negative ions (Figure 9), positive ions (Figure 10), and a combined curve of both (Figure 11). The DC characteristics were used to estimate the output current for any attractor voltage, such as in the prediction of the output voltage.

Spread of Data. As can be seen in Figures 9 and 10, a considerable spread in the data occurred for different runs. For example, with a  $V_a$  of 8 kv.,  $I_o$  varies from -60 to -150 micro-amps and with a  $V_a$  of -8 kv.,  $I_o$  varies from 15 to 95 micro-amps. The spread of data probably resulted from a combination of several effects. Variations in temperature could have resulted in a variation in output voltage since  $\phi_o$  and the fluid velocity  $V_f$  are both functions of  $T_o$ . Variations in the moisture content and composition of the air from day to day could have effected the ionization properties of the air. Voltage breakdown between the needles and the attractor occurred quite frequently and the resultant burning and pitting of the needles could have changed the ionization characteristics of the generator. Several preliminary DC runs were made without the 10 megohm resistor in place. It was found that the curve for increasing  $V_a$  (from zero to breakdown) differed considerably from the curve for decreasing  $V_a$  (from breakdown to zero).

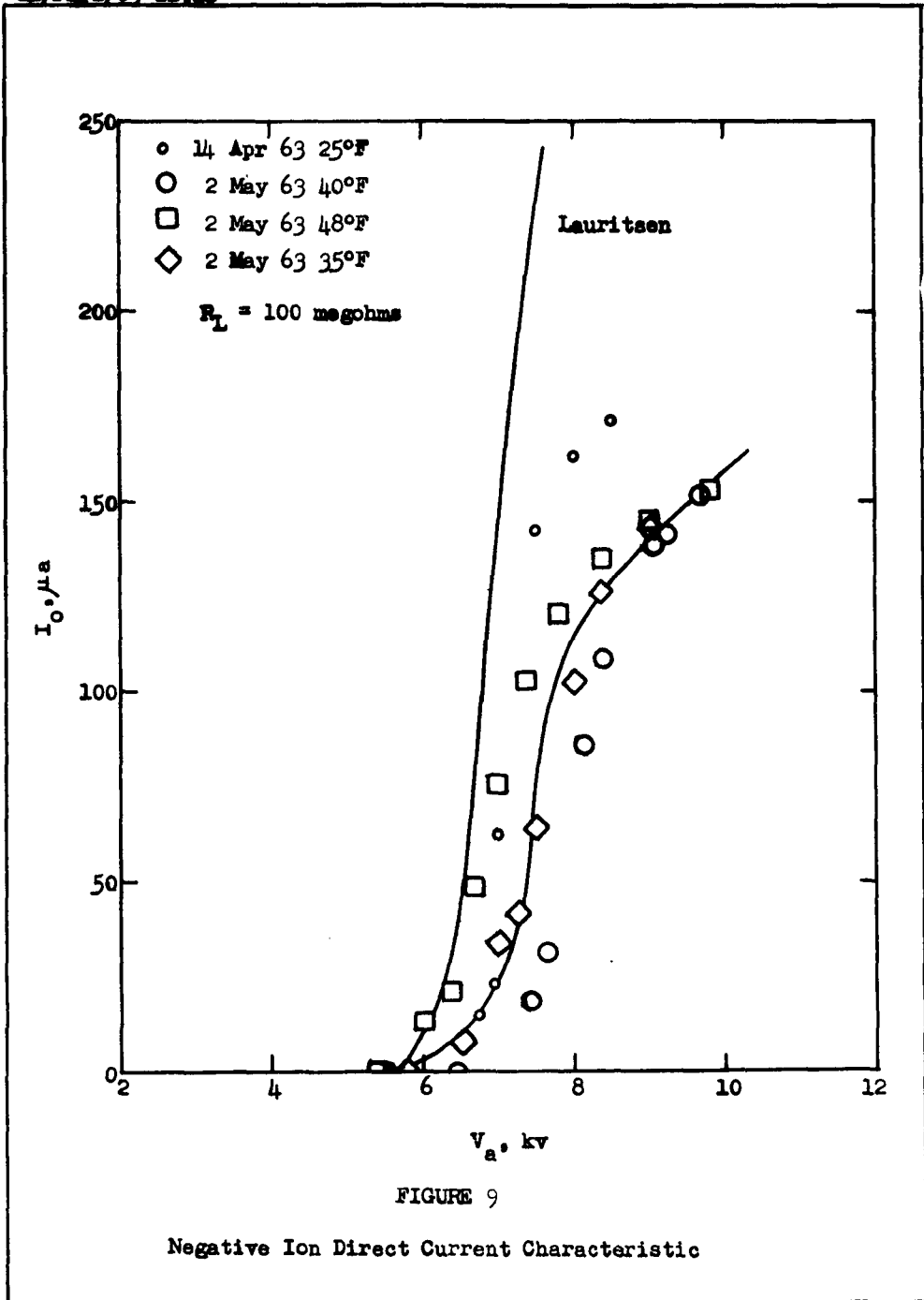
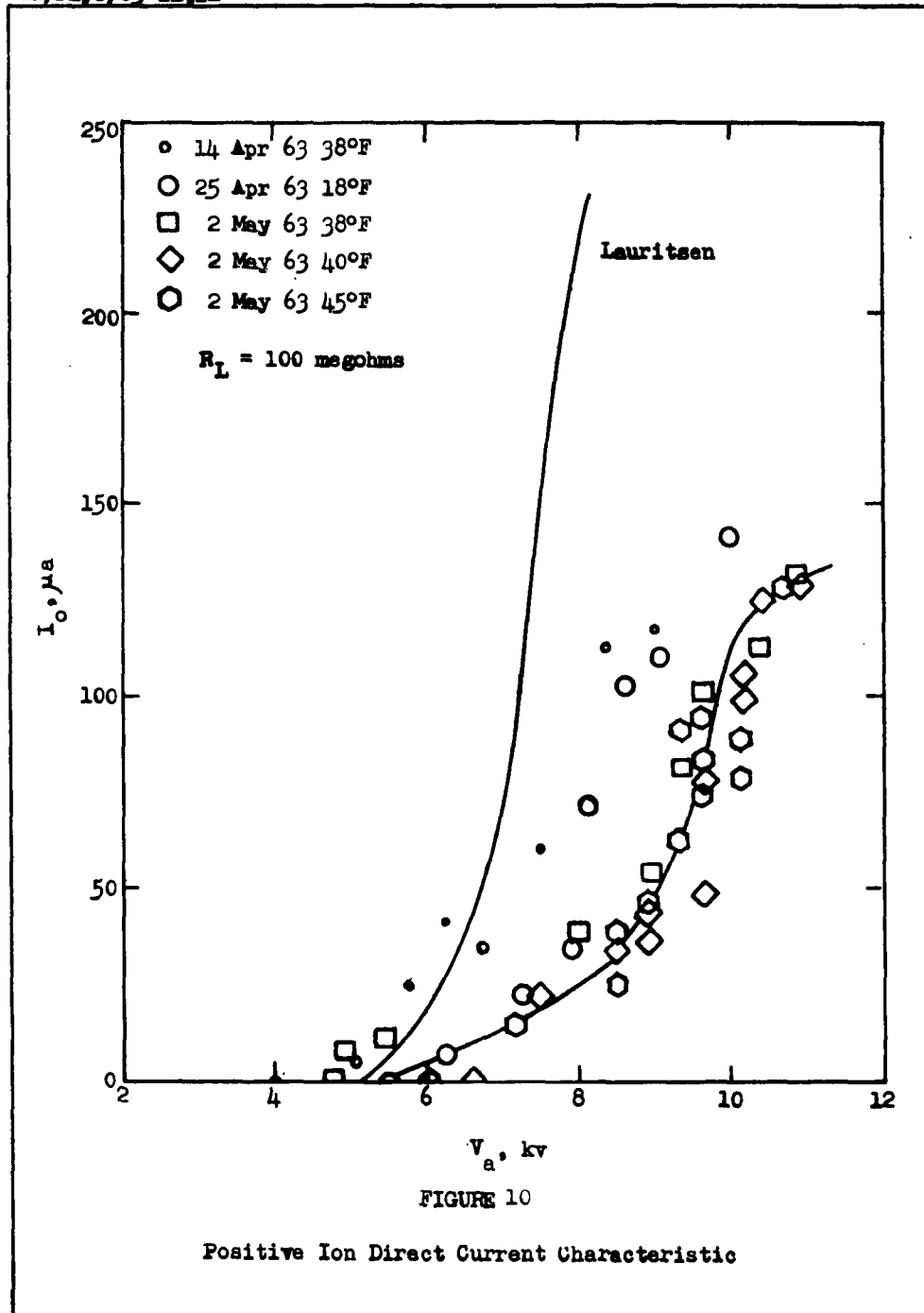
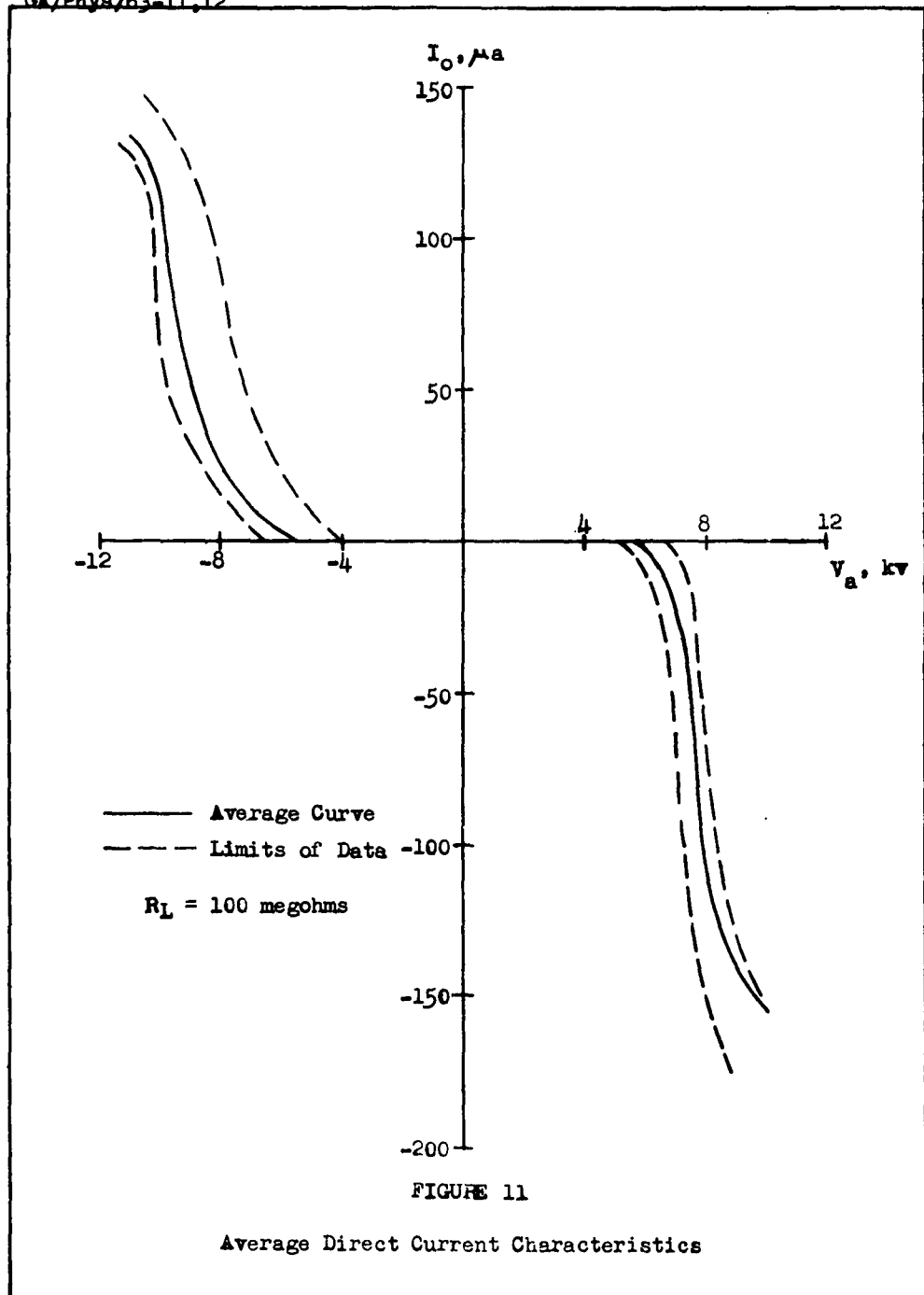


FIGURE 9

Negative Ion Direct Current Characteristic





GA/Phys/63-11, 12

This effect was undoubtedly caused by the heavy arcing which occurred at breakdown changing the ionization characteristic of the needles. With the large resistor in series only light arcing occurred and the up and down curves for any one run matched very closely. The large spread of data between runs, however, still persisted. Average DC characteristics are drawn through the points in Figures 9 and 10 and the limits of the spread of data are indicated on Figure 11.

Comparison with Previous Experiment. In order to compare the results of this study with those of Lauritsen, his corresponding curves are plotted in Figures 9 and 10. It can be seen that the lower portions of Lauritsen's curves match those of this investigation quite closely, but the upper portions of the curves are quite different. Lauritsen obtained much higher values of ion current at high attractor voltages. This occurred because Lauritsen's curves were obtained for the short-circuited condition and saturation did not take place.

Saturation of the output will occur at high attractor voltages when a load is connected to the output and a high voltage builds up on the collector. The phenomenon works in the following manner. As the ion current tends to increase due to an increase in attractor voltage, the potential difference across the load ( $I_o R_L$ ) also tends to increase. This higher voltage would normally result in an increase in the electric field in the transport region. However, if the electric field increases above a critical value, the air flow is not able to transport as many ions across the transport region and the ion current is decreased. An equilibrium condition is thus reached where the ion current and the output voltage rise to a maximum and level off regardless of how much

GA/Phys/63-11, 12

the attractor voltage is increased. This saturation phenomenon is reflected in the rounding off of the current and voltage characteristics at higher values of attractor voltage.

Since, Lauritsen's curves were plotted for zero load resistance (short-circuited output) the collector voltage was always zero. Therefore, saturation did not occur and his output was affected only by space charge limiting. This is a similar effect to that described above, except that the ion current is limited only by the electric field due to the space charge in the transport region and not by the electric field due to a voltage on the collector.

Another factor which could have contributed to the differences between Lauritsen's curves and those of this investigation was the burning of the needles by repeated voltage breakdown. The most severe damage probably occurred when preliminary DC runs were made without a series resistor between the power supply and the attractor. Further, there is the possibility that physical changes occurred in the generator during the months it lay unused. Such changes could be reflected in the electrical performance of the generator.

#### Peak Output Voltage Characteristics

Figures 12, 13 and 14 show the results of plotting peak to peak output voltage versus zero to peak attractor voltage at frequencies of 10, 20 and 30 cps for values of load resistance of 50, 100 and 200 megohms respectively.

Comparison with DC Results. If we take the curve for 10 cps at  $R_L = 100$  megohms (Figure 13) we find, at  $V_a = 8$  kv, that  $V_o = 27$  kv. Now, for the same  $V_a$  using the extreme limits on the DC characteristics

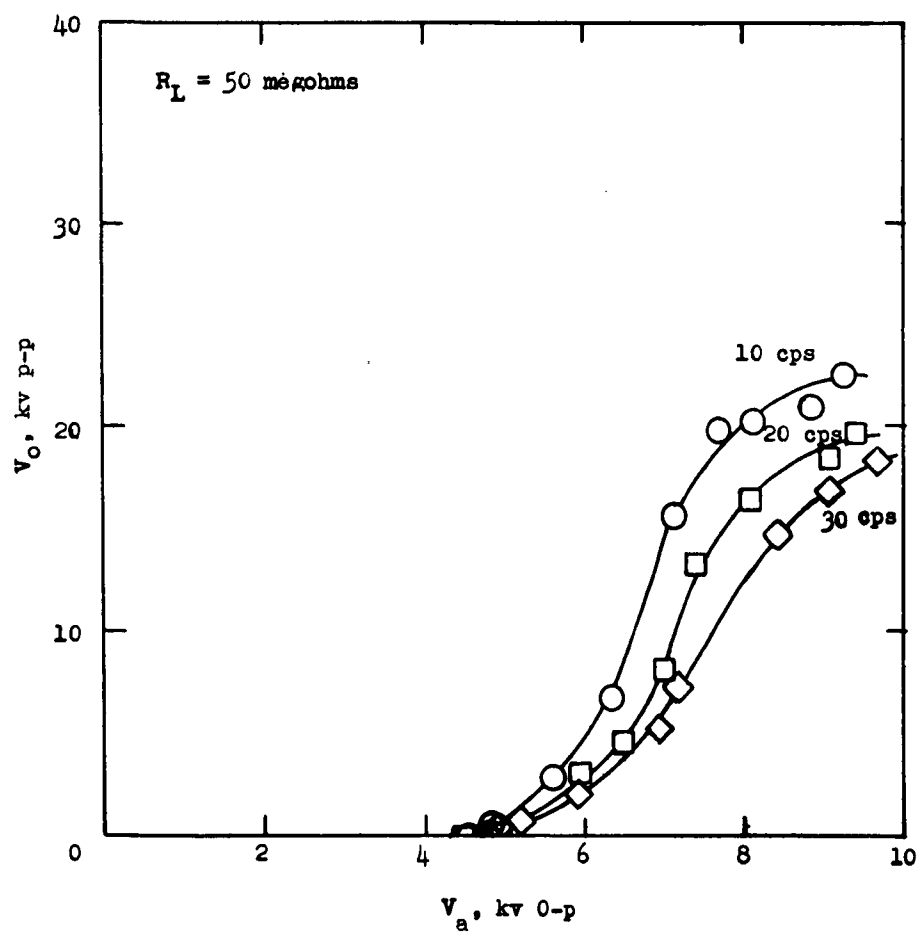


FIGURE 12

Peak Voltage Characteristics ( $R_L = 50$  megohms)

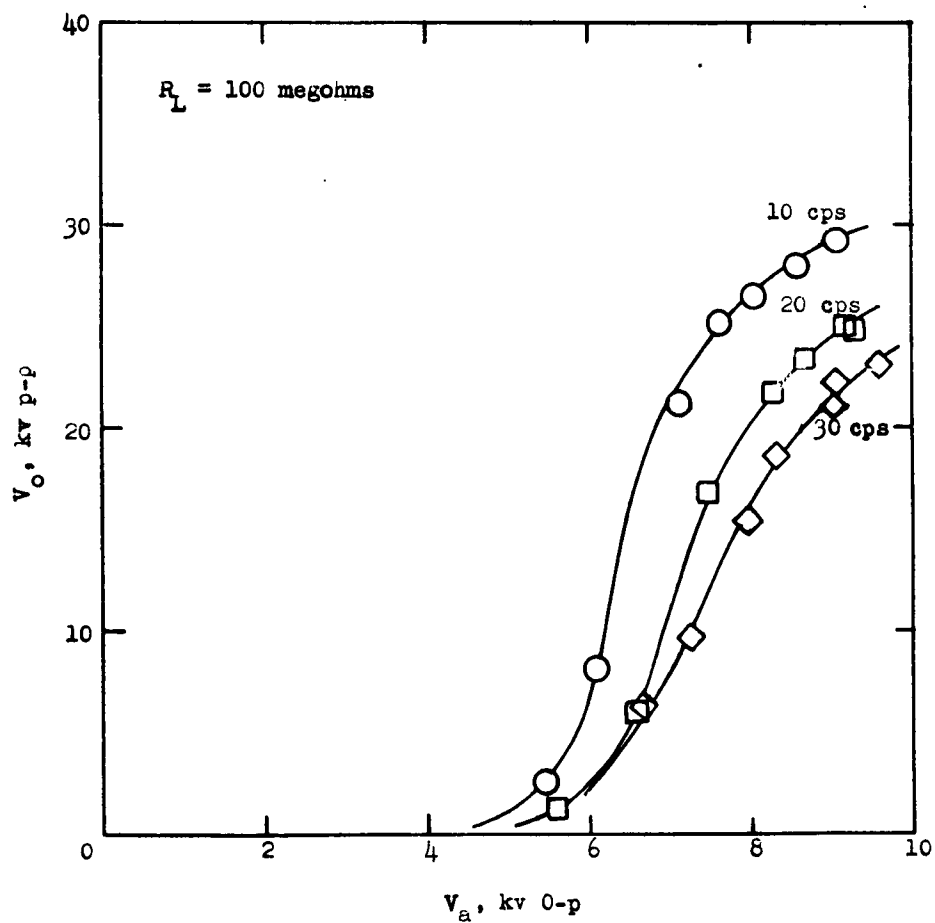


FIGURE 13

Peak Voltage Characteristics ( $R_L = 100$  megohms)

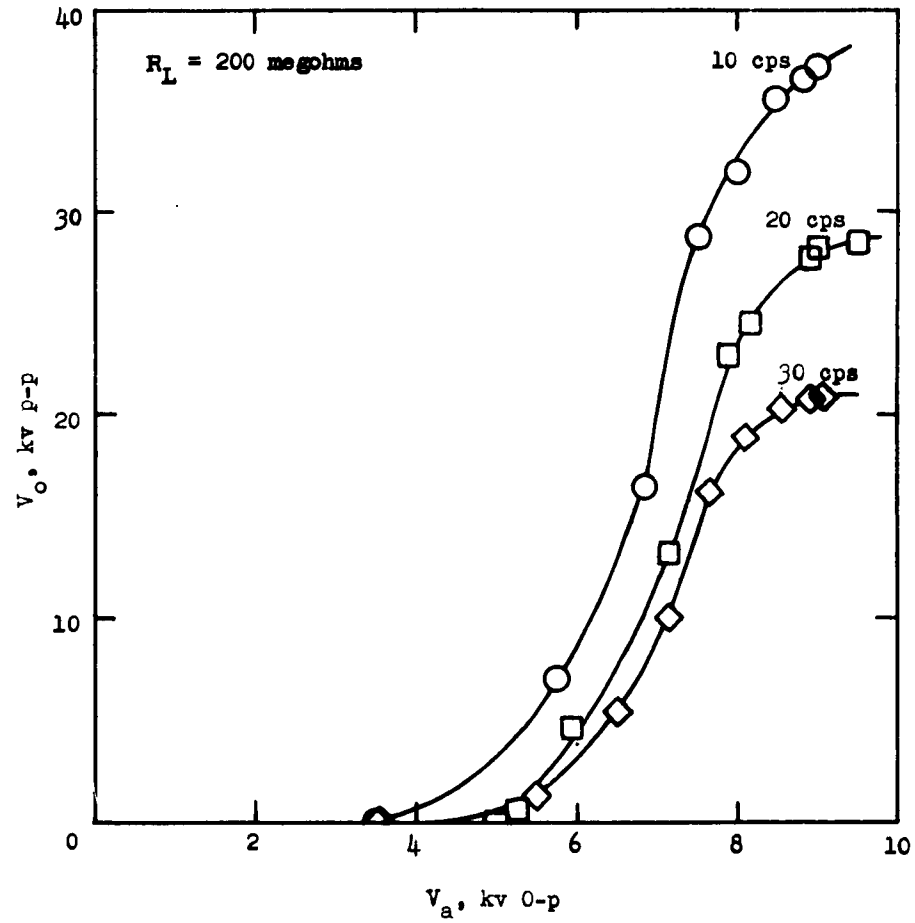


FIGURE 14

Peak Voltage Characteristics ( $R_L = 200$  megohms)

GA/Phys/63-11, 12

(Figure 11), the sum of the two  $V_0$ 's for positive and negative ions ( $I_0 R_L$ ) is 24.5 kv. These values correspond quite closely, although one would expect the value for the sine wave characteristic to be slightly less than that for the DC characteristics, since there will be some attenuation due to  $C_0$  even at 10 cps. It should be noted also that the shape of the peak output voltage curve corresponds very closely with the shape of the DC curve.

Effect of Load Resistance. It is apparent from Figures 12, 13 and 14, that as load resistance increases at any frequency, the output voltage also increases. This is to be expected since, for a given ion current, the IR drop and hence the voltage across the load, will increase as the resistance increases. This phenomenon is consistent with the results obtained by Wheeler (Ref 7:66) and is discussed more fully in the section on RMS output voltage results.

Effect of Frequency. Figures 12, 13, and 14 also indicate that, for a given value of load resistance, the output voltage decreases as the frequency increases. This phenomenon is not surprising since the effect of the output capacitance in attenuating the generator output will become more pronounced as the frequency increases. A further discussion of this effect is also contained in the section on RMS output voltage results.

#### RMS Output Voltage Characteristics

Figures 15, 16 and 17 are plots of RMS output voltage versus RMS attractor voltage at sine wave frequencies of 10, 25, and 40 cps for values of 50, 100 and 200 megohms respectively. Figures 18, 19 and 20 are the corresponding curves for a square wave input. Plots of output

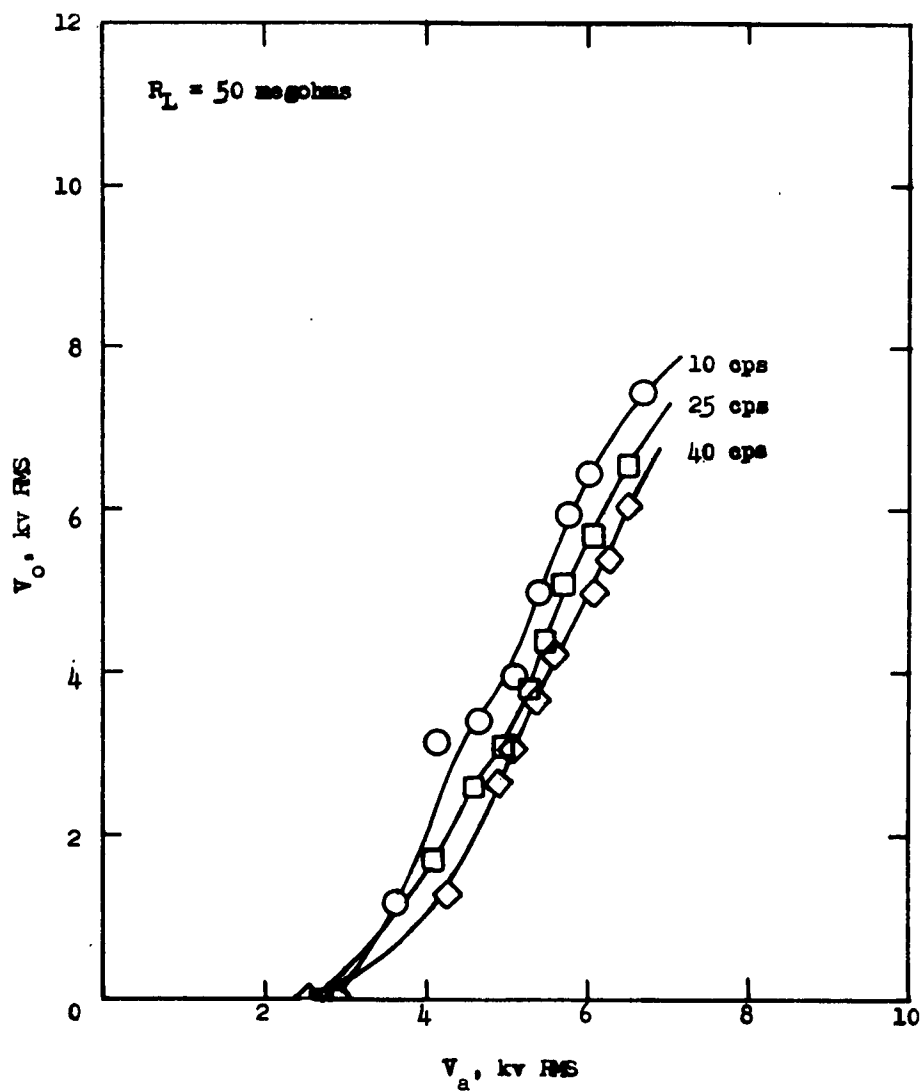


FIGURE 15

RMS Voltage Characteristics for Sine Wave Input  
( $R_L = 50$  megohms)

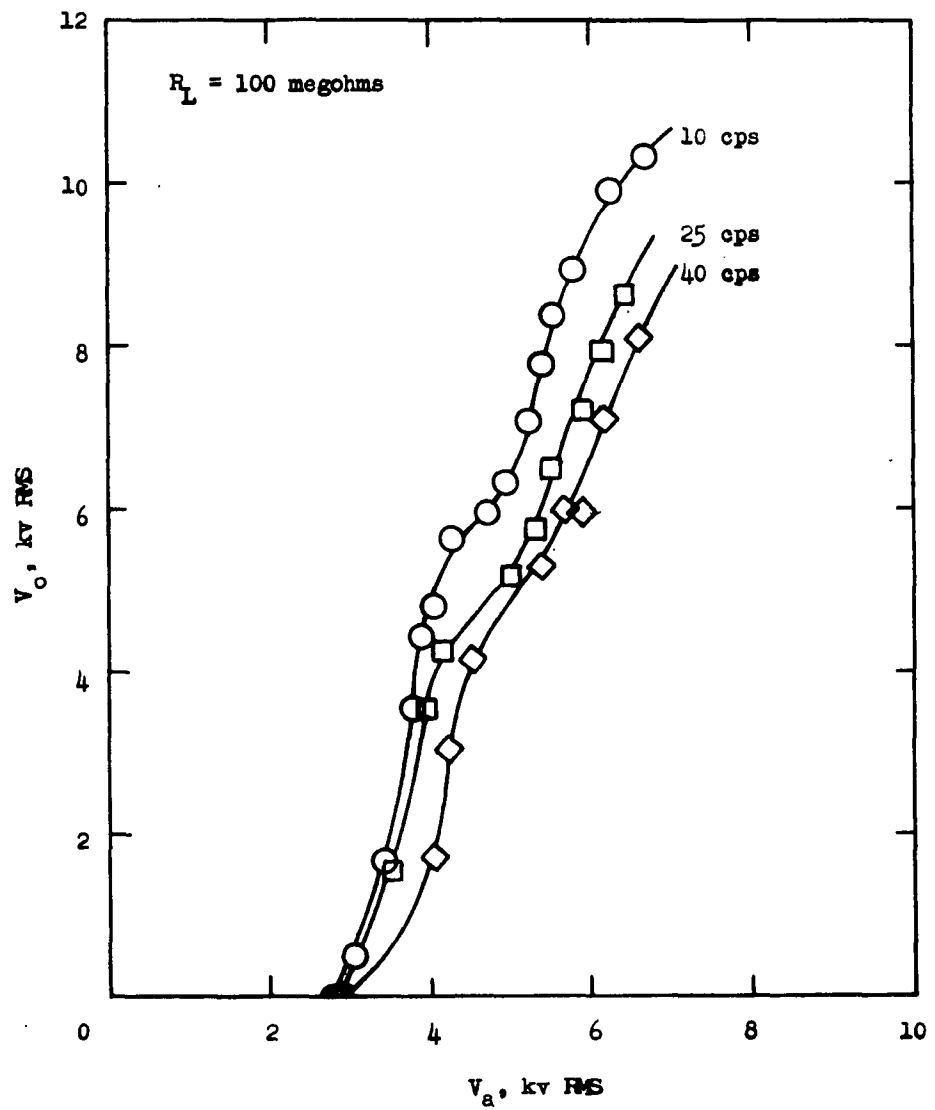


FIGURE 16

RMS Voltage Characteristics for Sine-Wave Input  
( $R_L = 100$  megohms)

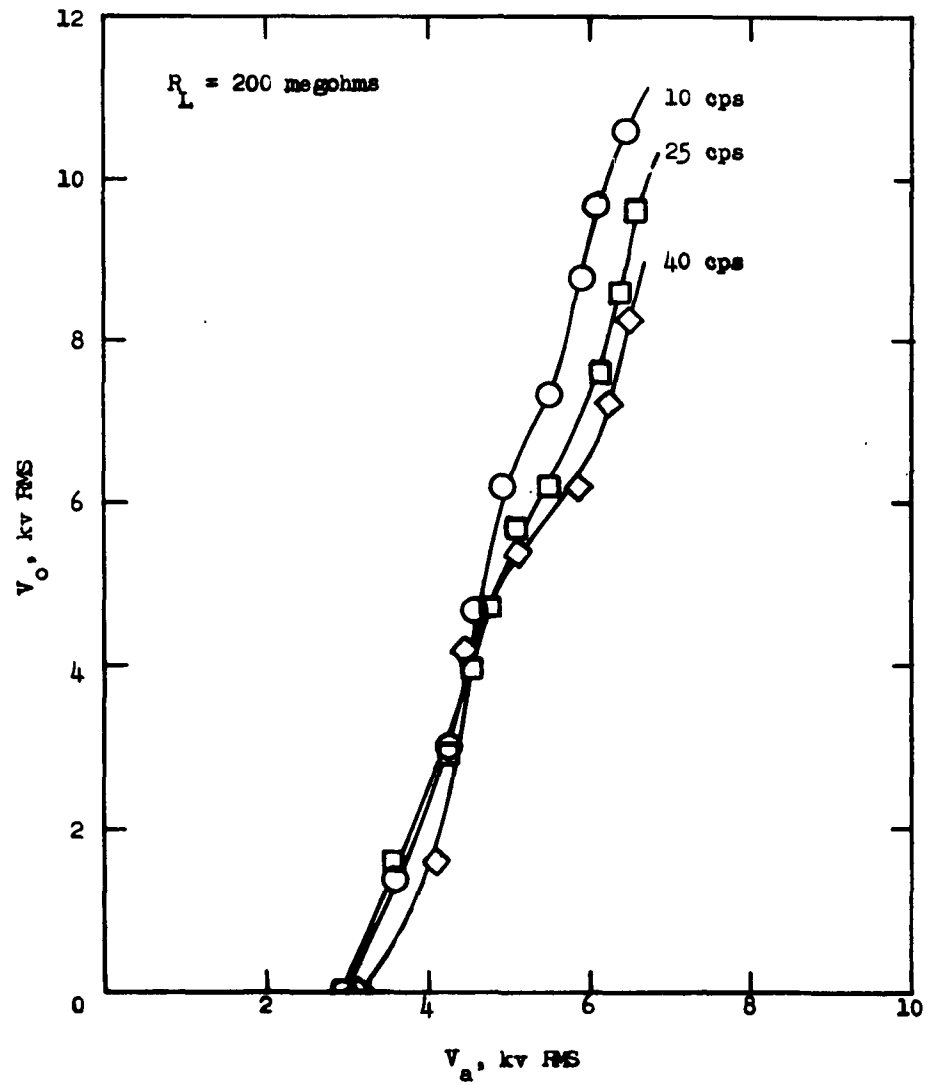


FIGURE 17

RMS Voltage Characteristics for Sine Wave Input  
( $R_L = 200$  megohms)

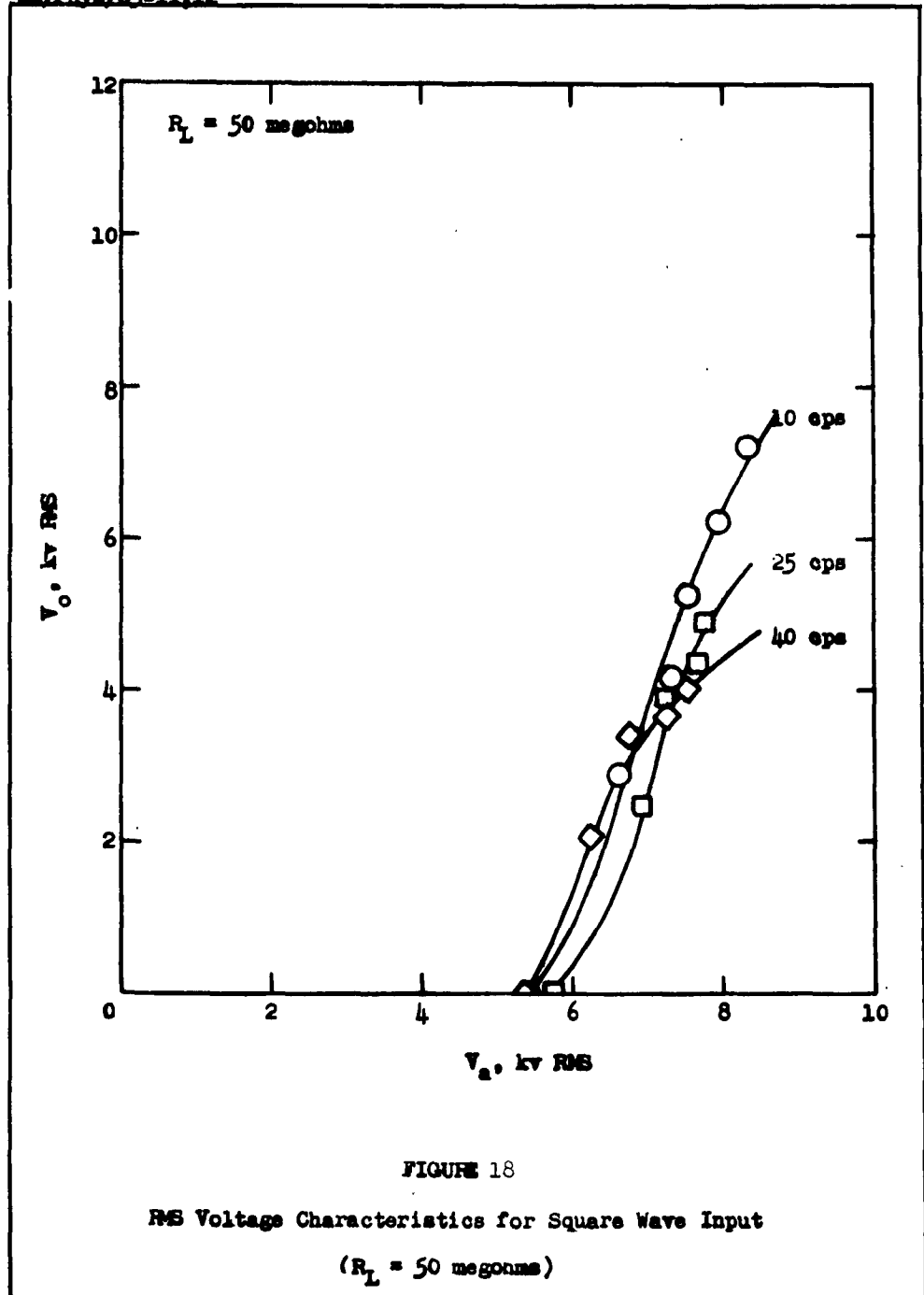


FIGURE 18

RMS Voltage Characteristics for Square Wave Input

( $R_L = 50$  megohms)

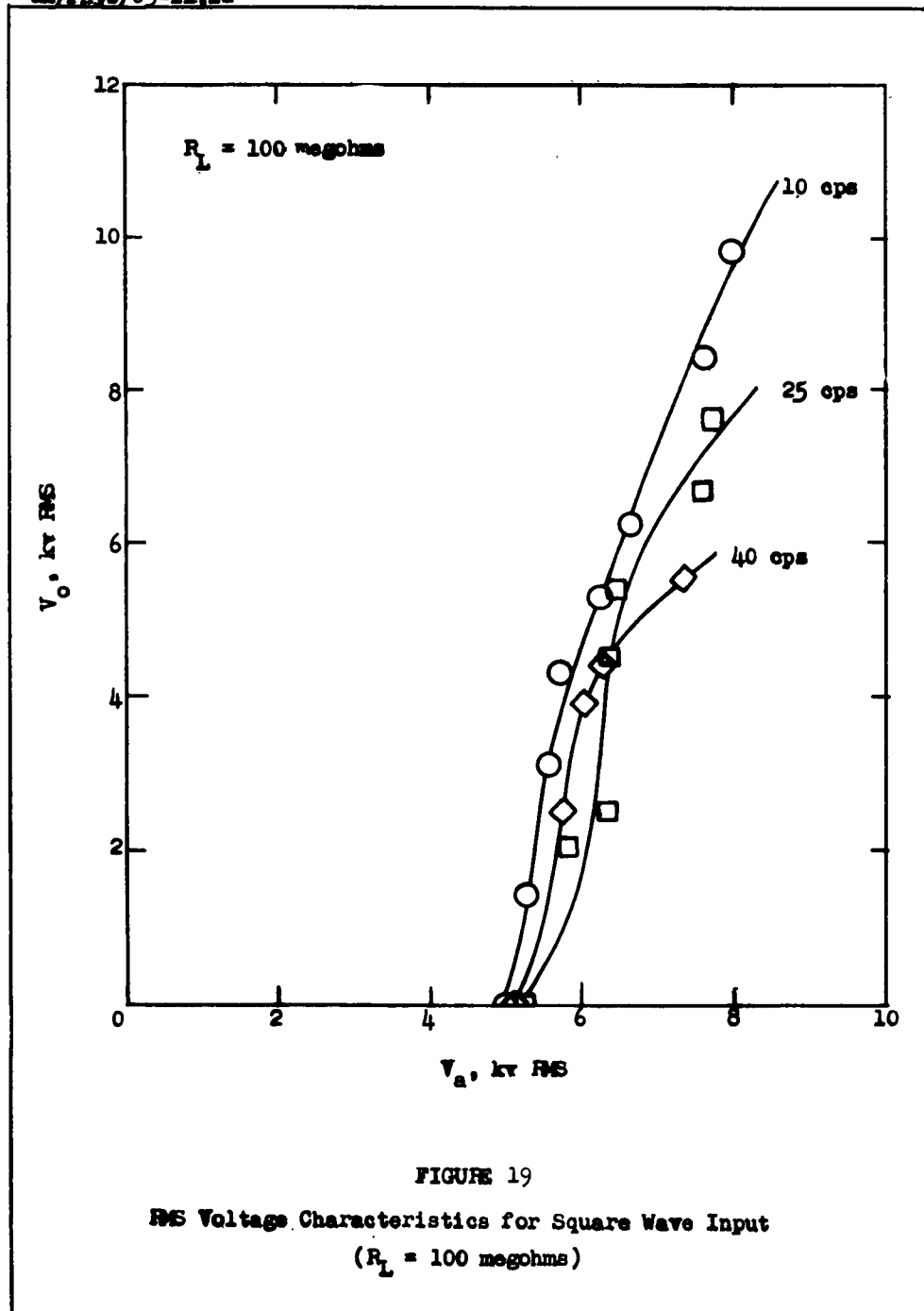


FIGURE 19

RMS Voltage Characteristics for Square Wave Input  
( $R_L = 100$  megohms)

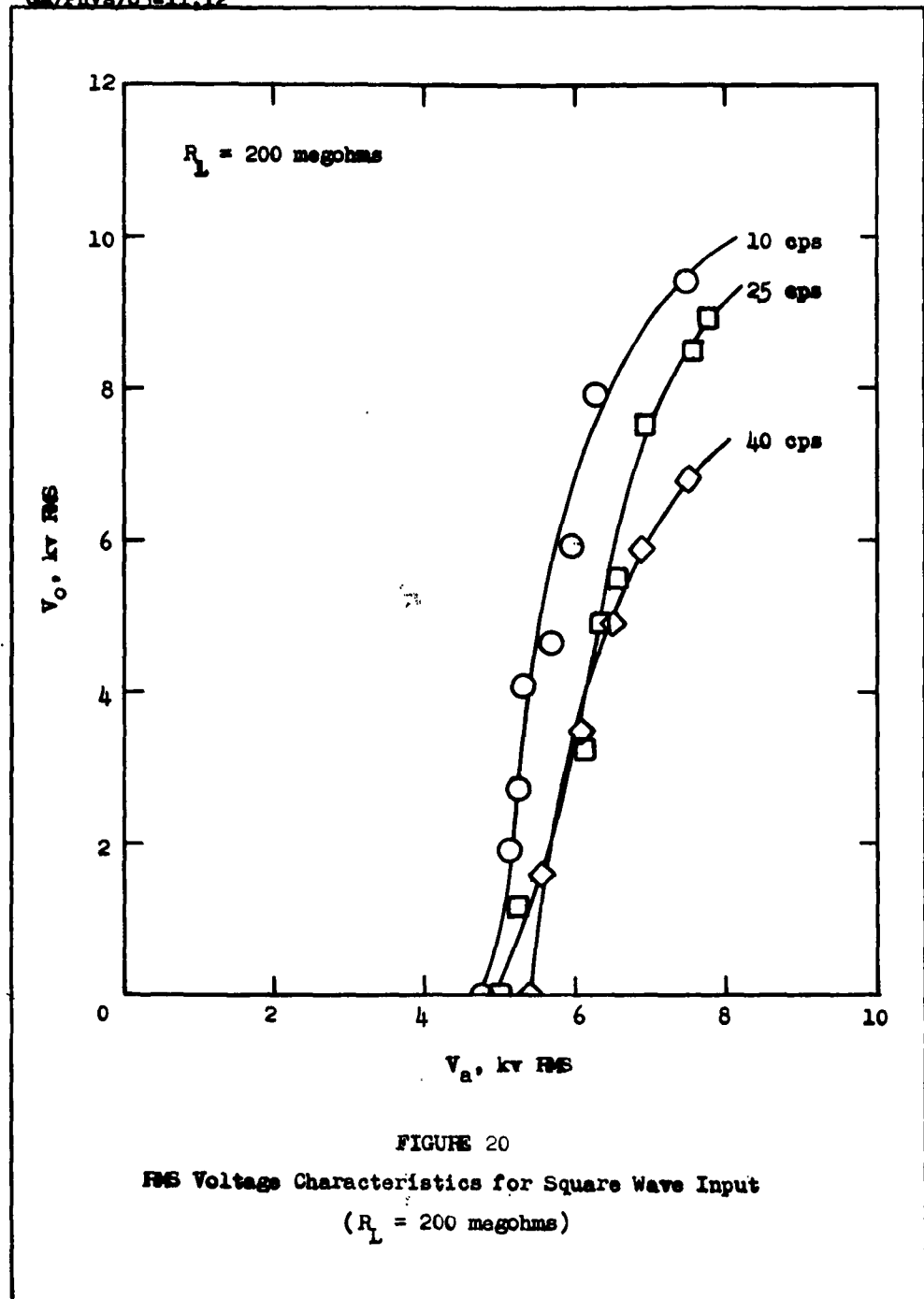


FIGURE 20

RMS Voltage Characteristics for Square Wave Input

 $(R_L = 200 \text{ megohms})$

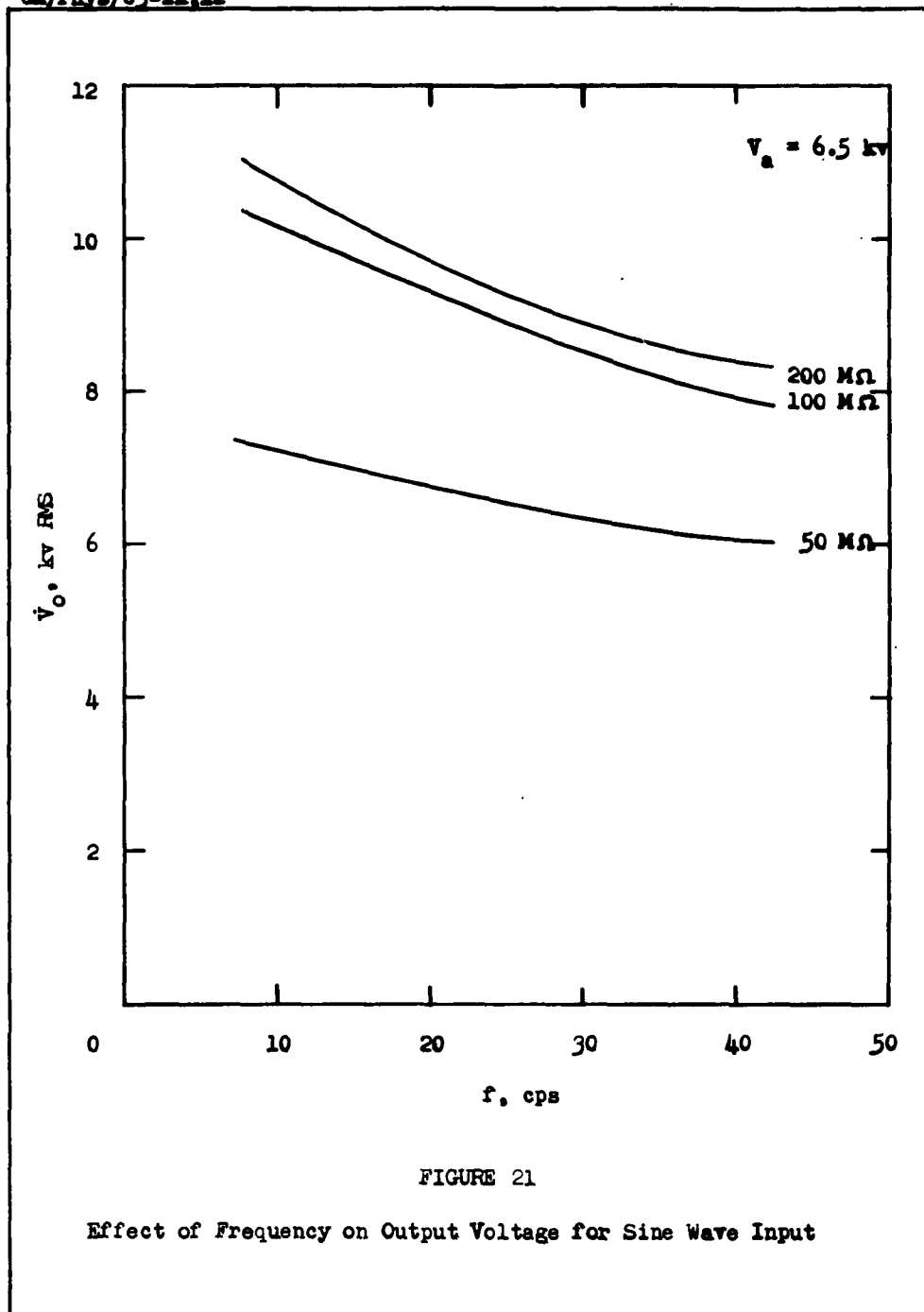


FIGURE 21

Effect of Frequency on Output Voltage for Sine Wave Input

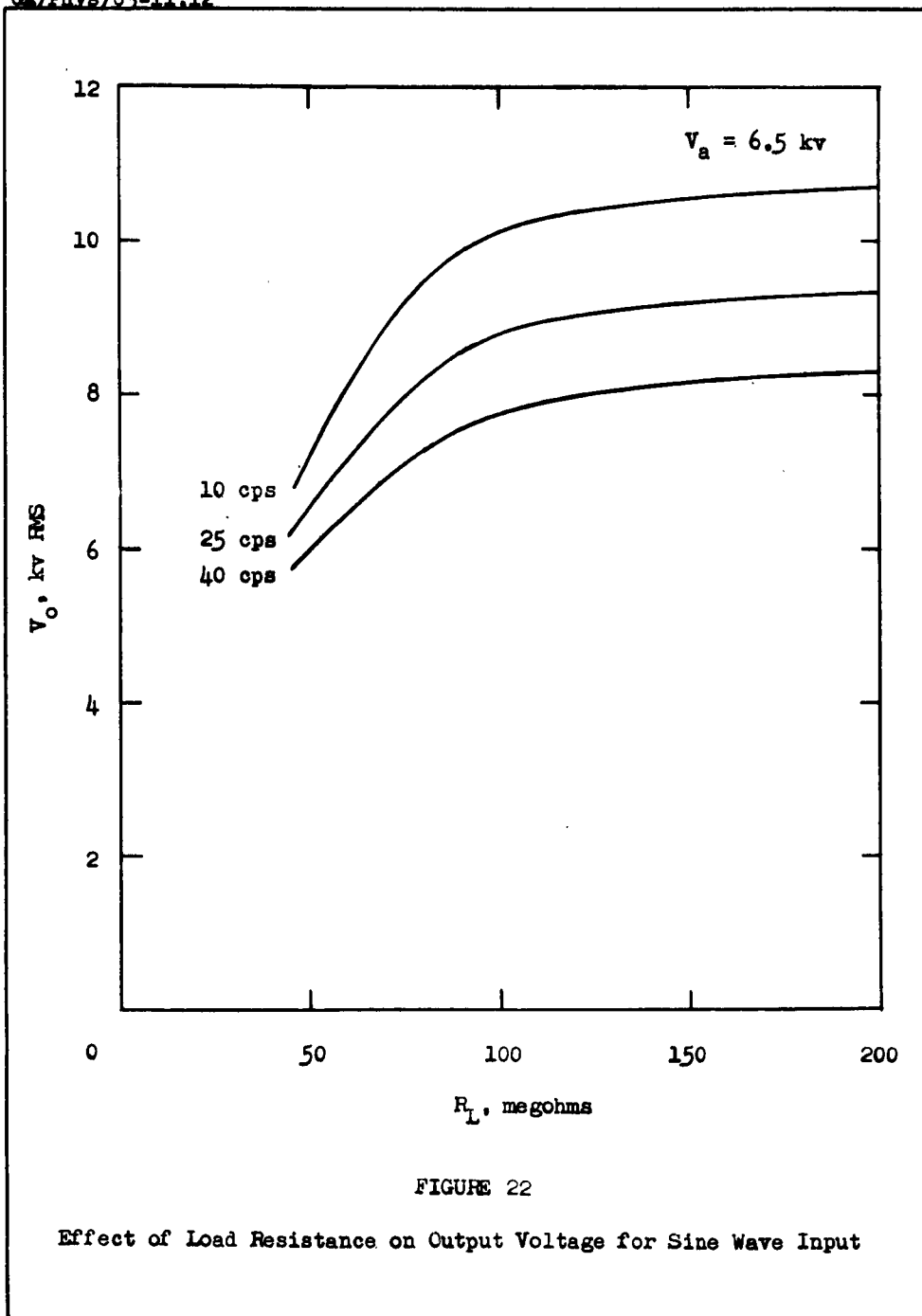


FIGURE 22

Effect of Load Resistance on Output Voltage for Sine Wave Input

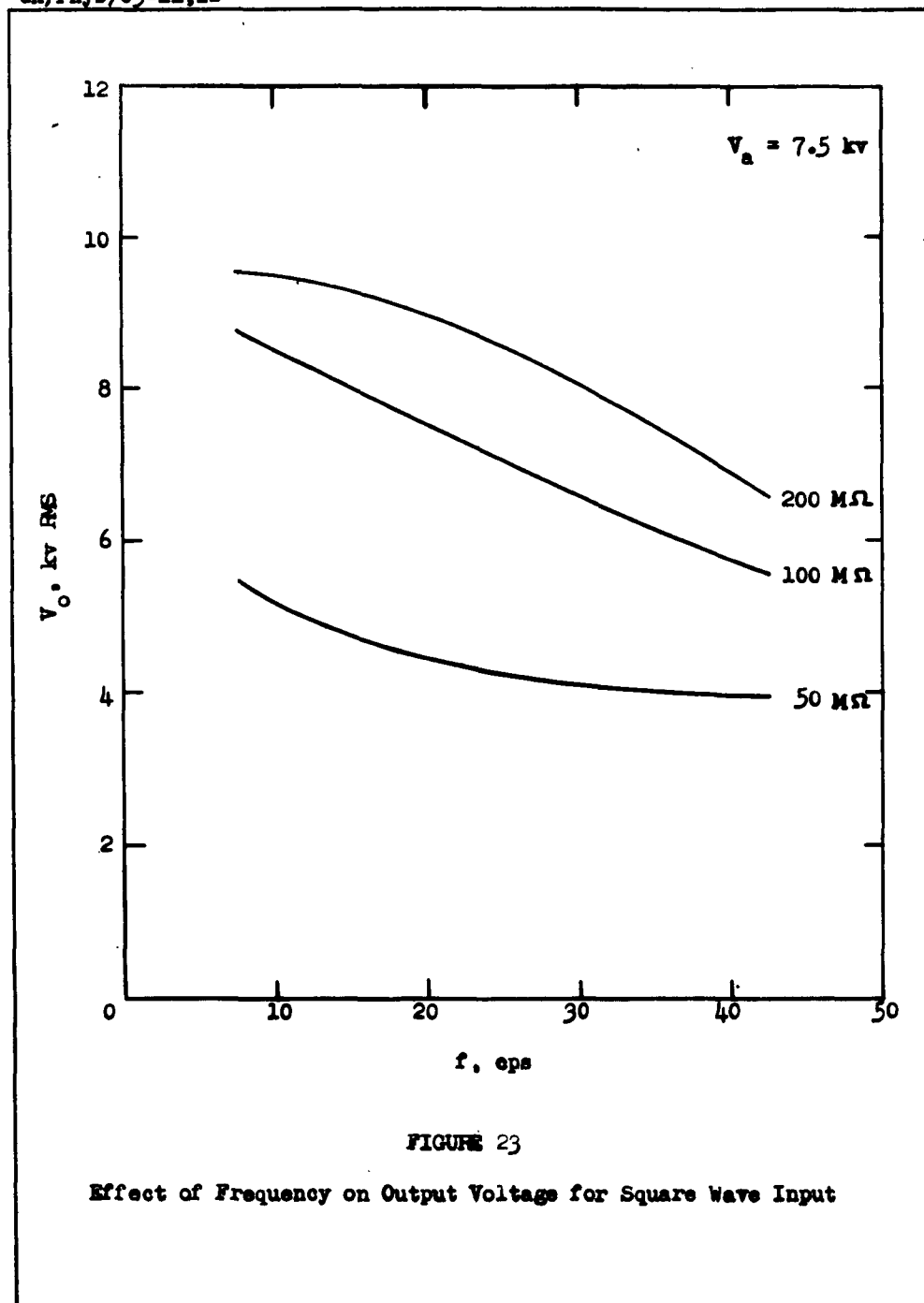


FIGURE 23

Effect of Frequency on Output Voltage for Square Wave Input

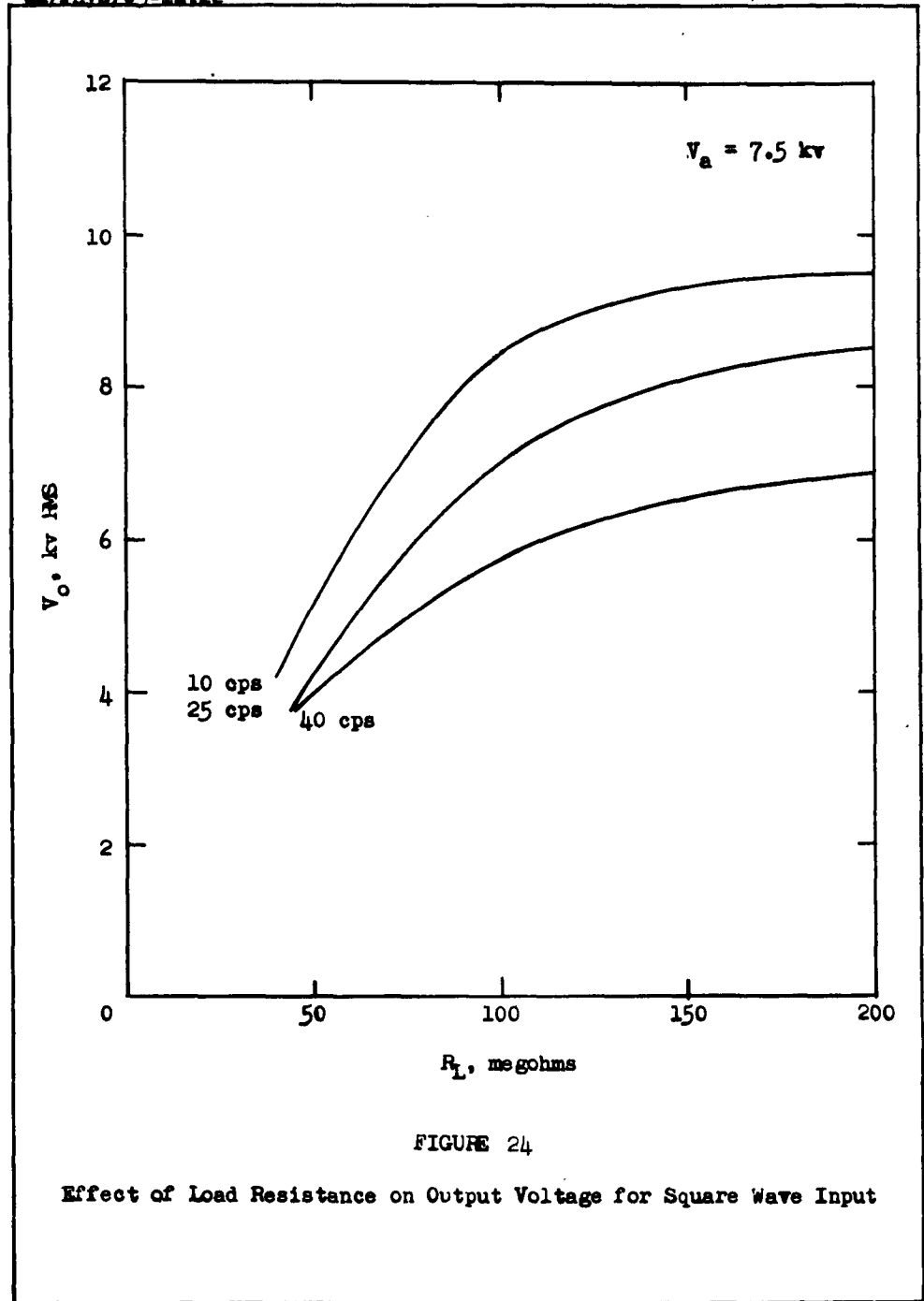


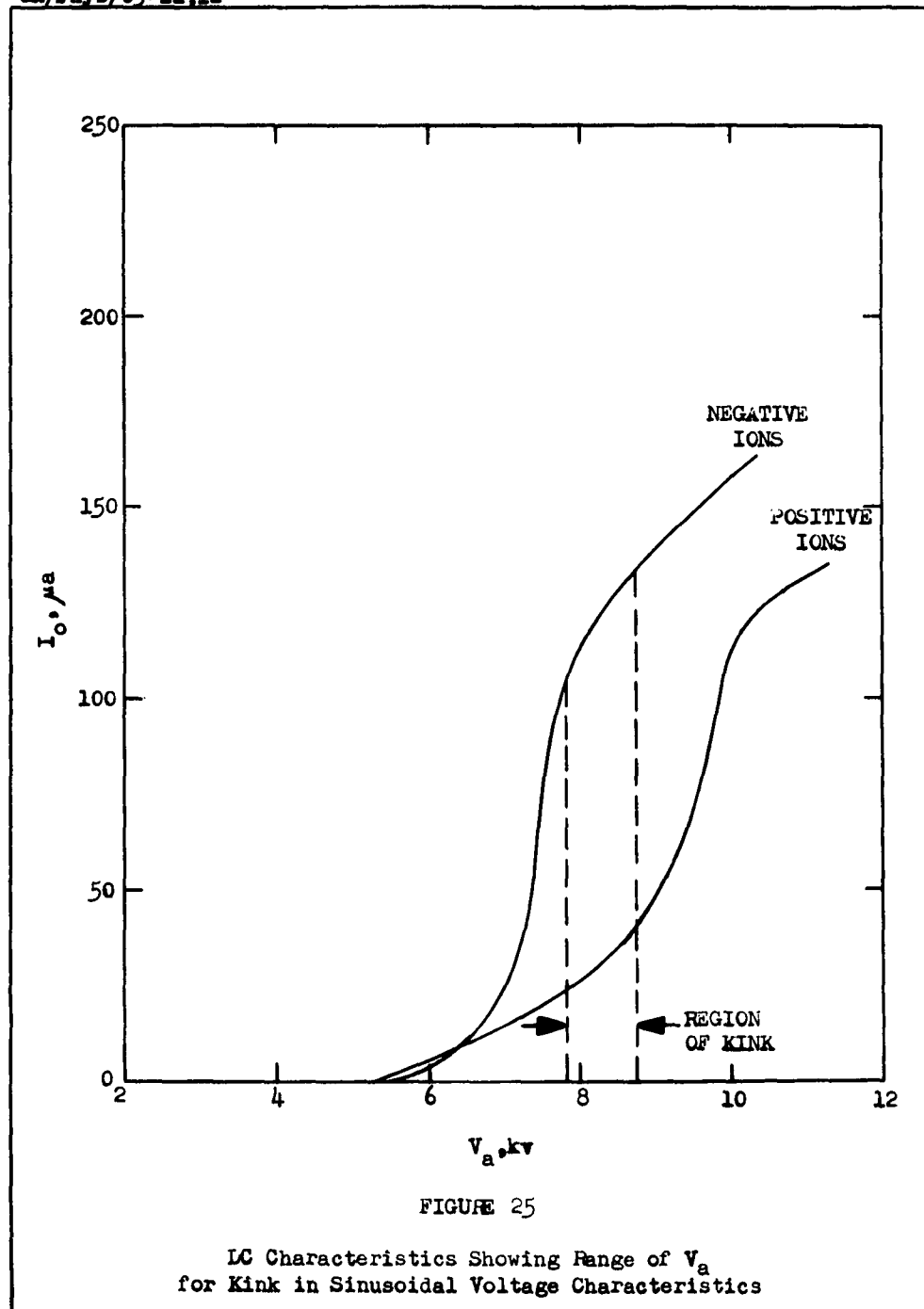
FIGURE 24

Effect of Load Resistance on Output Voltage for Square Wave Input

GA/Phys/63-11, 12

voltage versus frequency and output voltage versus load resistance are given for fixed values of sine wave and square wave input voltage (Figures 21 and 22 and Figures 23 and 24 respectively). These last four graphs are plotted from smoothed data; that is, the points for these curves were taken from the smooth curves drawn through the experimental points on the original RMS voltage characteristic curves. These curves were drawn from three points only and, therefore, it might be expected that slight errors or variations in the original data would strongly influence the shape of the curves. They are valid, however, for indicating trends.

Comparison with Peak Output Voltage Characteristics. The RMS voltage curves are, in general, similar in shape to the p-p output voltage characteristics with the exception of a kink in the sine wave curves for values of  $V_a$  between 5.2 to 6.2 kv RMS (7.3 to 8.8 kv p-p). This kink is probably caused by the change in the wave shape with attractor voltage as shown in the photographs of Figure 33. An examination of the DC characteristics helps to explain this phenomenon. Figure 25 shows the DC characteristics for positive and negative ions plotted on the same graph. Note that between the dotted lines, in the areas marked "Region of Kink", the negative ion curve has begun to taper off while the positive ion curve has not yet reached its steepest slope. Consequently, the rate of rise of output voltage decreases with attractor voltage in this region. Once  $V_a$  gets above 8.8 kv the steep part of the positive ion curve is reached and the output voltage once again rises rapidly as before. The rapid rise, decrease in rate of rise, and rapid rise again appears to account for the kink in the output voltage curves.



Effect of Load Resistance. Wheeler discovered that the output voltage increased with load resistance up to 60 megohms, tending to level off as it increased (Ref 7:66). For a given ion current, as the load resistance increases, the output voltage increases. The field in the transport region also increases correspondingly opposing the flow of ion current. Saturation will then take place as the output voltage reaches a maximum above which it cannot increase further. This effect was observed in both the square wave and the sine wave results. The output voltage was nearly constant for values of load resistance above 150 megohms (Figure 22 and 24).

Effect of Frequency. As the frequency increases, the output voltage of the generator would be expected to decrease owing to the effect of the output capacitance. Figures 21 and 23 show that, for given values of  $V_a$  and  $R_L$ ,  $V_o$  does decrease with frequency for both square and sine wave inputs. Now, if the output voltage of the generator were sinusoidal, the rate of attenuation of the output voltage by the capacitor would be expected to increase and the slopes of the  $V_o$  versus  $f$  curves would become more negative. However, the output of the generator for a sine wave input is not sinusoidal and, for a given peak to peak voltage, the RMS content of the output waveform increases with frequency (see Figure 31). Hence, the rate of attenuation of the output voltage for this waveform will not increase with frequency but, rather, it will decrease owing to the relatively greater RMS content. This fact accounts for the shape of the  $V_o$  versus  $f$  curves for the sine wave input. The same thing is not true, however, for the square wave input curves where the RMS content of the output waveform actually does decrease with frequency. The curve

GA/Phys/63-11, 12

for 200 megohms in Figure 23 does show an increase in the rate of attenuation, the curve for 100 megohms shows an almost linear attenuation and that for 50 megohms shows a decrease in the rate of attenuation. The trend of the latter two curves is contrary to what was expected and a satisfactory explanation could not be found for this inconsistency. Perhaps here, as in the case of the sine wave, distortion in the wave shape was the cause.

Comparison of Square and Sine Wave Results. The shapes of the square and sine wave characteristics are quite similar as may be seen by comparing Figures 15, 16, and 17 with Figures 18, 19 and 20. Ionization occurs at the lower RMS value of attractor voltage for the sine wave than it does for the square wave since the peak of the sine wave goes above the ionization potential while the RMS value is still considerably below. Slightly higher values of  $V_0$  were obtained at the upper end of the curves for the sine wave input. This can be attributed to two factors:

1. For a given RMS attractor voltage, the peak of the sine wave is 1.4 times as high as the peak of the square wave. Therefore, the generator will be operating on a higher portion of the DC characteristic, thus giving a larger ion current and a higher output voltage.
2. Since a definite time is required for the voltage breakdown to occur inside the generator, a sinusoidal voltage, whose peak rises above the breakdown potential for a small fraction of each half cycle, could be applied to the attractor at some frequencies without causing breakdown. A square wave voltage

GA/Phys/63-11, 12

of the same peak value, whose peak is above the breakdown potential for the entire half cycle, would cause breakdown at the same frequencies. Thus, a higher peak to peak sine wave voltage can be applied to the attractor and a correspondingly higher output voltage can be generated.

#### Output Power Characteristics

Output power was calculated in all cases from the output voltage and load resistance. Plots of output power versus attractor voltage for a frequency of 10 cps and three values of load resistance are given in Figures 26 and 27 for sine and square wave inputs respectively. Also plotted are curves of output power versus load resistance for a fixed value of attractor voltage and three frequencies for sine and square wave inputs (Figures 28 and 29). The latter are derived from the smoothed data of Figures 15 to 20, and the fact that they are derived from only three points should be borne in mind as their shape is examined. As might be expected, the shape of the curves is similar to the shape of the RMS voltage characteristics. However, their slopes are different. It is interesting to note that, for both sine wave and square wave inputs, the highest value of output power obtained was of the order of one watt. The maximum value of power obtained by Wheeler for the same conditions was 4.5 watts (Ref 7:63).

Effect of Load Resistance. For any electrical generator which is delivering power to a load, the maximum power is transferred when the impedance of the load is equal to the impedance of the generator. A plot of output power versus load resistance, then, should show a maximum

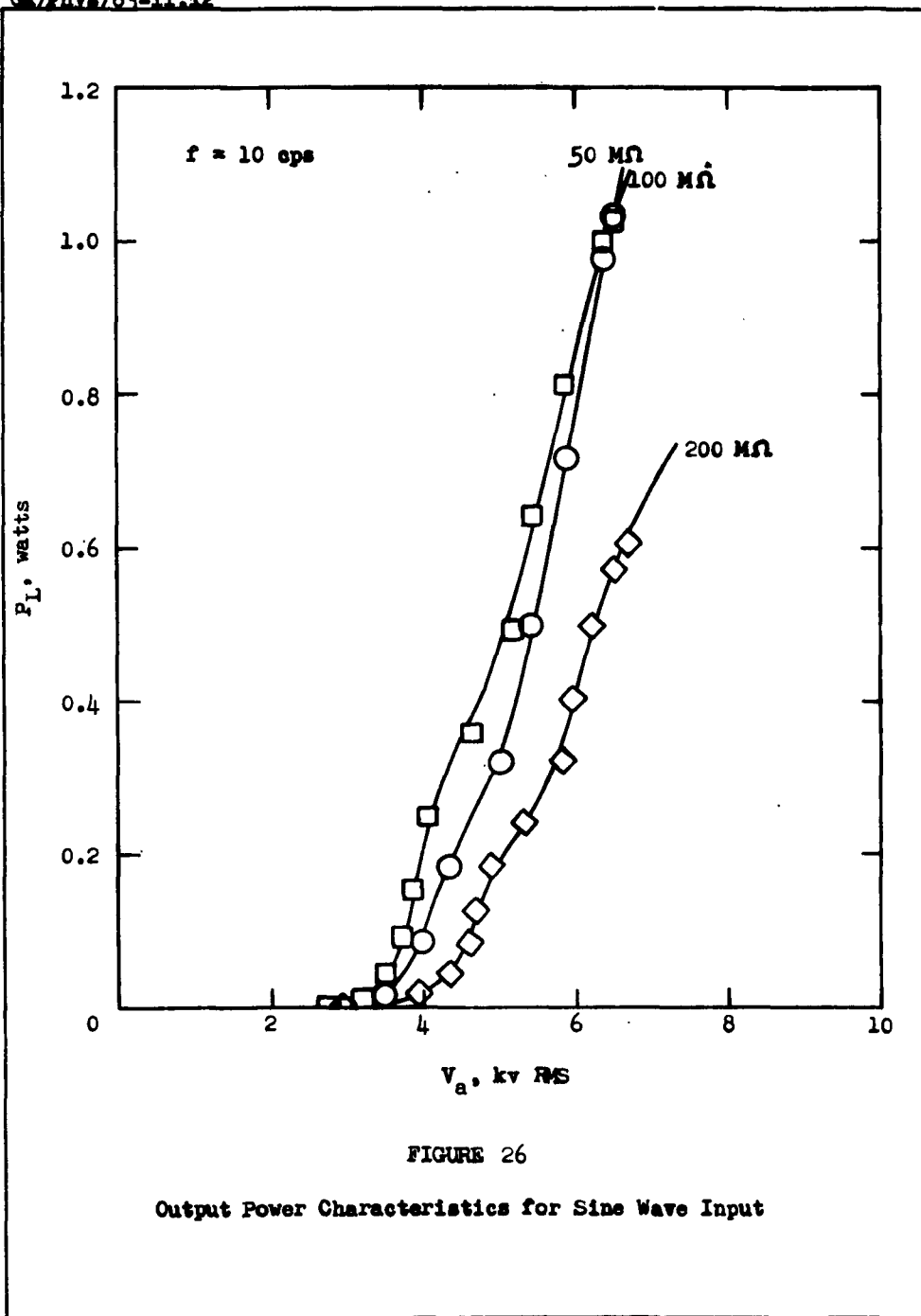


FIGURE 26

Output Power Characteristics for Sine Wave Input

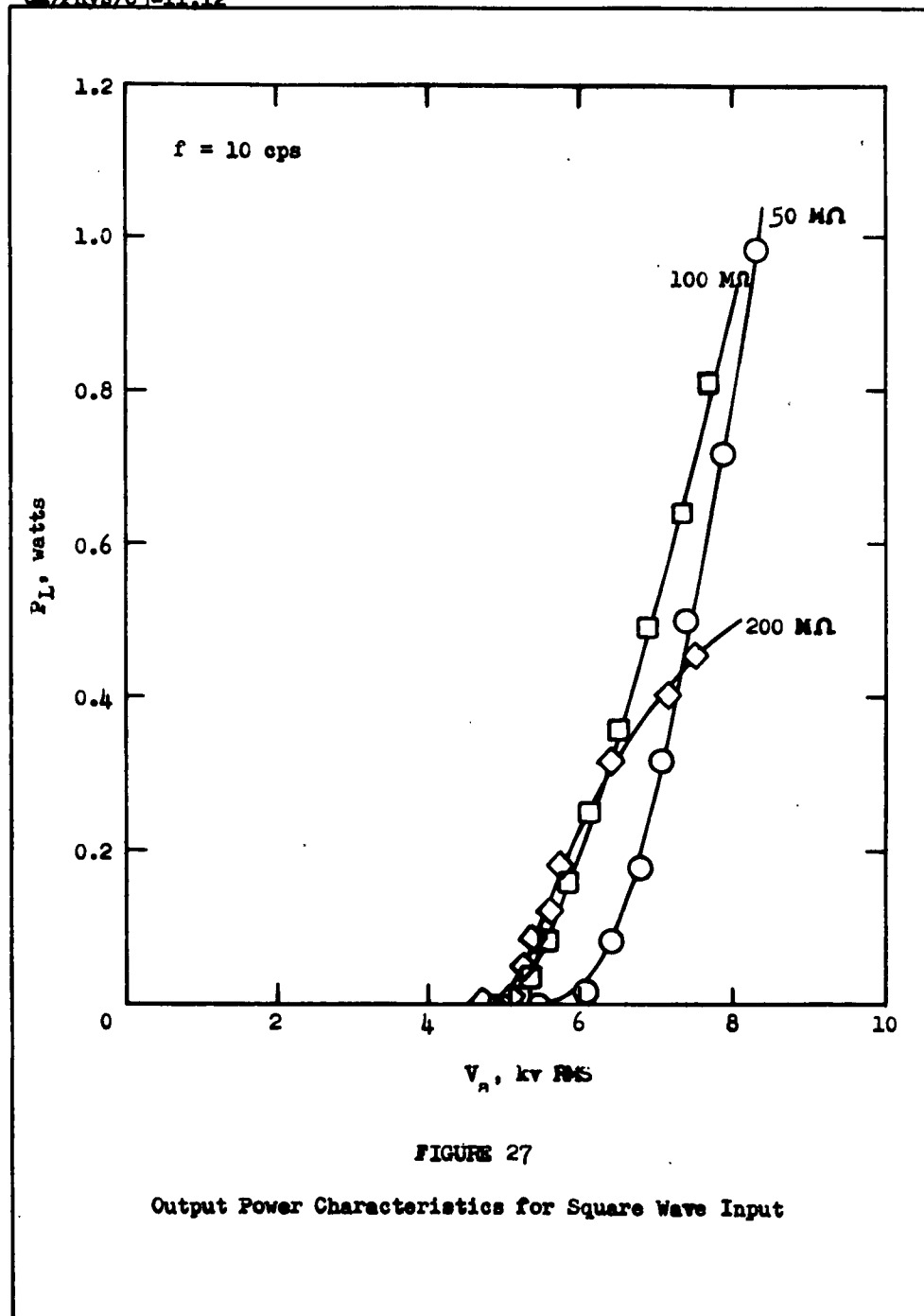


FIGURE 27

Output Power Characteristics for Square Wave Input

GA/Phys/63-11.12

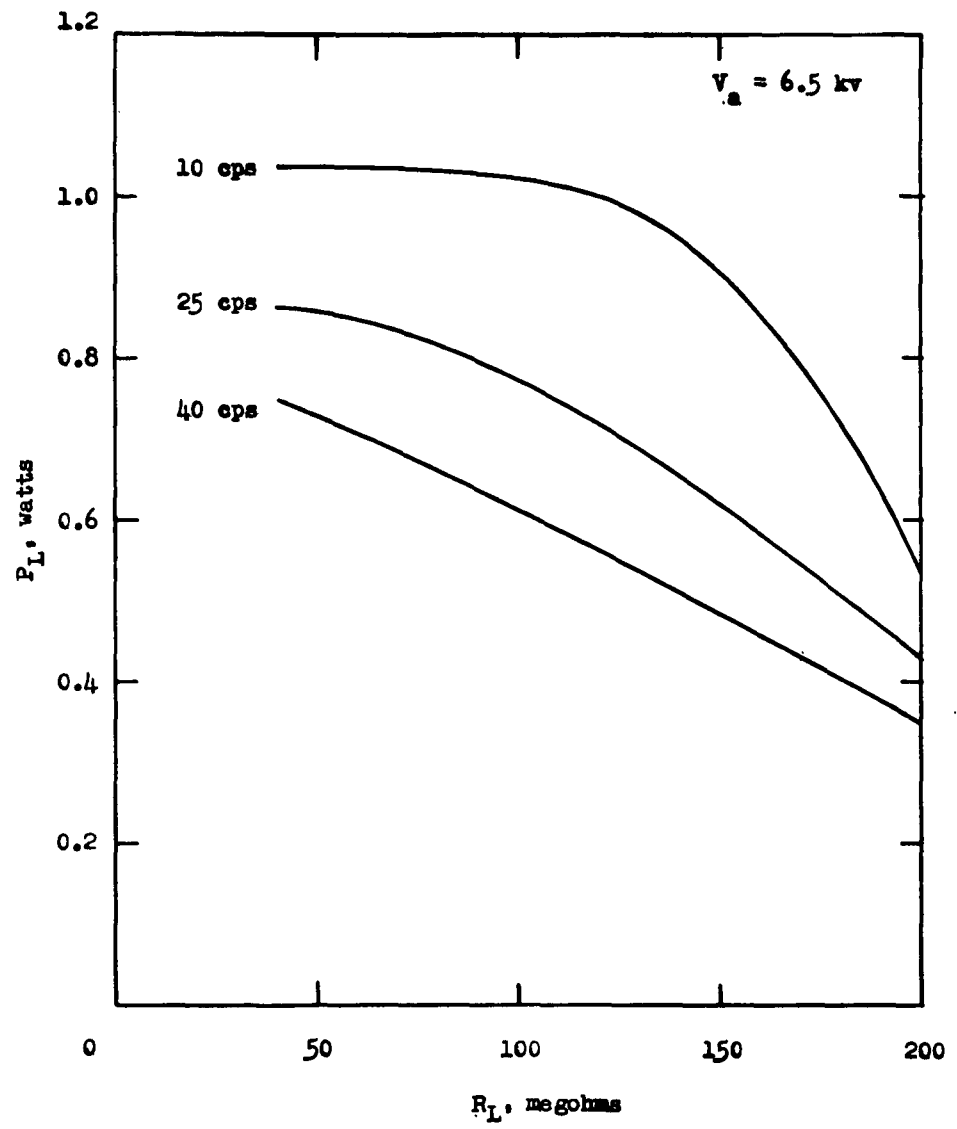


FIGURE 28

Effect of Load Resistance on Output Power for Sine Wave Input

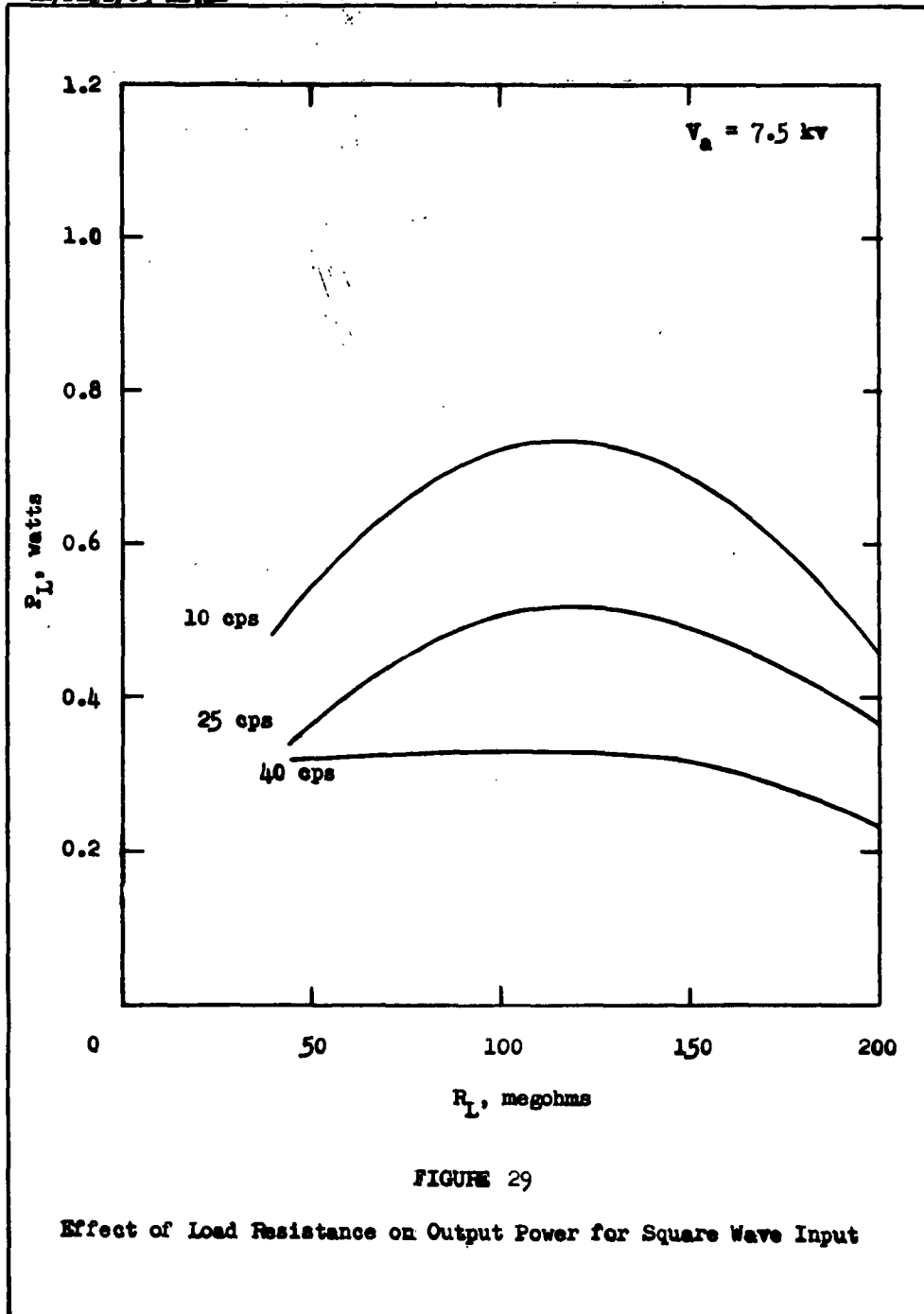


FIGURE 29

Effect of Load Resistance on Output Power for Square Wave Input

GA/Phys/63-11, 12

for some value of load resistance. This is exactly the case for the square wave curves. For an attractor voltage of 7.5 kv RMS, maximum output power occurs at all frequencies in the range of 100 to 150 megohms (see Figure 29). The sharpest maximum occurs on the 10 cps curve, while the broadest occurs on the 40 cps curve. This range of load resistance for maximum output power agrees very closely with Wheeler's results for DC maximum power. He obtained maximum output power for a load resistance of approximately 150 megohms (Ref 7:63).

The sine wave results did not conform to the expected pattern. None of the curves in Figure 28 shows a clear maximum. The curves for 10 and 25 cps tend to level off and perhaps go to a maximum at a value of  $R_L$  below 50 megohms, but the 40 cps curve shows no such tendency. It was decided to fix  $V_a$  at 6.5 kv RMS to keep it as close as possible to the  $V_a$  chosen for the square wave, but, had  $V_a$  been fixed at a lower value, the 10 and 25 cps curves would both have shown maxima for an  $R_L$  of approximately 100 megohms.

Effect of Frequency. For a given value of load resistance, the output voltage decreases as the frequency increases (Figures 28 and 29). Since the output power is a function of the square of the voltage, then it will also decrease with frequency. This was found to be true in all cases as is shown in Figures 28 and 29.

#### Comparison of Square and Sine Wave Powers

Output Power Characteristics. The sine wave input gives an output for a lower value of RMS input voltage than that of the square wave. This phenomenon occurs because the peak value of the sine wave voltage

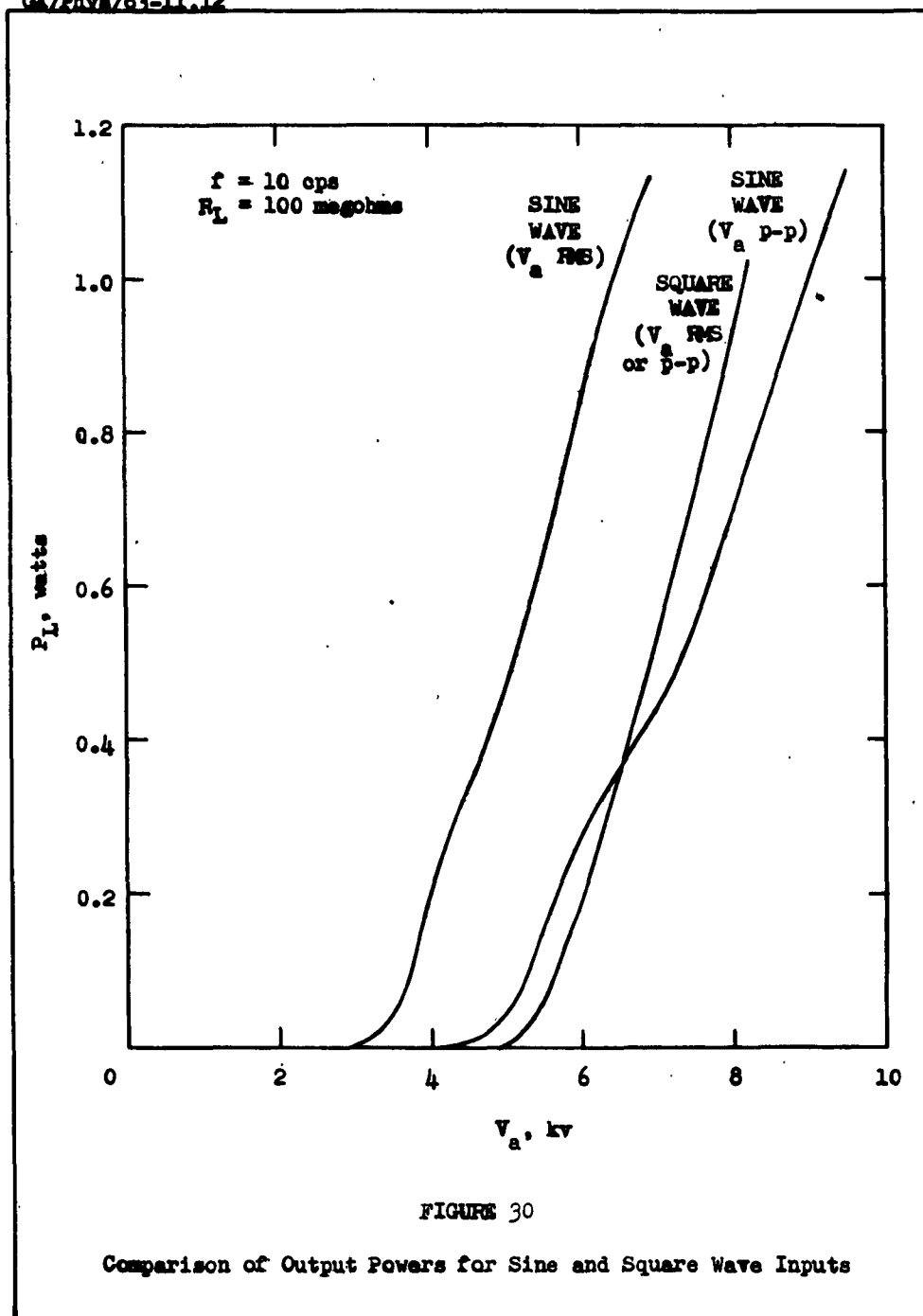


FIGURE 30

Comparison of Output Powers for Sine and Square Wave Inputs

GA/Phys/63-11, 12

reaches ionization potential while the RMS value of the voltage is still only about 70% of the ionization voltage. Thus the square wave will be only about 70% of its value for zero output when the sine wave reaches its zero output point. This is shown in Figure 30. The sine wave ( $V_a$  RMS) and the square wave curves rise with approximately the same slope, as would be expected since the input powers are nearly the same. However, the slope of the sine wave ( $V_a$  p-p) curve is less than the slope of the square wave curve. This occurs because, for any given increase in  $V_a$ , the increase in input power for the square wave will be considerably greater than the increase in input power for the sine wave ( $V_a$  p-p). Hence, for the square wave, the output will be higher and the slope of the curve greater. The sine wave ( $V_a$  p-p) curve in Figure 30 begins at a lower value of  $V_a$  than does the square wave curve. This is contrary to what was expected since, once the voltage reaches ionization potential, an output should be obtained. The two curves would, therefore, be expected to begin at the same value of  $V_a$  (p-p). The fact that they do not is probably the result of varying temperature and moisture conditions in the air flow since the runs were done on different days.

Input Power Ratio. Assuming pure sine wave and square wave voltage inputs, a ratio of sine wave power: square wave power for any given value of RMS voltage is given by the ratio of the areas under the curves of the square of the voltage. For the sine wave input, power is only being put in during that part of the cycle in which the voltage is above the ionization voltage. In this calculation a value of RMS voltage was chosen of 6.5 kv and the ionization potential of 5.5 kv was taken from

GA/Phys/63-11, 12

Figure 11. The integration of the squares of the voltage which is shown in Appendix E, yielded:

$$\frac{\text{Sine wave power in}}{\text{Square wave power in}} = 0.896$$

Output Power Ratio. From Figure 30 a ratio of observed output powers can be obtained for the same value of RMS input. Again picking 6.5 kv, we get,

$$\frac{\text{Sine wave power out}}{\text{Square wave power out}} = 4.71$$

Hence, for the same input power, the sine wave will produce  $\frac{4.71}{0.896} = 5.25$  times as much output power as the square wave.

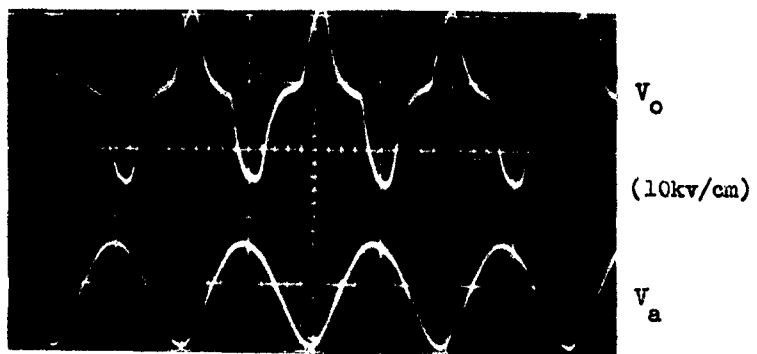
From the DC characteristics (Figure 11) a value of instantaneous current for each instantaneous voltage was obtained. The areas under the curves of the square of the output current for the two input wave shapes were computed by plotting the curves and adding squares (see Appendix E). The ratio of these two areas gave the output power ratio. By making allowance for the experimental spread in the DC characteristics, the following ratio was obtained:

$$\frac{\text{Sine wave power out}}{\text{Square wave power out}} = 9.22$$

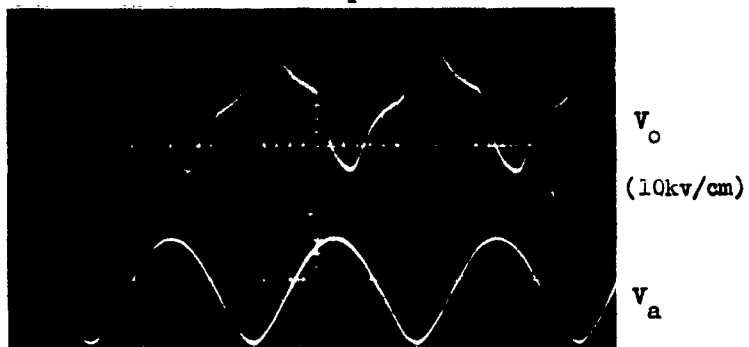
which is less than a factor of two above the observed value.

#### Output Wave Shape

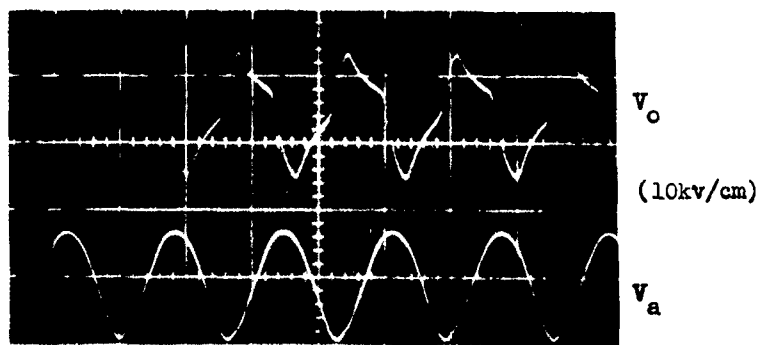
Examination of the photographs of output wave shapes (Figures 31 to 34) shows the distorting effect of the generator on the input wave shape. In the first place, there is the effect of the output capacitance. This shows up as an exponential rise superimposed on the increasing portion of the input voltage and an exponential decay super-



$f = 10$  cps



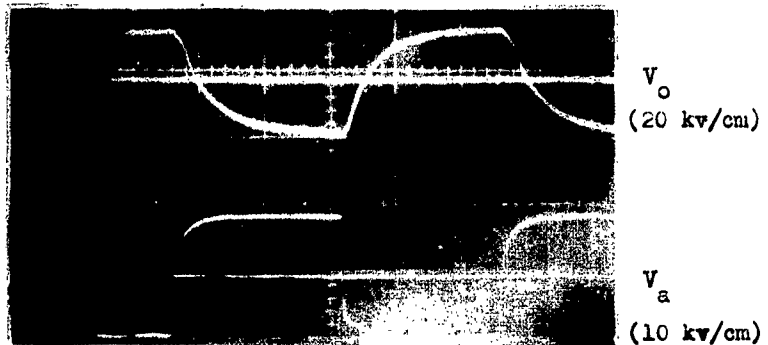
$f = 20$  cps



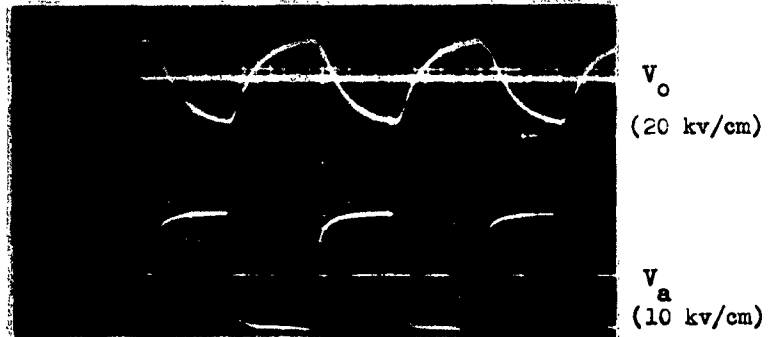
$f = 30$  cps

FIGURE 31

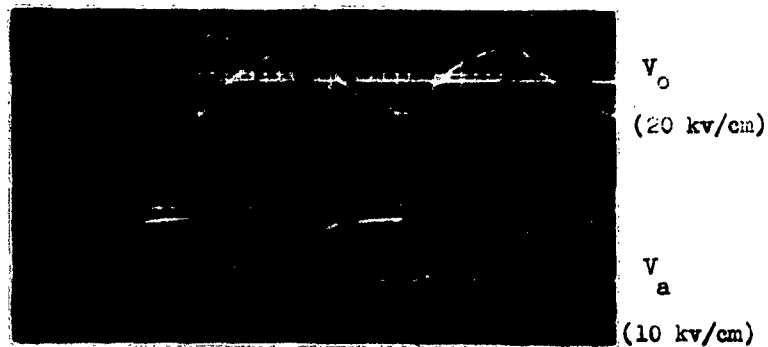
Oscilloscope Photographs Showing Change of Output  
Wave Shape with Frequency - Sine Wave Input  
( $V_a = 15.5$  kv p-p,  $R_L = 100$  megohms)



$f = 10$  cps



$f = 20$  cps



$f = 30$  cps

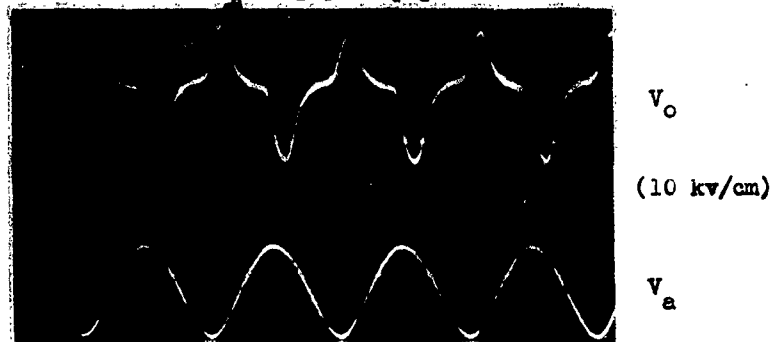
FIGURE 32

Oscilloscope Photographs Showing Change of Output  
Wave Shape with Frequency - Square Wave Input

( $V_a = 18.0$  kv p-p,  $R_L = 200$  megohms)



$V_a = 15.3$  kv p-p



$V_a = 14.3$  kv p-p



$V_a = 12.2$  kv p-p

FIGURE 33

Oscilloscope Photographs Showing Change of Output  
Wave Shape with Attractor Voltage - Sine Wave Input

( $f = 10$  cps,  $R_L = 100$  megohms)

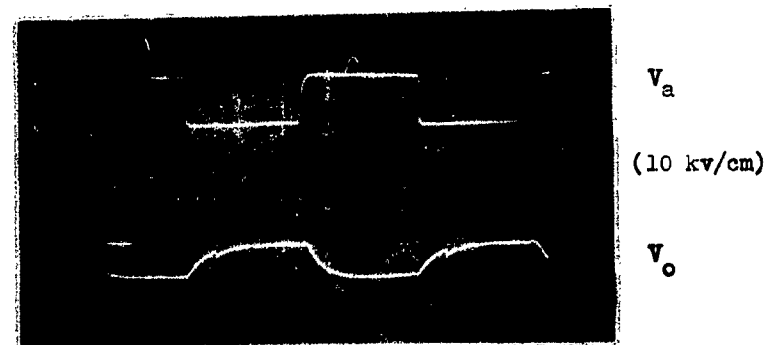
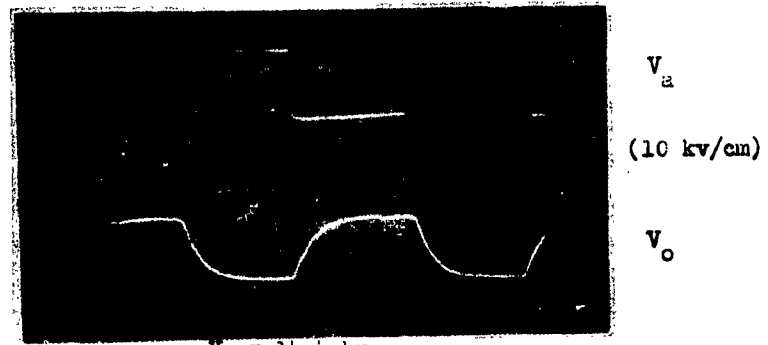
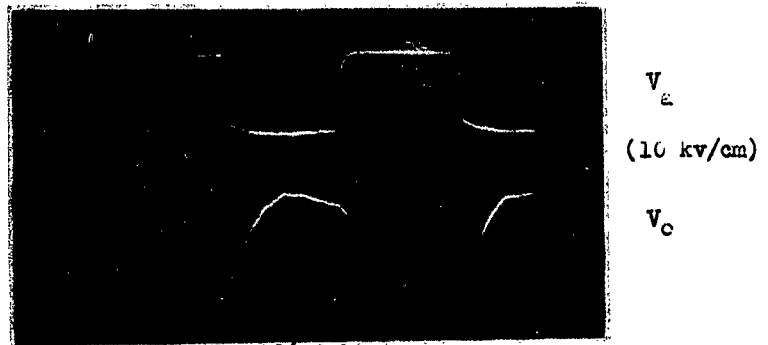


FIGURE 34

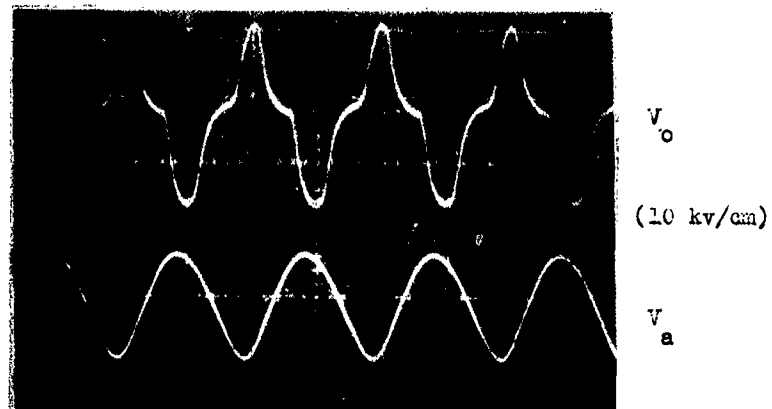
Oscilloscope Photographs Showing Change of Output  
Wave Shape with Attractor Voltage - Square Wave Input

( $f = 10 \text{ cps}$ ,  $R_1 = 100 \text{ megohms}$ )

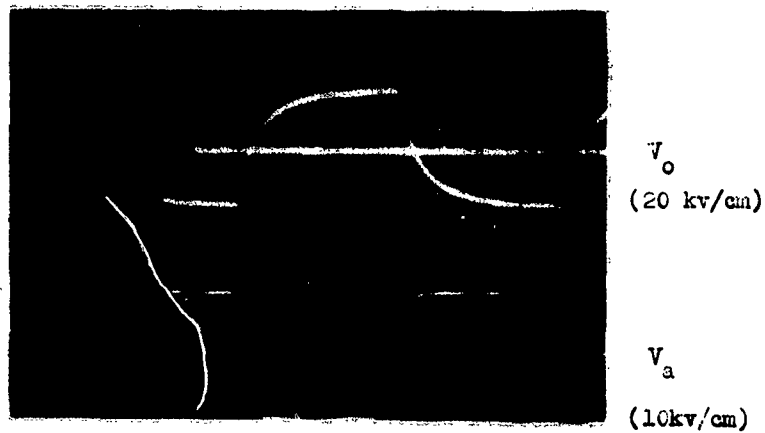
GA/Phys/63-11, 12

imposed on the decreasing portion of the input voltage. Since the effect of the capacitance increases with frequency, the distortion in the output wave shape would be expected to increase with frequency. Examination of Figures 31 and 32 shows this to be the case. In the second place, there is the effect of the direct current characteristics. When the instantaneous input voltage is less than the ionization potential, there is no output with the result that a flat portion occurs in the output wave form every time the input reverses polarity. This effect is insignificant with a square wave input. However, with a sine wave input where the instantaneous voltage is below the ionization potential over a considerable fraction of the cycle, it results in an output which resembles a series of peaks separated by intervals of zero output (Figure 33). The direct current characteristics also explain the asymmetrical wave shape at lower values of  $V_a$ . It can be seen from Figure 25 that the negative ion characteristic rises more steeply at a lower value of  $V_a$  than does the positive ion characteristic. Therefore, the negative half cycle of the output for an alternating input would be expected to develop more rapidly at low attractor voltages than the positive half cycle. Although this effect will occur for either the sine wave or the square wave input, it is most obvious with the sine wave (Figure 33).

Comparison of Actual and Predicted Sine Wave Outputs. The derivation of the predicted output wave shape for a given set of conditions was given in Chapter III. Figure 35(a) shows the actual output wave shape for the same set of conditions. Both the theoretical and experimental wave shapes are plotted for comparison in Figure 36. The shapes of the two waveforms correspond very closely but their magnitudes do not.



(a)  
Sine Wave Input ( $V_a = 17.1$  kv p-p)



(b)  
Square Wave Input ( $V_a = 18.4$  kv p-p)

FIGURE 35

Oscilloscope Photographs Showing Output Wave Shapes  
Used for Comparison with Predicted Output Wave Shapes

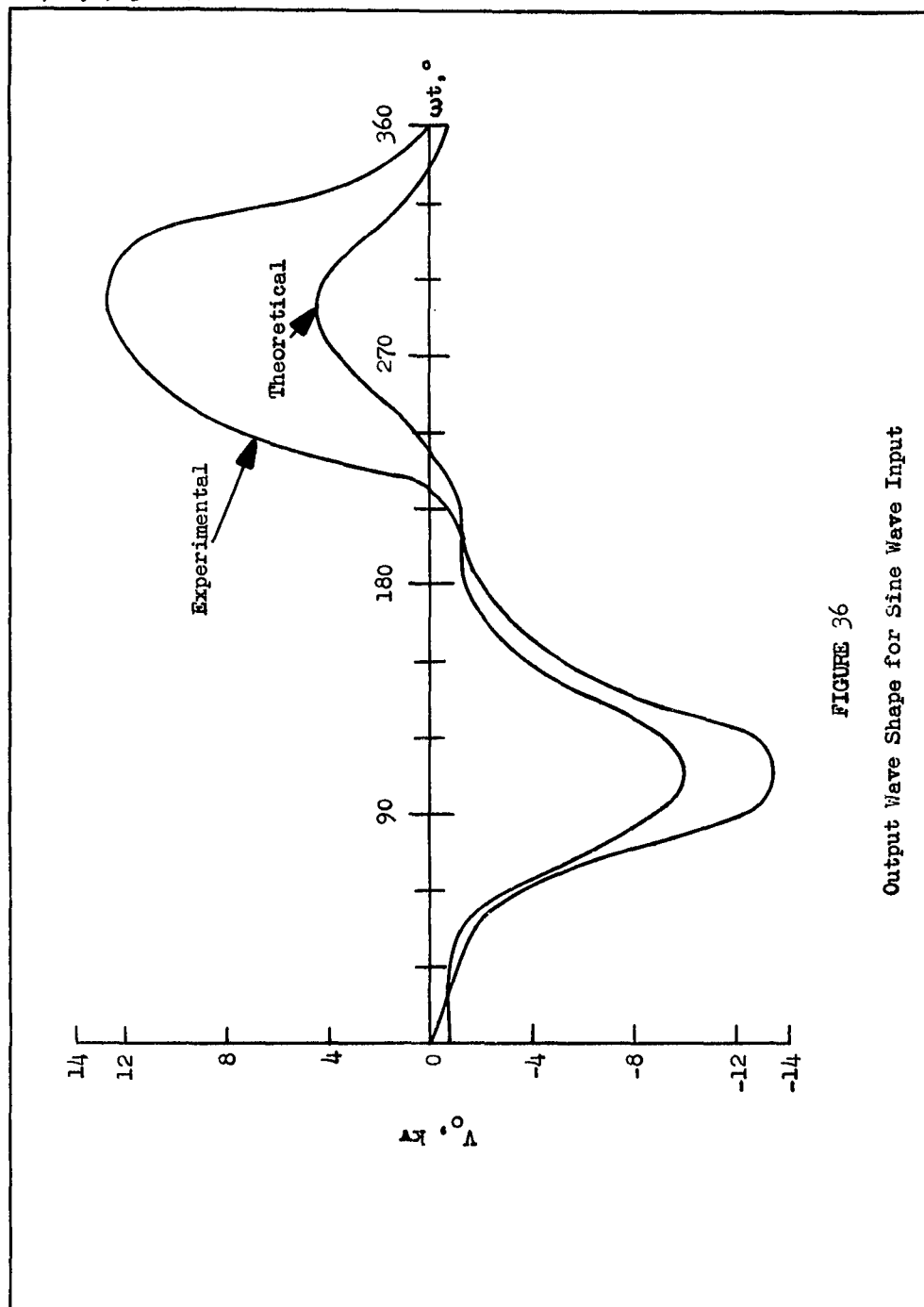


FIGURE 36  
Output Wave Shape for Sine Wave Input

GA/Phys/63-11, 12

For the negative half cycle, the theoretical peak was -10 kv while the actual peak was -13.5 kv. If we go to the average DC characteristics, (Figure 11) for  $V_a = 8.55$  kv, which was the peak input voltage, we find that  $I_o$  ranges from -110 to -170  $\mu$ a. Had a value of -170  $\mu$ a (instead of -130  $\mu$ a) been selected as the maximum  $I_o$  for the theoretical analysis, then a peak value of  $V_o$  of approximately -13.1 kv would have been found. For the positive half cycle, the theoretical peak was 4.5 kv and the actual peak was 12.5 kv. Applying the same argument as before, for  $V_a = -8.55$  kv,  $I_o$  ranges from 25 to 115  $\mu$ a. Had the value of 115  $\mu$ a, instead of 38  $\mu$ a, been used to predict  $V_o$ , a peak value of  $V_o$  of approximately 13.6 kv would have been found. These facts represent sufficient justification to attribute the large discrepancy in the theoretical and experimental peak output voltage to the accuracy of the average DC characteristics.

The difference between the positive and negative ion DC characteristics then explains the fact that the positive theoretical peak (or the area under the positive half cycle of the curve) is less than the negative peak (or the area under the negative half cycle of the curve). This is equivalent to a negative DC component in the output voltage.

Comparison of Actual and Predicted Square Wave Outputs. The derivation of the predicted output wave shape for a given set of conditions was given in Chapter III. Figure 35(b) shows the actual output wave shape for the same set of conditions. Both the theoretical and experimental wave shapes are plotted for comparison in Figure 37. As was the case with the comparison of the sine wave outputs, the shapes of the two waveforms correspond quite closely but their magnitudes do not.

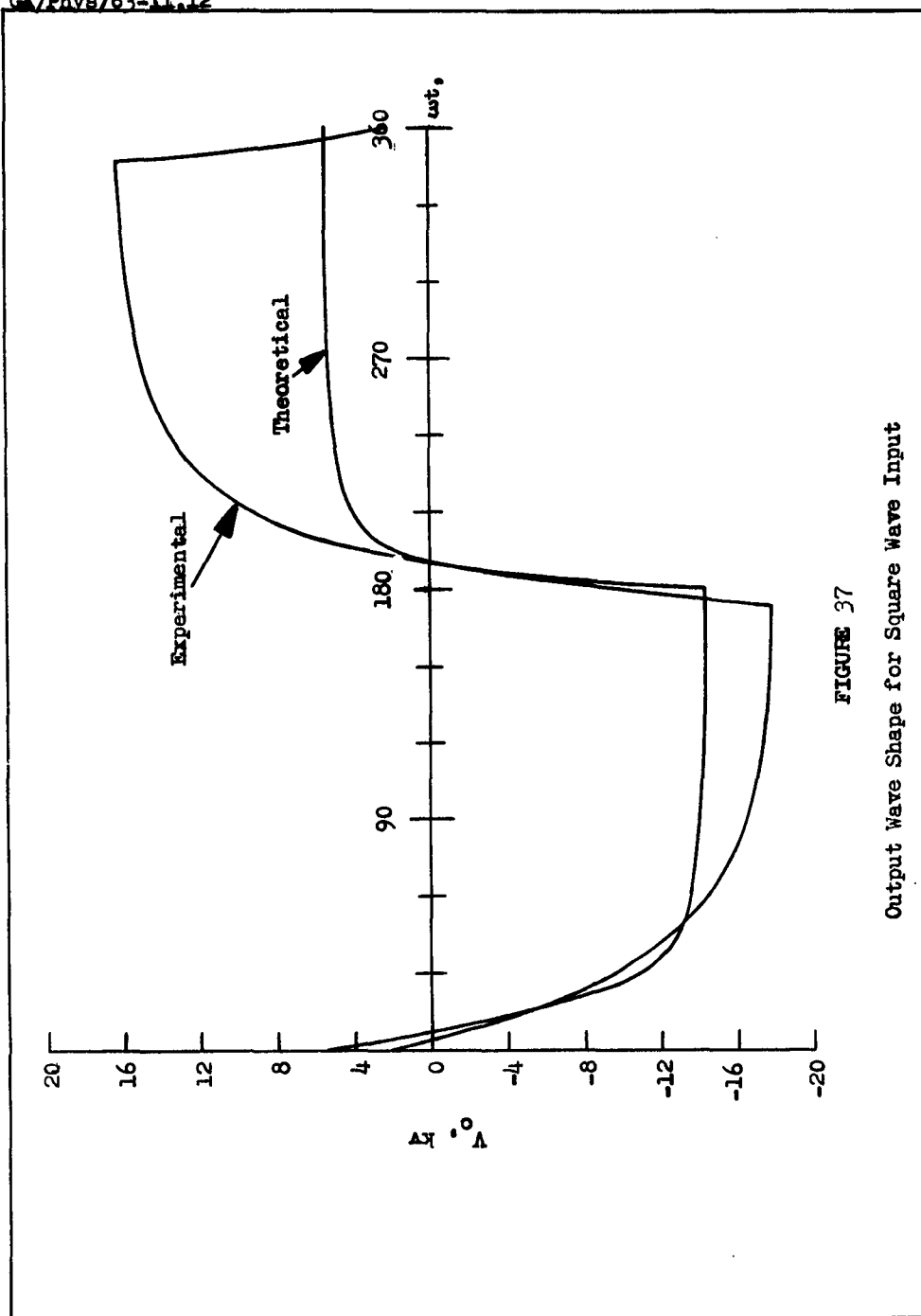


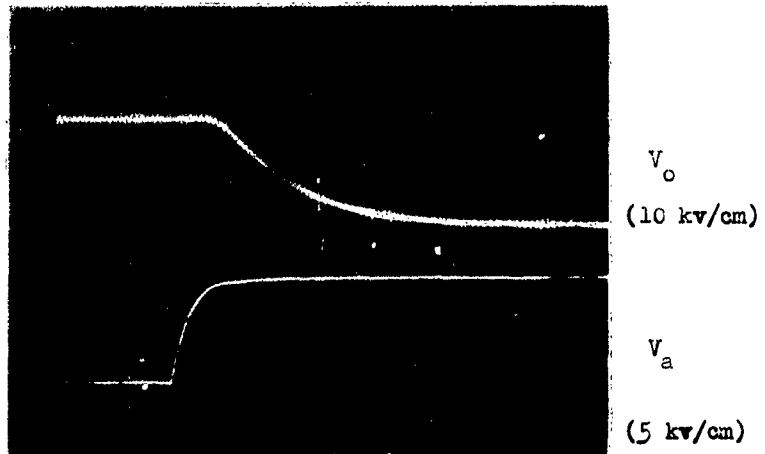
FIGURE 37

Output Wave Shape for Square Wave Input

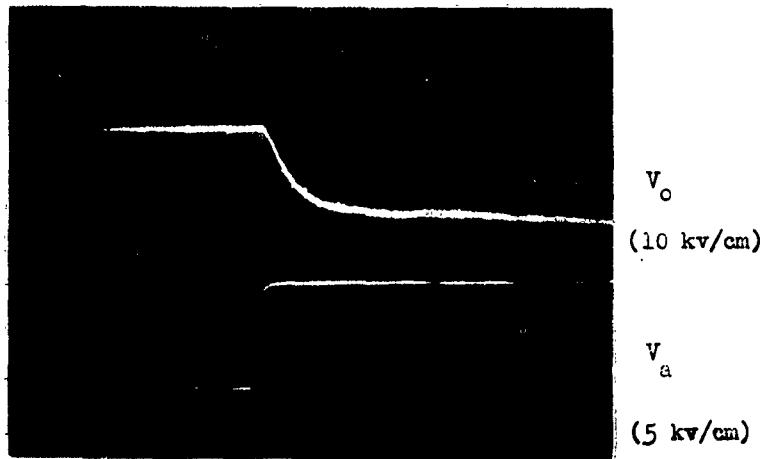
GA/Phys/63-11, 12

Considering the negative half cycle as before, the theoretical maximum was -14 kv and the actual maximum was -17.5 kv. For a peak input voltage of 9.2 kv, from the average DC characteristic (Figure 11), the highest  $I_0$  is -180  $\mu$ a. If this figure had been used instead of -143  $\mu$ a in the analysis, the maximum value of  $V_0$  would have been -17.6 kv. Now, for the positive half cycle, the theoretical maximum was 5.5 kv as opposed to the actual maximum of 16 kv. Once again, from the average DC characteristic for  $V_a = -9.2$  kv, the highest  $I_0$  is 130  $\mu$ a. If this value had been used instead of 54  $\mu$ a, the predicted maximum  $V_0$  would be 13.2 kv, slightly lower than the value actually obtained. Once again, the discrepancy between the two curves can be attributed to the spread of the DC data and the accuracy of the average DC characteristic.

Comparison of Actual and Predicted Step Function Outputs. The derivation of the predicted output wave shape for a given set of conditions was given in Chapter III. Figure 38 shows the actual output wave shape for the same set of conditions. The theoretical and experimental (data taken from Figure 38(a)) wave shapes are plotted for comparison in Figure 39. The two are seen to correspond very closely both in shape and magnitude. The reason why there is very little discrepancy between the theoretical curve and the experimental curve lies in the fact that a different method was used in the analysis. The prediction of the output voltages for the square wave and the sine wave was based on the average DC characteristic, but the prediction of the output voltage for the step input was not. It was based on the experimental value of  $V_{0\max} = -16.2$  kv. If  $V_{a\max} = 7.8$  kv had been the criterion, then, from the



(a)  
 $t = 5 \text{ msec/cm}$



(b)  
 $t = 20 \text{ msec/cm}$

FIGURE 38

Oscilloscope Photographs

Step Input ( $V_{o_{\max}} = 16.2 \text{ kv}$ )

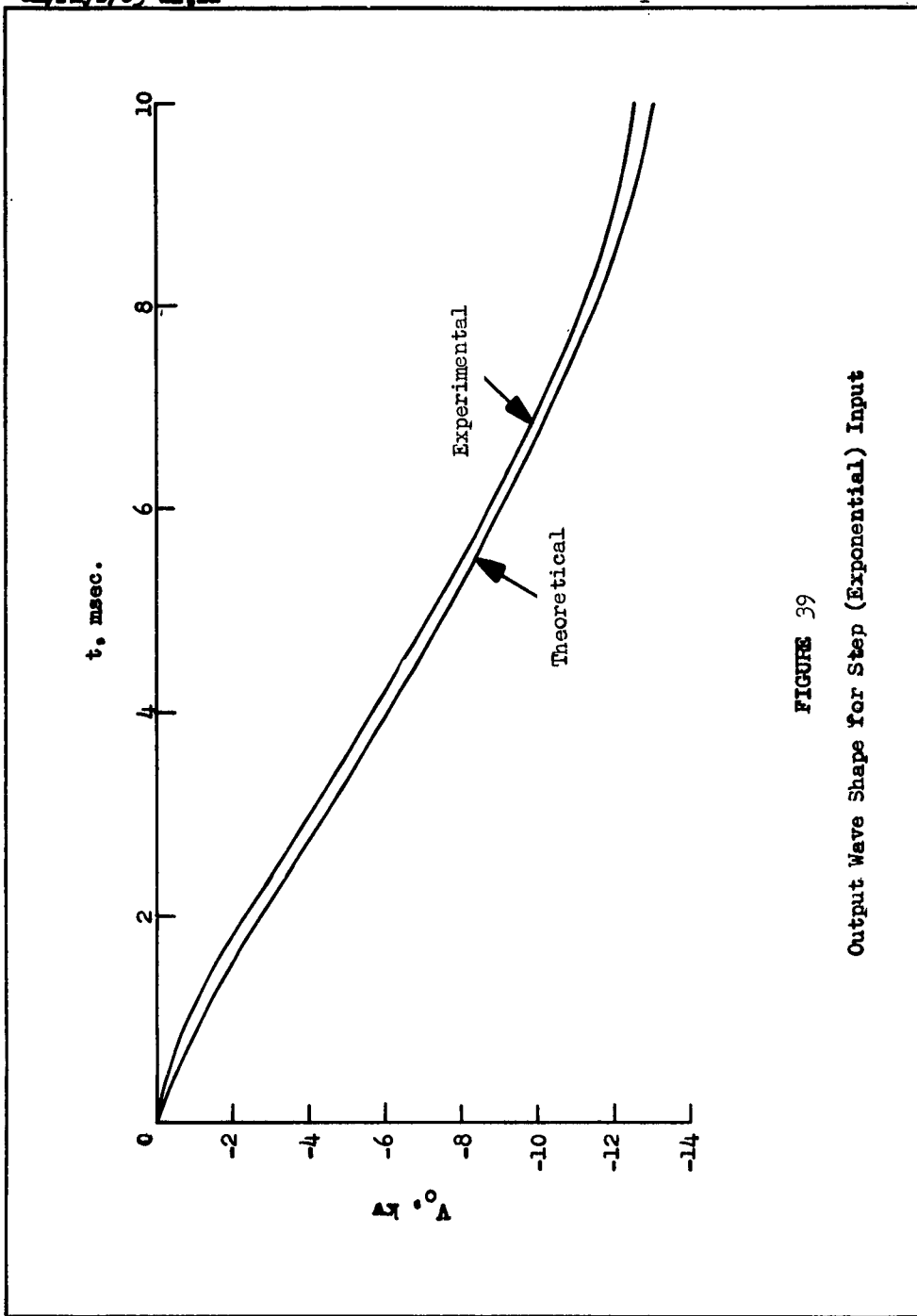


FIGURE 39  
Output Wave Shape For Step (Exponential) Input

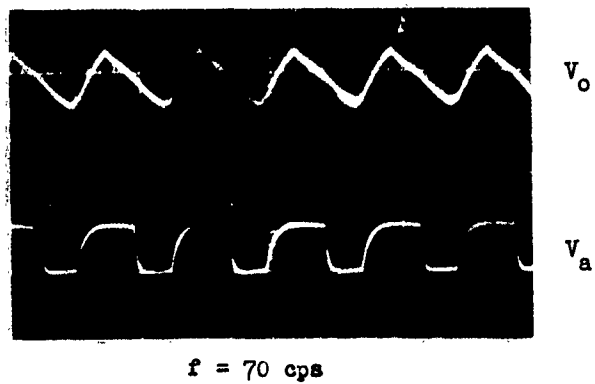
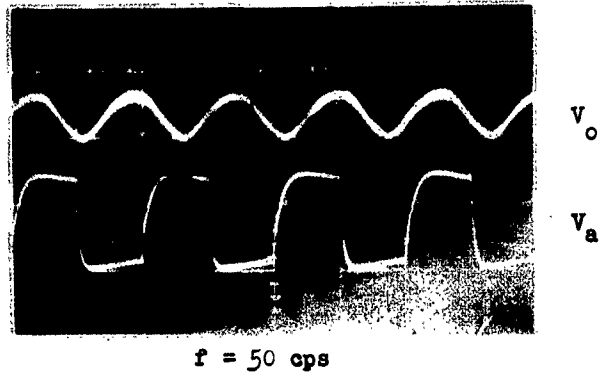


FIGURE 40

Oscilloscope Photographs Showing Unusual  
Output Wave Shapes for Square Wave Input

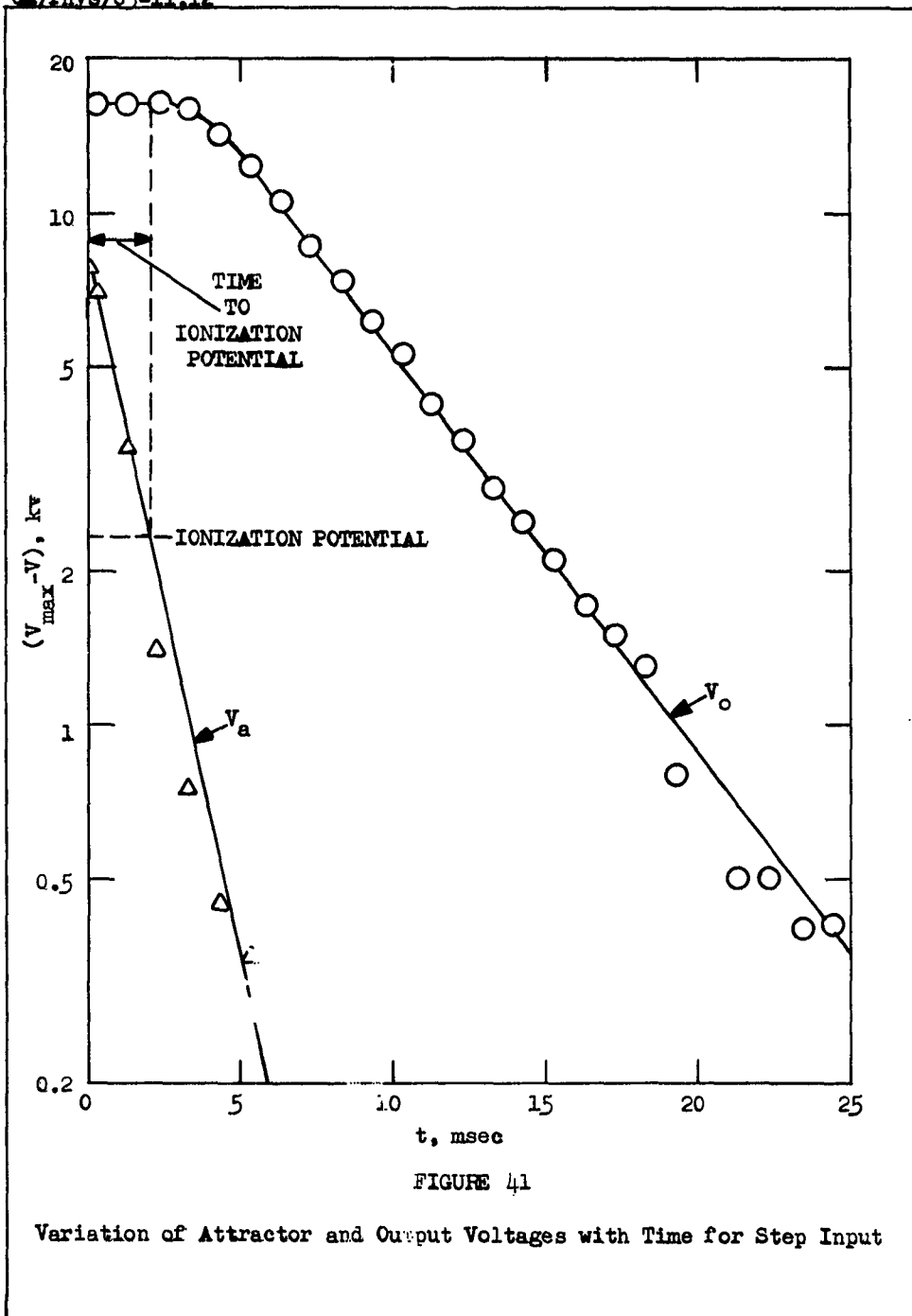
GA/Phys/63-11, 12

average DC characteristic (Figure 11),  $V_{o_{max}}$  would have been -12 kv or, for the upper limit of the DC characteristic, -15.5 kv. The theoretical curve appeared to build up more quickly than the experimental. This effect is equivalent to a time lag in the experimental wave shape which is fully discussed in the next section.

Unusual Wave Shapes. Throughout the experimental phase of the investigation unusual output wave shapes would occasionally occur. Output wave shapes for the sine wave input invariably showed a great deal of distortion and typical wave shapes are shown in Figures 31, 33, and 35. Two output wave shapes which are typical of a RC circuit for a square wave input are shown in Figure 40. At 50cps, the output is seen to resemble a sine wave, while at 70 cps it is seen to resemble a triangular wave. These wave shapes have little significance in this study and are pointed out as a matter of interest only.

#### Output Voltage for a Step Input

Determination of Input and Output Time Constants and Output Capacitance. The output voltage data (Table IV) for a step input was gotten from the oscilloscope photograph shown in Figure 38 (a). The natural logarithm of  $(V_{o_{max}} - V_o)$  and the natural logarithm of  $(V_{a_{max}} - V_a)$  were both plotted against  $t$ . These curves are shown in Figure 41. The slope of the straight line portion of the curve is equal to  $-\frac{1}{RC}$ . Therefore we get  $R_1C_1 = 1.57$  msec from the input voltage curve, where  $R_1C_1$  represents the generator input time constant, and  $R_LC_o = 5.56$  msec from the output voltage curve. Then, since the load resistance  $R_L = 100$  megohms, the output capacitance,  $C_o = 55.6$   $\mu$ pf.



GA/Phys/63-11, 12

The output capacitance as measured with a Q meter was found to be 69.1  $\mu\text{pf}$ . This measurement was made at several kilocycles and with the generator not operating. The value of 55.6  $\mu\text{pf}$  was considered to be the true dynamic output capacitance of the generator and consequently is used in all calculations throughout this report.

Effect of Exponential Input. Due to the input capacitance of the generator, the attractor voltage was not a true step function, but exponential as shown by the straight line of the  $(V_{a\text{max}}-V_a)$  curve of Figure 41. This resulted in the rounded portion of the  $(V_{o\text{max}}-V_o)$  curve which was calculated theoretically in the step input analysis of Chapter III and is replotted as  $\log (V_{o\text{max}}-V_o)$  versus  $t$  and compared with the exponential curve in Figure 42. A consistent shift to the right is evident in the experimental curve when compared with the theoretical. Since the theoretical analysis considered only the effect of an exponential input, the shift in the curve could represent a time lag due to ion current build-up, ion diffusion in the transport region, and ion transit time. A more detailed analysis is not justified since the experimental results are well within the experimental error. Further, the effect of the non-linearity of the direct current characteristics was ignored in the theoretical analysis and this would undoubtedly contribute to the difference between the curves.

Time to Reach Ionization Potential. From the DC characteristic (Figure 11), a value of ionization potential was chosen. This value was then plotted on Figure 41 and a horizontal line drawn to intersect the input voltage curve  $V_a$ . The intersection of these two lines represents the point where ionization occurs, and the distance along the

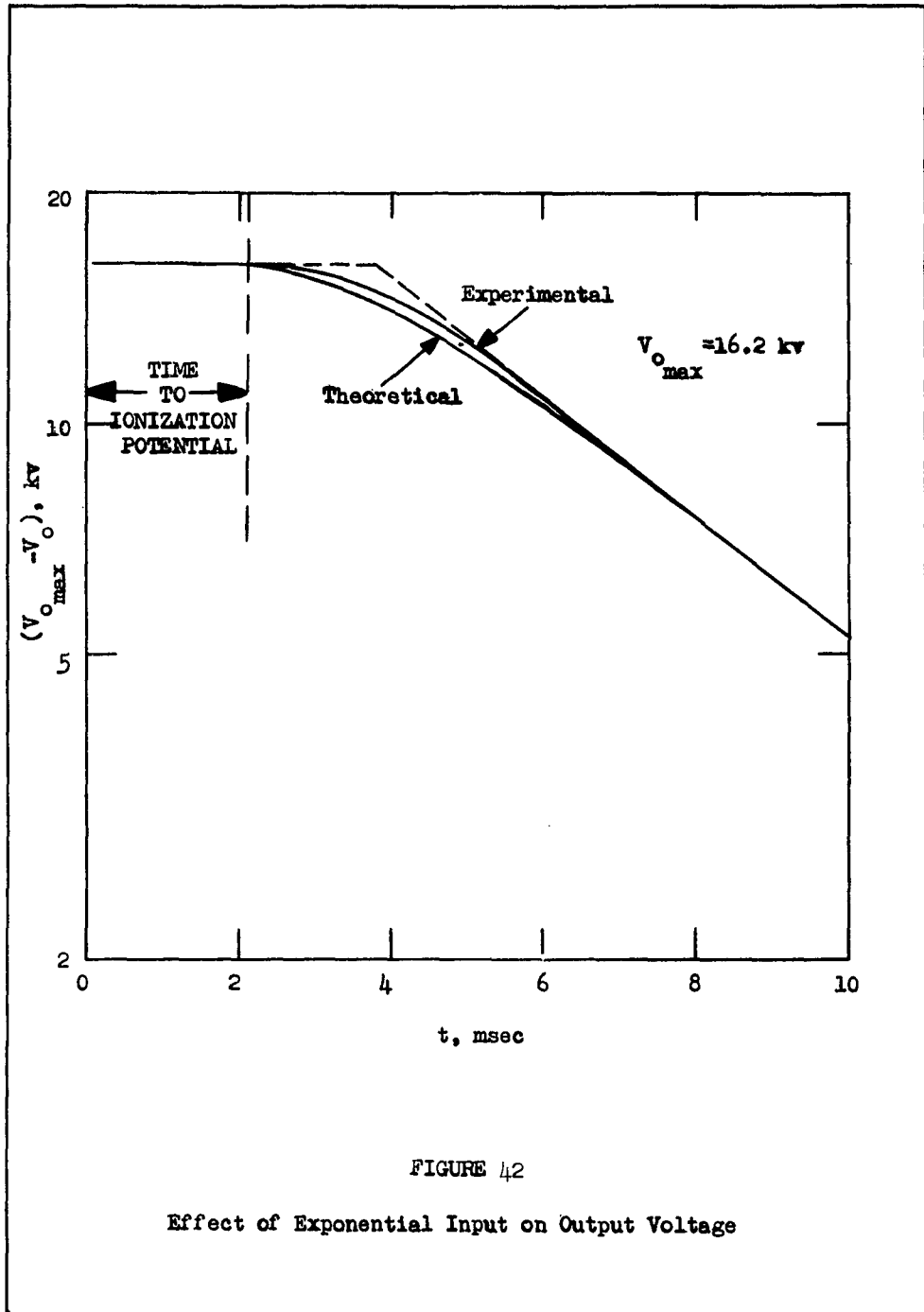


FIGURE 42

Effect of Exponential Input on Output Voltage

GA/Phys/63-11, 12

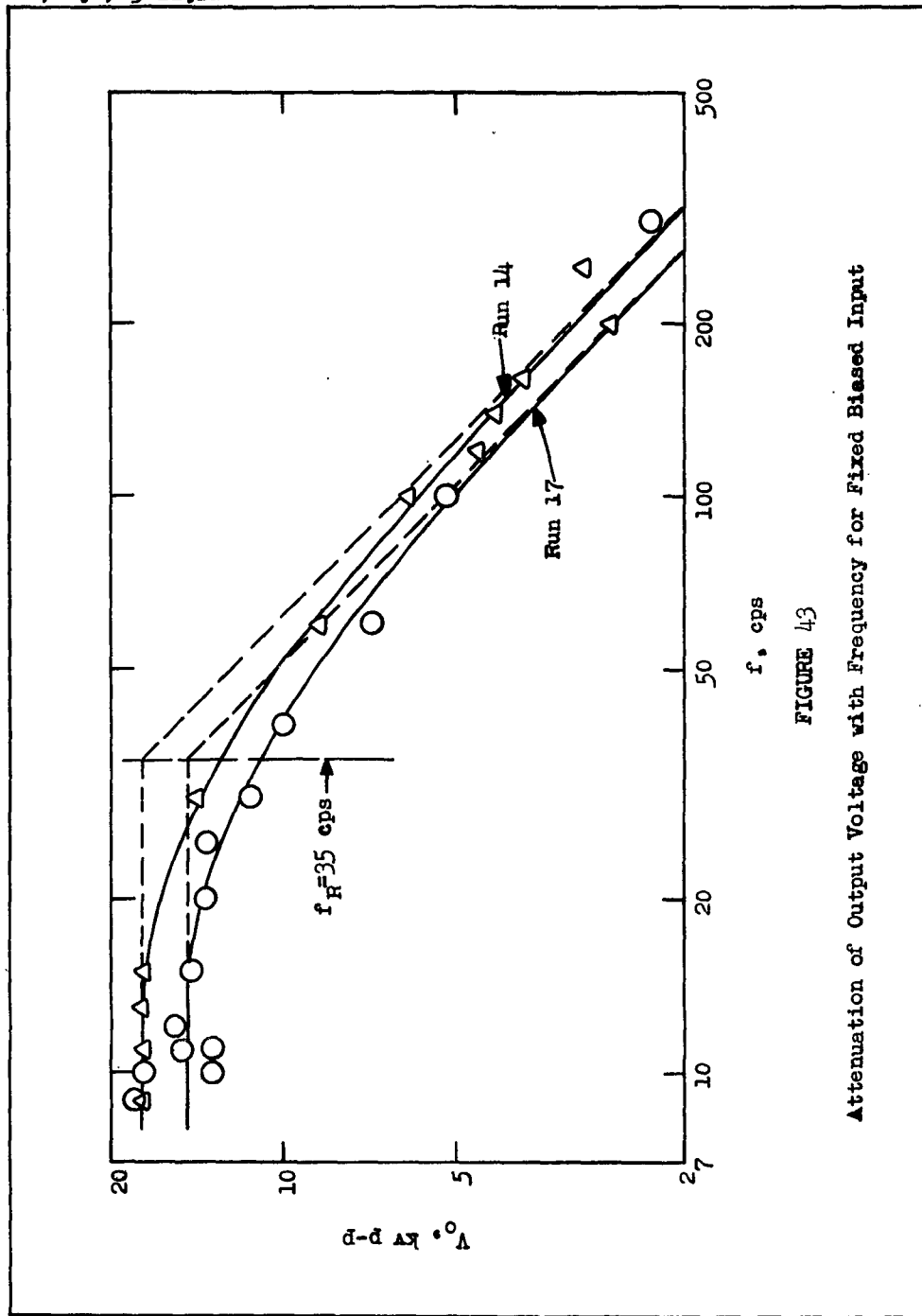
abscissa to this point gives the time for the attractor voltage to reach ionization potential. When the theoretical curve was drawn on Figure 42, its straight line portion was superimposed as closely as possible on the straight line portion of the experimental curve. The break in the theoretical curve is seen to occur at 2.1 msec. This is the same as the time to ionization which resulted from the experimentally selected ionization potential.

Transit Time. Since the transit time is approximately 0.06 msec (as shown in Appendix C), it will produce a negligible effect on the experimental curve. Such a small time interval cannot be observed on Figure 42 and hence its effects must be considered within other delaying effects, experimental errors, and errors due to the assumptions.

#### Output Voltage for Biased Alternating Input

Determination of Output Capacitance and Roll-off Frequency. The plot of output voltage versus frequency (Figure 43) shows a constant output up to a certain frequency and then a decrease in output above that frequency. This is similar to the plot for a RC filter circuit. The theoretical decrease for a RC circuit is 6 db per octave which can be represented by a straight line drawn at  $45^\circ$  on a log-log plot. This line intersects the extension of the horizontal portion of the output voltage curve at the roll-off frequency for the circuit. From Figure 43, the roll-off frequency is seen to be 35 cps for the two runs plotted. Since the roll-off frequency,  $f_R$ , is given by

$$f_R = \frac{1}{2\pi R_1 C_0}$$



$f$ , cps

FIGURE 43

Attenuation of Output Voltage with Frequency for Fixed Biased Input

GA/Phys/63-11, 12

then the output capacitance, for a load resistance  $R_L = 100$  megohms, is

$$C_0 = \frac{1}{2\pi R_L f_R} = \frac{1}{2\pi \times 100 \times 10^6 \times 35} = 45.5 \mu\mu\text{f}$$

This value of output capacitance is 10.1  $\mu\mu\text{f}$  or 18% lower than the value obtained from the step input data.

Comparison of Frequency and Wave Shape with Unbiased Input. The output wave shape was much closer to the input wave shape for the biased case than for the unbiased case. This was expected since, in the unbiased case, the input voltage must build up to ionization potential before any output is possible, while, in the biased case, there is continuous ionization and hence all changes in the input are immediately reflected in the output. It is therefore possible to operate the generator at a higher frequency (say a few hundred cycles) and still obtain a reasonable wave shape (Figure 44). The limiting factor is the output capacitance. The photographs of Figure 45 show a comparison of biased and unbiased operation at a frequency of 10 cps. It must be remembered, of course, that when operating biased the output does not alternate about ground potential. To obtain only the alternating output a blocking capacitor could be used in the output circuit.

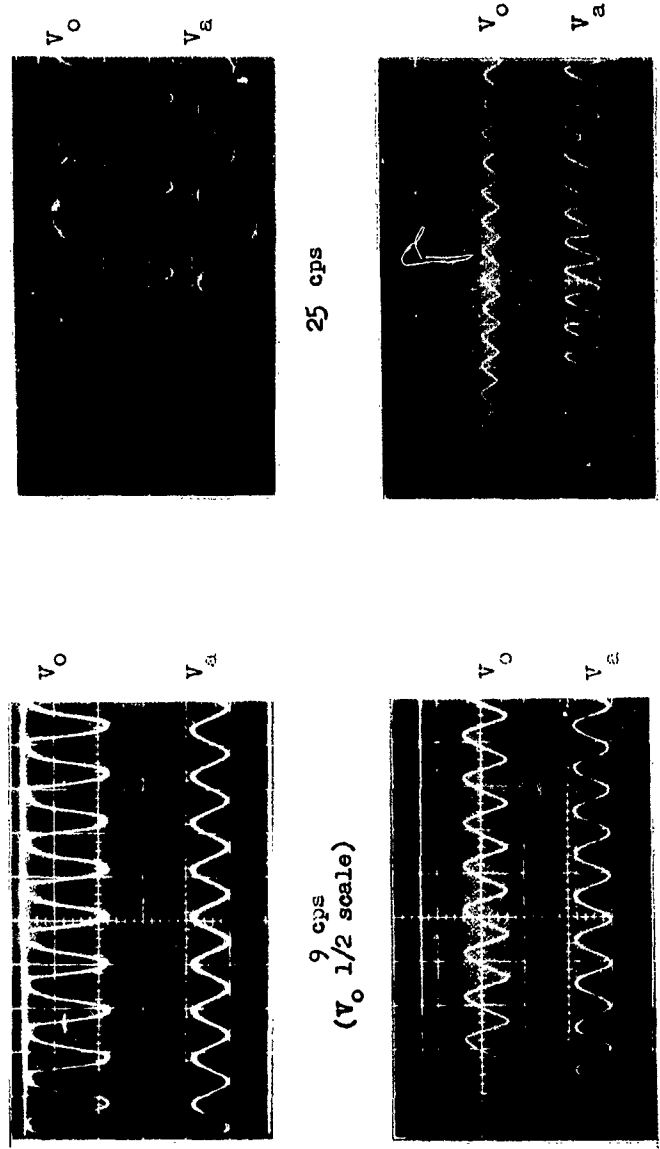
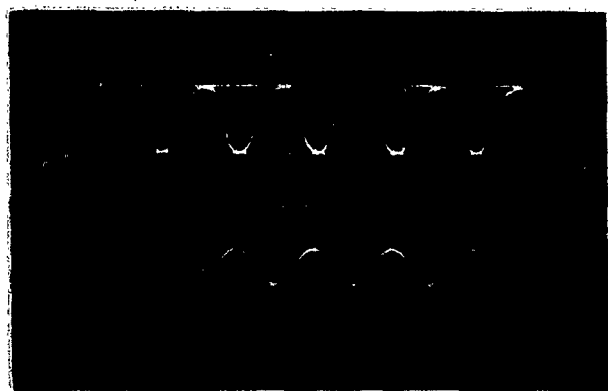


FIGURE 44

Oscilloscope Photographs Showing Variation of Output Wave Shape with Frequency for Biased Sine Wave Input



Unbiased ( $f = 10 \text{ cps}$ )



Biased ( $f = 10 \text{ cps}$ )

FIGURE 45

Comparison of Output Wave Shapes for  
Biased and Unbiased Sine wave Inputs

## VI. Conclusions

A number of conclusions which may be drawn from the results of this study are listed below. The first seven are valid for any EHD generator, while the remaining two apply only to the generator investigated.

1. AC power generation with an EHD generator is quite feasible.

The output power levels, however, are lower than those which can be obtained from the same generator with a DC input.

2. The frequency for maximum output power from an EHD generator is zero, i.e. direct current. As the frequency increases from zero the output power drops off. The optimum frequency for any EHD generator would depend on how the output was to be used. If the output was to be transformed before it was used then the output power would have to be compromised in favor of a higher frequency to ensure good transformation.
3. For a given RMS attractor voltage, a sine wave input gives a greater output power than a square wave input. If, however, the same peak-to-peak input voltages are used then the square wave gives the greater output power.
4. The quasi-static assumption is valid for low operating frequencies. This was verified by the good results obtained in the prediction of output voltages.
5. Self-sustained oscillation of an EHD generator is theoretically possible and with a suitably designed generator might be practical. Since the auxiliary equipment requirements were so stringent for the feed back circuit of the EHD generator used, self-sustained oscillation was not practical in this case.

6. Maximum output power is obtained for some specific value of load resistance when the EHD generator is operated with an alternating input. For the EHD generator used, the optimum load was found to be between 100 and 150 megohms. This is in good agreement with the results found by Wheeler (Ref 7:52) for the DC case.
7. AC power generation with a biased alternating input is feasible and, in fact, has some advantages over unbiased operation. The output wave shape closely resembles the input wave shape and the attenuation and distortion of the output with frequency is much less in the biased case. These factors might well make voltage amplification at low frequencies practical.
8. The assumption that the output capacitance  $C_0$  was the only significant effect other than the ionization potential which caused distortion of the output wave shape was justified. The good results obtained from the use of the differential equation with the step input verified this. It was further verified in the biased runs where the output was found to be rapidly attenuated over 35 cps. If the output capacitance had not existed, a maximum frequency of around 8 kc would have been expected.
9. The generator used in this study had three major shortcomings which limited the depth of experimentation possible. First, voltage breakdown within the generator forced premature cut-off on many of the runs, second, the output capacitance of the generator imposed a low maximum frequency of operation, and third, day to day variations in the generator and air supply character-

GA/Phys/63-11, 12

ized by the wide spread in the DC characteristic data made  
it virtually impossible to relate the performance of the  
generator to a standard condition.

VII. Recommendations

The field of AC power generation by electro-fluid dynamic energy conversion is worthy of further study. Specific recommendations arising from the investigation are as follows:

1. Although the generator used in this study would have very little value in further investigations with an alternating input, it would be well worthwhile to design and build a new generator for this purpose. In addition to improvements in aerodynamic efficiency, ion generation and collection, and voltage breakdown elimination an attempt should be made to minimize the output capacitance. By proper design of the collector it should be feasible to reduce the output capacitance by a factor of six to ten.
2. Since variations in flow conditions strongly influence the electrical performance of an EHD generator, the possibility of closely regulating the temperature and moisture content of the air supply should be considered.
3. Power generation with a biased alternating input should be investigated. In addition to an expected improvement in output wave shape and frequency response, high output levels may be possible because of the continuous ion current flow. Also, the feasibility of separating the AC and DC components of the output so that both may be separately utilized should be determined.

GA/Phys/63-11, 12

4. Self-sustained oscillation of an EHD generator should be examined. For a generator, designed specifically for AC operation, the additional circuitry required for oscillation would not be as unique as that required for the generator used in this study.

Bibliography

1. Gourdine, M. C. Power Generation by Means of the "Electric Wind". Jet Propulsion Laboratory Technical Report 32-6. Pasadena, California: California Institute of Technology, 1960.
2. Luitzen, T. N. Ion Production and Flow in an Electrohydrodynamic Generator. Unpublished thesis. Wright-Patterson Air Force Base, Ohio: Air Force Institute of Technology, 1962.
3. Lawson, M., H. Von Ohain, and F. Wattendorf. Performance Potentialities of Direct Energy Conversion Processes Between Electrostatic and Fluid Dynamic Energy. Aeronautical Research Laboratory Technical Report 178. Wright-Patterson Air Force Base, Ohio: Aeronautical Research Laboratory, 1961.
4. Hoakes, G. R., Electrical Fundamentals, (Volume I). London: H. M. Stationery Office, 1956.
5. Smith, J. M., Theoretical Study of the Electrohydrodynamic Generator. Space Sciences Laboratory Technical Report R61SD192. King of Prussia, Pennsylvania: General Electric Company, 1961.
6. Werner, F. D., and R. L. Geronimo. Investigation of a Corona Discharge for Measurements in Air Flow. Rosemount Aeronautical Laboratories Research Report 84. Minneapolis, Minnesota; University of Minnesota, 1952.
7. Wheeler, H. P., Jr., The Volt-Ampere Characteristics of an Electrohydrodynamic Generator. Unpublished thesis. Wright-Patterson Air Force Base, Ohio: Air Force Institute of Technology, 1962.

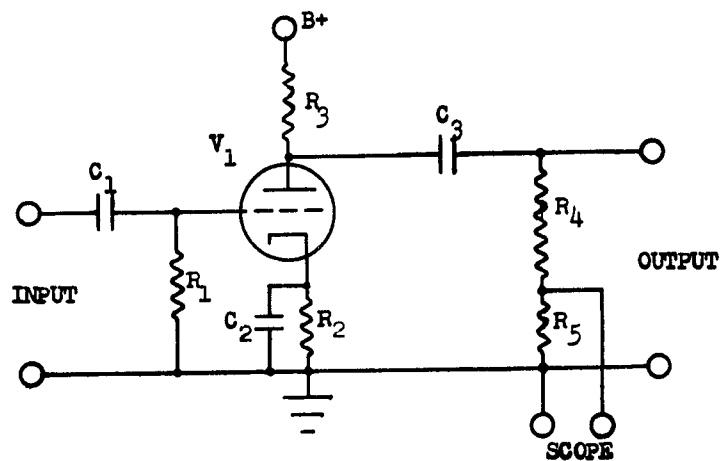
Appendix A

High-Voltage Alternating Power Source Specifications and Design

To carry out this study, an alternating power source was required that would produce sine and square wave outputs of 0 to 20,000 v p-p at frequencies from DC to 100 cps. Several designs were investigated which included staged amplification, multivibration, crow-bar switching, R-F pulsing and rectification, and mechanical commutation. The design which was chosen was a single-stage, high-gain amplifier powered by a 30 kv, 1 ma DC power supply and driven by low voltage sine and square wave signal generators. The final configuration of this amplifier as designed and built by the authors is shown in the schematic of Figure A 1, and the photographs of Figure A 2.

The completed power source gave square and sine wave outputs of 0 to 20,000 v p-p. The voltage gain was of the order of 2000. The frequency range over which the distortion in the output wave shape was low was 10 to 100 cps for the square wave, and 10 to 200 cps for the sine wave. The output power was approximately 10 watts. Since the input capacitance of the generator was around 50 uuf with a RC time constant of 1.57 msec., The amplifier did not have sufficient output power to drive it at high frequencies without distortion of the wave shape. The limiting frequencies were therefore 50 cps for the square wave and 100 cps for the sine wave.

The 6BK4 tube of the amplifier gave off x-rays at voltages over 14,000, so it was necessary to shield the tube with sheet lead. This was removed when the photograph was taken to allow a clearer view of the circuitry.



List of Components

- $V_1$  6BK4 Vacuum Tube  
 $C_1$  Capacitor, 1.0 uf, 400 v  
 $C_2$  Electrolytic Capacitor, 50 uf, 50 v  
 $C_3$  Tubular Capacitor, 0.01 uf, 30,000 v  
 $R_1$  Resistor, 3 megohm, 1 watt  
 $R_2$  Resistor, 1 kilohm, 1/2 watt  
 $R_3$  22 Resistors, 1 megohm, 2 watt  
 $R_4$  10 Carbon Film Precision Resistors, 10 megohm, 1/2 watt  
 $R_5$  Precision Resistor, 1 megohm, 2 watt  
 $B+$  DC Power Supply, 30 kv, 10 ma  
 Filament Transformer, 6.3 v, 0.2 amp (not shown)

FIGURE A1

The High-Voltage Power Source

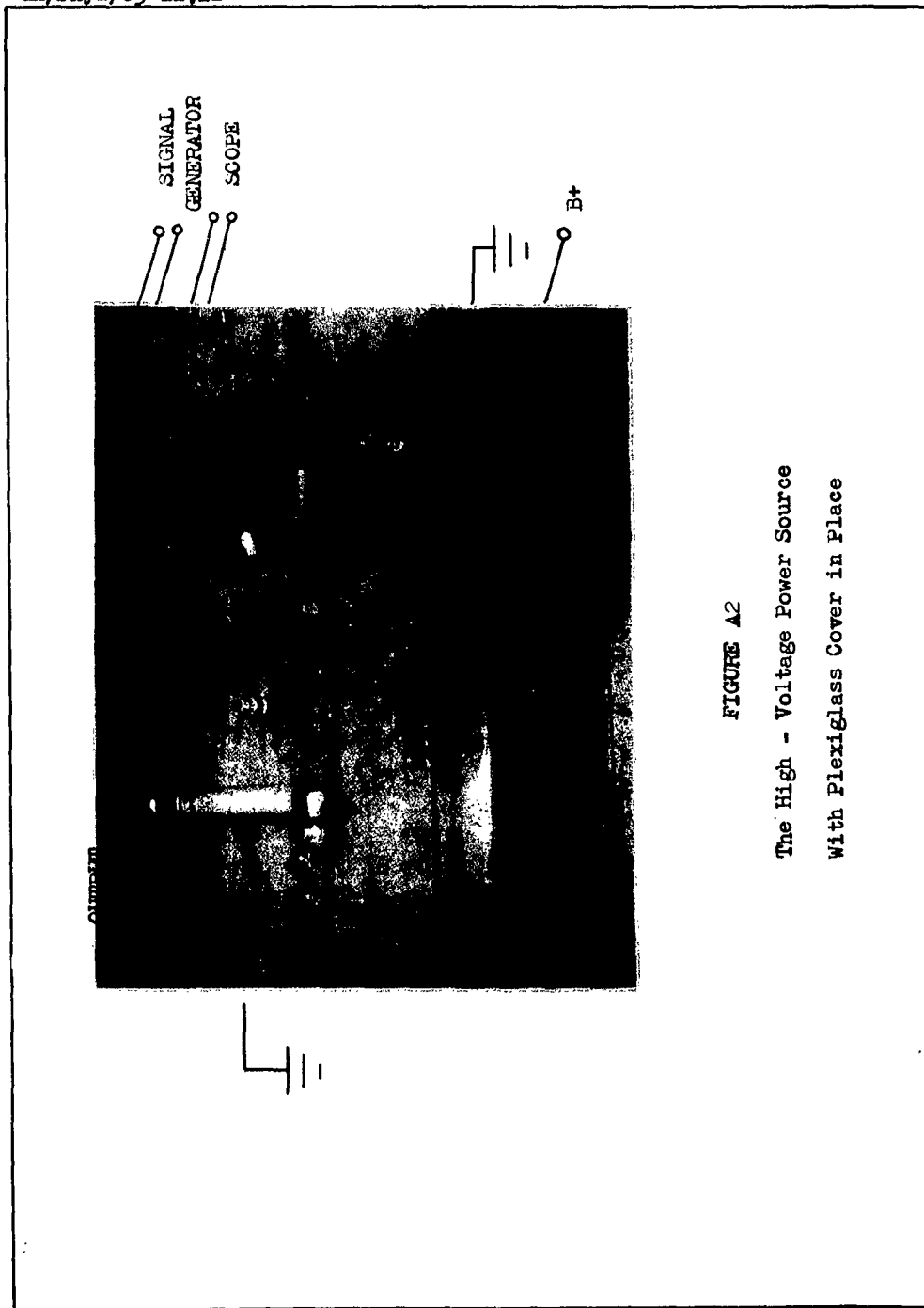


FIGURE A2

The High - Voltage Power Source  
With Plexiglass Cover in Place

## Appendix B

Prediction of Output Voltages  
for Selected Input VoltagesSine Wave Input

This section gives a detailed derivation of an expression for  $V_o$  as a function of time ( or phase angle ) for a sinusoidal input at a given set of operating conditions. The operating conditions selected were:

$$f = 10 \text{ cps or } \omega = 20 \pi$$

$$V_a = 17.1 \text{ kv p-p}$$

$$R_L = 100 \text{ megohms}$$

Therefore, we have

$$V_a = 8.55 \sin 20 \pi t$$

or, since it is more convenient to deal with angles,

$$V_a = 8.55 \sin \omega t$$

$30^\circ$  intervals for  $\omega t$  were taken and instantaneous values of  $V_a$  were found. These are tabulated in Table I. Corresponding values of  $I_o$  were found from the DC characteristic, Figure 11, and these are also shown in Table I.

An approximate expression for  $I_o$  as a function of  $\omega t$  was derived by Fourier analysis. The method used, the 12 - Ordinate Method (Ref 4:473), is shown below. Where  $I_o$  is a periodic function, we can write;

$$I_o(\omega t) = \left[ a_0 + a_1 \sin \omega t + a_2 \sin 2\omega t + \dots + a_n \sin n\omega t \right. \\ \left. + b_1 \cos \omega t + b_2 \cos 2\omega t + \dots + b_n \cos n\omega t \right] \times 10^{-6}$$

where  $a_0, a_1, a_2, a_n, b_1, b_2, b_n$  are given by the following expressions in terms of  $y_0, y_1, y_2, \dots, y_{11}$ , the instantaneous values of  $I_o$  in micro-amps corresponding to the values of  $\omega t$  of  $0^\circ, 30^\circ, 60^\circ, \dots, 330^\circ$ .

GA/Phys/63-11, 12

$$\begin{aligned}a_0 &= \frac{1}{12} (x_0 + x_1 + x_2 + \dots + x_{11}) \\ &= \frac{1}{12} (0 + 0 - 75 - 130 - 75 + 0 + 0 + 0 - 20 - 38 - 20 - 0) \\ &= -16.83\end{aligned}$$

$$\begin{aligned}a_1 &= \frac{1}{6} [(x_3 - x_9) + 0.866 (x_2 + x_4 - x_8 - x_{10}) \\ &\quad + 0.5 (x_1 + x_5 - x_7 - x_{11})] \\ &= \frac{1}{6} [(-130 - 38) + 0.866 (-75 - 75 - 20 - 20) + 0.5 (0 + 0 - 0 - 0)] \\ &= -55.5\end{aligned}$$

$$\begin{aligned}a_2 &= 0.1443 [(x_1 + x_2 + x_7 + x_8) - (x_4 + x_5 + x_{10} + x_{11})] \\ &= 0.1443 [(0 - 75 + 0 + 20) - (-75 + 0 + 20 + 0)] \\ &= 0\end{aligned}$$

$$\begin{aligned}a_3 &= \frac{1}{6} [(x_1 + x_5 + x_9) - (x_3 + x_7 + x_{11})] \\ &= \frac{1}{6} [38 + 130] \\ &= 28.0\end{aligned}$$

$$\begin{aligned}a_4 &= 0.1443 [(x_1 + x_4 + x_7 + x_{10}) - (x_2 + x_5 + x_8 + x_{11})] \\ &= 0.1443 [(0 - 75 + 0 + 20) - (-75 + 0 + 20 + 0)] \\ &= 0\end{aligned}$$

$$\begin{aligned}a_5 &= \frac{1}{6} [(x_3 - x_9) + 0.866 (x_8 + x_{10} - x_2 - x_4) \\ &\quad + 0.5 (x_1 + x_5 - x_7 - x_{11})] \\ &= \frac{1}{6} [(-130 - 38) + 0.866 (20 + 20 + 75 + 75) \\ &\quad + 0.5 (0 + 0 - 0 - 0)] \\ &= -0.55\end{aligned}$$

GA/Phys/63-11, 12

$$b_1 = \frac{1}{6} \left[ (y_0 - y_6) + 0.866 (y_1 + y_{11} - y_5 - y_7) \right. \\ \left. + 0.5 (y_2 + y_{10} - y_4 - y_8) \right]$$

$$= \frac{1}{6} \left[ (0 - 0) + 0.866 (0 + 0 - 0 - 0) \right. \\ \left. + 0.5 (-75 + 20 + 75 - 20) \right]$$

$$= 0$$

$$b_2 = \frac{1}{6} \left[ (y_0 + y_6) + 0.5 (y_1 + y_5 + y_7 + y_{11}) \right. \\ \left. - 0.5 (y_2 + y_4 + y_8 + y_{10}) \right]$$

$$= \frac{1}{6} \left[ (0 + 0) + 0.5 (0 + 0 + 0 + 0) - 0.5 (-75 - 75 + 20 + 20) \right]$$

$$= 9.16$$

$$b_3 = \frac{1}{6} \left[ (y_0 + y_4 + y_8) - (y_2 + y_6 + y_{10}) \right]$$

$$= \frac{1}{6} \left[ (0 - 75 + 20) - (-75 + 0 + 20) \right]$$

$$= 0$$

$$b_4 = \frac{1}{6} \left[ (y_0 + y_3 + y_6 + y_9) - 0.5 (y_1 + y_2 + y_4 \right. \\ \left. + y_5 + y_7 + y_8 + y_{10} + y_{11}) \right]$$

$$= \frac{1}{6} \left[ (0 - 130 + 0 + 38) - 0.5 (0 - 75 - 75 + 0 \right. \\ \left. + 0 + 0 + 20 + 20 + 0) \right]$$

$$= -6.16$$

$$b_5 = \frac{1}{6} \left[ (y_0 - y_6) + 0.866 (y_5 + y_7 - y_1 - y_{11}) \right. \\ \left. + 0.5 (y_2 + y_{10} - y_4 - y_8) \right]$$

$$= \frac{1}{6} \left[ (0 - 0) + 0.866 (0 + 0 - 0 - 0) + 0.5 (-75 + 20 + 75 - 20) \right]$$

$$= 0$$

then, substitution yields

$$I_o(\omega t) = \left[ -16.83 - 55.5 \sin \omega t + 28.0 \sin 3\omega t \right. \\ \left. - 0.55 \sin 5\omega t + 9.16 \cos 2\omega t - 6.16 \cos 4\omega t \right]$$

$$\times 10^{-6}$$

(B - 1)

GA/Phys/63-11, 12

Now, the differential equation of the generator is,

$$\frac{dV_0}{dt} + \frac{1}{R_L C_0} V_0 - \frac{I_0}{C_0} = 0$$

and its solution is

$$V_0(t) = \frac{e^{-t/R_L C_0}}{C_0} \int_0^t e^{t/R_L C_0} I_0(t) dt \quad (B-2)$$

Substitution of (B-1) into (B-2) yields

$$V_0(t) = \frac{10^{-6}}{C_0} e^{-t/R_L C_0} \int_0^t e^{t/R_L C_0} [-16.83 - 55.5 \sin \omega t$$

$$+ 28.0 \sin 3\omega t - 0.55 \sin 5\omega t + 9.16 \cos 2\omega t - 6.16 \cos 4\omega t] dt$$

If we integrate and simplify, then,

$$V_0(t) = R_L \times 10^{-6} \left[ -16.83 (1-B) - \frac{55.5}{(1+A^2)} \left\{ \sin \omega t \right. \right. \\ \left. \left. - A (\cos \omega t - B) \right\} + \frac{28.0}{(1+9A^2)} \left\{ \sin 3\omega t \right. \right. \\ \left. \left. - 3A (\cos 3\omega t - B) \right\} - \frac{0.55}{(1+25A^2)} \left\{ \sin 5\omega t \right. \right. \\ \left. \left. - 5A (\cos 5\omega t - B) \right\} + \frac{9.16}{(1+4A^2)} \left\{ (\cos 2\omega t - B) \right. \right. \\ \left. \left. + 2A \sin 2\omega t \right\} - \frac{6.16}{(1+16A^2)} \left\{ \cos 4\omega t - B \right\} \right. \\ \left. + 4A \sin 4\omega t \right]$$

$$\text{where } A = \omega R_L C_0 \text{ and } B = e^{-t/R_L C_0} \quad (B-3)$$

Substitution of  $C_0 = 55.6 \times 10^{-12}$ ,  $R_L = 10^8$ ,  $\omega = 20\pi$  and

$$A = \omega R_L C_0 = 20\pi \times 10^8 \times 55.6 \times 10^{-12} = 0.3493$$

into (B-3) yields

GA/Phys/63-11, 12

$$\begin{aligned}
 V_o(\omega t) = 10^2 & \left[ -16.83 (1-B) - 49.4 \{ \sin \omega t \right. \\
 & - 0.3493 (\cos \omega t - B) \} + 13.34 \{ \sin 3 \omega t \\
 & - 1.047 (\cos 3 \omega t - B) \} - 0.1358 \{ \sin 5 \omega t \\
 & - 1.745 (\cos 5 \omega t - B) \} + 6.16 \{ (\cos 2 \omega t - B) \\
 & + 0.6986 \sin 2 \omega t \} - 2.085 \{ (\cos 4 \omega t - B) \\
 & \left. + 1.3972 \sin 4 \omega t \} \right]
 \end{aligned}$$

$$\text{where } B = e^{-t/R_L C_o} = e^{-\omega t / \omega R_L C_o} = e^{-\omega t / 0.3493} \quad (B-4)$$

After the output voltage is established,  $t$  approaches  $\infty$  and  $B$  in (B-4) approaches 0.

We can then write

$$\begin{aligned}
 V_o(\omega t) = 10^2 & \left[ -16.83 - 49.4 \{ \sin \omega t - 0.3493 \cos \omega t \} \right. \\
 & + 13.34 \{ \sin 3 \omega t - 1.047 \cos 3 \omega t \} \\
 & - 0.1358 \{ \sin 5 \omega t - 1.745 \cos 5 \omega t \} \\
 & + 6.16 \{ \cos 2 \omega t + 0.6986 \sin 2 \omega t \} \\
 & \left. - 2.085 \{ \cos 4 \omega t + 1.3972 \sin 4 \omega t \} \right] \quad (B-5)
 \end{aligned}$$

For  $\omega t$  intervals of  $15^\circ$ , values of  $V_o$  were found from (B-5) using the IBM 1620 computer. The computer output is shown in Table II and the wave shape is plotted as the theoretical curve in Figure 36.

GA/Phys/63-11, 12

TABLE I

$I_o$  Coefficients for Output Voltage Prediction

For Sine Wave Input

<u><math>\omega t</math> (<math>^\circ</math>)</u>	<u><math>V_a</math> (kV)</u>	<u><math>I_o</math> (mA)</u>	<u><math>Y_n</math></u>
0	0	0	$Y_0$
30	4.27	0	$Y_1$
60	7.40	-75	$Y_2$
90	8.55	-130	$Y_3$
120	7.40	-75	$Y_4$
150	4.27	0	$Y_5$
180	0	0	$Y_6$
210	-4.27	0	$Y_7$
240	-7.40	20	$Y_8$
270	-8.55	38	$Y_9$
300	-7.40	20	$Y_{10}$
330	-4.27	0	$Y_{11}$

TABLE II

## Computer Data

Predicted Output Voltage for Values of  
Phase Angle for Sine Wave Input

Values of  $V_o$  are given in volts.

Unidentified numbers in table represent phase angle in degrees.

0.	$V_o \text{ } \emptyset \text{ F WT} = -922.96$	195.	$V_o \text{ } \emptyset \text{ F WT} = -1627.76$
15.	$V_o \text{ } \emptyset \text{ F WT} = -954.03$	210.	$V_o \text{ } \emptyset \text{ F WT} = -1481.39$
30.	$V_o \text{ } \emptyset \text{ F WT} = -819.30$	225.	$V_o \text{ } \emptyset \text{ F WT} = -694.90$
45.	$V_o \text{ } \emptyset \text{ F WT} = -1393.39$	240.	$V_o \text{ } \emptyset \text{ F WT} = 733.37$
60.	$V_o \text{ } \emptyset \text{ F WT} = -3256.89$	255.	$V_o \text{ } \emptyset \text{ F WT} = 2408.16$
75.	$V_o \text{ } \emptyset \text{ F WT} = -6114.66$	270.	$V_o \text{ } \emptyset \text{ F WT} = 3780.12$
90.	$V_o \text{ } \emptyset \text{ F WT} = -8795.11$	285.	$V_o \text{ } \emptyset \text{ F WT} = 4387.40$
105.	$V_o \text{ } \emptyset \text{ F WT} = -9963.76$	300.	$V_o \text{ } \emptyset \text{ F WT} = 4025.96$
120.	$V_o \text{ } \emptyset \text{ F WT} = -9049.41$	315.	$V_o \text{ } \emptyset \text{ F WT} = 2826.31$
135.	$V_o \text{ } \emptyset \text{ F WT} = -6636.00$	330.	$V_o \text{ } \emptyset \text{ F WT} = 1225.40$
150.	$V_o \text{ } \emptyset \text{ F WT} = -4007.72$	345.	$V_o \text{ } \emptyset \text{ F WT} = -183.05$
165.	$V_o \text{ } \emptyset \text{ F WT} = -2250.30$	360.	$V_o \text{ } \emptyset \text{ F WT} = -922.98$
180.	$V_o \text{ } \emptyset \text{ F WT} = -1628.04$		

GA/Phys/63-11, 12

Square Wave Input

This section gives a detailed derivation of an expression for  $V_o$  as a function of time (or phase angle) for a square wave input at a given set of operating conditions. The operating conditions selected were

$$f = 10 \text{ cps or } \omega = 20 \pi$$

$$V_a = 18.4 \text{ kv p-p}$$

$$R_L = 100 \text{ megohms}$$

Therefore, we have

$$V_a = \begin{cases} 9.2, & 0 < \omega t < \pi \\ -9.2, & \pi < \omega t < 2\pi \end{cases}$$

From the DC characteristic (Figure 11), we can write

$$I_o = \begin{cases} -143 \times 10^{-6}, & 0 < \omega t < \pi \\ 54 \times 10^{-6}, & \pi < \omega t < 2\pi \end{cases} \quad (\text{B} - 6)$$

The solution of the differential equation of the generator is the same as before,

$$V_o(t) = \frac{e^{-t/R_L C_o}}{C_o} \int_0^t e^{t/R_L C_o} I_o(t) dt \quad (\text{B} - 2)$$

Substitution of (B - 6) into (B - 2) yields

$$V_o(t) = \begin{cases} \frac{e^{-t/R_L C_o}}{C_o} \int_0^t -143 \times 10^{-6} e^{t/R_L C_o} dt, & 0 < \omega t < \pi \\ \frac{e^{-t/R_L C_o}}{C_o} \int_0^t 54 \times 10^{-6} e^{t/R_L C_o} dt, & \pi < \omega t < 2\pi \end{cases}$$

If we integrate, then

GA/Phys/63-11, 12

$$V_0(t) = \begin{cases} -143 \times 10^{-6} R_L (1 - e^{-t/R_L C_0}), & 0 < \omega t < \pi \\ 54 \times 10^{-6} R_L (1 - e^{-t/R_L C_0}), & \pi < \omega t < 2\pi \end{cases} \quad (B-7)$$

Substitution of  $C_0 = 55.6 \times 10^{-12}$ ,  $R_L = 10^8$  and  $\omega = 20\pi$  into (B-7) yields

$$V_0(\omega t) = \begin{cases} -143 \times 10^2 (1 - e^{-\omega t/0.3493}), & 0 < \omega t < \pi \\ 54 \times 10^2 (1 - e^{-\omega t/0.3493}), & \pi < \omega t < 2\pi \end{cases} \quad (B-8)$$

For  $\omega t$  intervals of  $30^\circ$ , values of  $V_0$  were found from (B-8). These are tabulated in Table III and the wave shape is plotted as the theoretical curve in Figure 37.

GA/Phys/63-11, 12

TABLE III

Predicted Output Voltage for Square Wave Input

<u><math>\omega t, ^\circ</math></u>	<u><math>V_o(\omega t), \text{KV}</math></u>
0	0
30	-11.12
60	-13.59
90	-14.14
120	-14.27
150	-14.30
180	-14.30 ( 0 )
210	4.20
240	5.13
270	5.34
300	5.39
330	5.40
360	5.40 ( 0 )

GA/Phys/63-11, 12

Step (Exponential) Input

This section gives a detailed derivation of an expression for  $V_o$  as a function of time for a step input at a given set of operating conditions. In this derivation, the ion current is assumed to be a linear function of attractor voltage above the ionization potential and therefore the DC characteristic is not used. The operating conditions selected were:

$$V_o \text{ max} = 16.2 \text{ kv}$$

$$R_L = 100 \text{ megohms}$$

$$R_1 C_1 = 1.57 \times 10^{-3} \text{ sec (from P. 8*)}$$

Since the input of the generator is, in fact, an RC network, for a step input we may write

$$V_a(t) = V_a \text{ max} (1 - e^{-t/R_1 C_1})$$

and, therefore, by our assumption,

$$I_o(t) = I_{o\text{max}} (1 - e^{-t/R_1 C_1}) \quad (\text{B-9})$$

The solution of the differential equation of the generator is

$$V_o(t) = \frac{e^{-t/R_L C_o}}{C_o} \int_0^t e^{t/R_L C_o} I_o(t) dt \quad (\text{B-2})$$

Substitution of (B-9) into (B-2) yields

$$V_o(t) = \frac{e^{-t/R_L C_o}}{C_o} \int_0^t e^{t/R_L C_o} I_{o\text{max}} (1 - e^{-t/R_1 C_1}) dt$$

If we integrate and simplify, then

$$V_o(t) = I_{o\text{max}} R_L \left[ 1 - \frac{e^{-t/R_L C_o}}{B R_L C_o} - \left(1 - \frac{1}{B}\right) \frac{e^{-t/R_1 C_1}}{R_1 C_1} \right]$$

$$\text{where } B = \frac{1}{R_L C_o} - \frac{1}{R_1 C_1} \quad (\text{B-10})$$

GA/Phys/63-11, 12

Substitution of  $I_0 \max R_L = V_0 \max = 16.2 \times 10^3$ ,  $R_1 C_1 = 1.57 \times 10^{-3}$   
and  $R_2 C_2 = 5.56 \times 10^{-3}$  into (B-10) yields

$$V_0(t) = 16.2 \times 10^3 \left[ 1 + 0.393 e^{-10^3 t/1.57} - 1.393 e^{-10^3 t/5.56} \right] \quad (\text{B-11})$$

The transport phenomena discussion utilizes this result but in the following slightly different form:

$$(V_0 \max - V_0) = 16.2 \times 10^3 \left[ 1.393 e^{-10^3 t/5.56} - 0.393 e^{-10^3 t/1.57} \right] \quad (\text{B-12})$$

Values of  $V_0$  and  $(V_0 \max - V_0)$  were calculated for values of  $t$  up to 10 msec. These are tabulated in Table IV and the wave shape ( $V_0$  versus  $t$ ) is plotted as the theoretical curve in Figure 39.

GA/Pays/63-11, 12

TABLE IV

Predicted Output Voltage for Step Input

<u>t, msec.</u>	<u>V<sub>o</sub>, kv</u>	<u>(V<sub>o</sub> max - V<sub>o</sub>), kv</u>
0	0	16.20
0.25	0.05	16.14
0.5	0.18	16.01
1.0	0.70	15.50
1.5	1.43	14.77
2.0	2.22	13.98
2.5	3.11	13.10
3.0	3.97	12.23
3.5	4.89	11.31
4.0	5.68	10.52
5.0	7.30	8.90
6.0	8.67	7.53
7.0	9.87	6.33
8.0	10.90	5.29
9.0	11.74	4.46
10.0	12.46	3.74

## Appendix C

Flow Parameters in the Transport RegionFluid Velocity Calculations

The following calculations are based on Wheeler's assumed average value of Mach Number of 1.4 throughout the transport region (Ref 7:53). Also, the average  $T_0$  is taken as  $40^\circ\text{F}$  and for isentropic flow of a perfect gas  $\gamma = 1.4$

Now,

$$\frac{T_0}{T} = 1 + \frac{\gamma - 1}{2} M^2$$

where  $T$  = fluid temperature in transport region

$T_0$  = stagnation temperature

$M$  = Mach Number in transport region

Then

$$T = \frac{500}{1 + 0.2 (1.4)^2} = 359^\circ\text{R}$$

Now the velocity of sound,  $c = 49.1 \sqrt{T} = 930$  fps

and  $M = \frac{V_f}{c}$  where  $V_f$  = fluid velocity in transport region

therefore,  $V_f = M \times c = 1.4 \times 930 = 1302$  fps

Fluid Density Calculations

$$\text{Density } \rho = \rho_0 \left( 1 + \frac{\gamma - 1}{2} M^2 \right)^{\frac{1}{\gamma - 1}}$$

where  $\rho_0$  = the stagnation density

$$\text{But } \rho_0 = \frac{P_0}{RT_0} = \frac{164.7 \times 144}{53.3 \times 500} = 0.890 \text{ lbm/ft}^3$$

Therefore the density of fluid in transport region is

$$\rho = \frac{0.890}{2.286} = 0.389 \text{ lbm/ft}^3$$

GA/Phys/63-11, 12

Transit Time Calculation

$V_t$  = transit velocity of ions

$V_f$  = fluid velocity

$u$  = drift velocity of ions

Then,

$$V_t = V_f + u \quad (C-1)$$

and,

$$u = kE \quad (\text{Ref 6:2}) \quad (C-2)$$

where

$k = K \frac{\rho_a}{\rho} =$  ion mobility

$K = 1.6 \times 10^{-4} \frac{\text{m/sec}}{\text{volt/m}}$  for positive ions and

$K = 2.2 \times 10^{-4} \frac{\text{m/sec}}{\text{volt/m}}$  for negative ions.

$$\rho_a = \text{density of air at } 0^\circ\text{C \& 760 mm Hg} = \frac{P}{RT} = \frac{14.7 \times 144}{53.3 \times (460 + 32)} \\ = 0.0807 \text{ lbm/ft}^3$$

But  $\rho = 0.389$

Then  $k^+ = 3.32 \times 10^{-5}$

and  $k^- = 4.56 \times 10^{-5}$

From Gouridine (Ref 1:2), taking the case for maximum power, we

get

$$\tilde{X}_x = -1 + \left[ 1 - \tilde{J} (1 - \tilde{X})^{\frac{1}{2}} \right]$$

where

$\tilde{X}_x = \frac{E_x k}{V_f}$  and  $E_x$  = electric field strength at position  $x$  in the transport region

$$\tilde{J} = \frac{I}{L}$$

Now, for optimum operation,  $\tilde{J} = 1.00$

GA/Phys/63-11, 12

$$\text{Then, } E_x = \left[ -1 + \left(\frac{x}{L}\right)^{\frac{1}{2}} \right] \frac{V_f}{K}$$

But

$$u = k \times E_x \\ = \left[ \left(\frac{x}{L}\right)^{\frac{1}{2}} - 1 \right] V_f \quad (C-3)$$

Substitution of (C-3) into (C-1) gives

$$V_t = V_f + V_f \left[ \left(\frac{x}{L}\right)^{\frac{1}{2}} - 1 \right]$$

$$\text{then, } \frac{dx}{dt} = V_f \left[ 1 + \left(\frac{x}{L}\right)^{\frac{1}{2}} - 1 \right]$$

or

$$\frac{dx}{\left(\frac{x}{L}\right)^{\frac{1}{2}}} = V_f dt$$

If we integrate,

$$t_r = \frac{1}{V_f} \int_0^L \frac{dx}{\left(\frac{x}{L}\right)^{\frac{1}{2}}} \\ t_r = \frac{1}{V_f} \left[ 2 L \left(\frac{x}{L}\right)^{\frac{1}{2}} \right]_0^L \\ t_r = \frac{2L}{V_f} = \frac{2 \left(\frac{1}{1302}\right)}{1302} = 0.0641 \text{ msec}$$

Therefore, under maximum power conditions the ion transit

time  $t_r = 0.0641$  msec.

In general,

$$\frac{L}{V_f} < t_r < \infty$$

Since when  $E_x = 0$ ,  $u = 0$

so  $V_t = V_f$ , and  $t_r = \frac{L}{V_f} = 0.032$  msec.

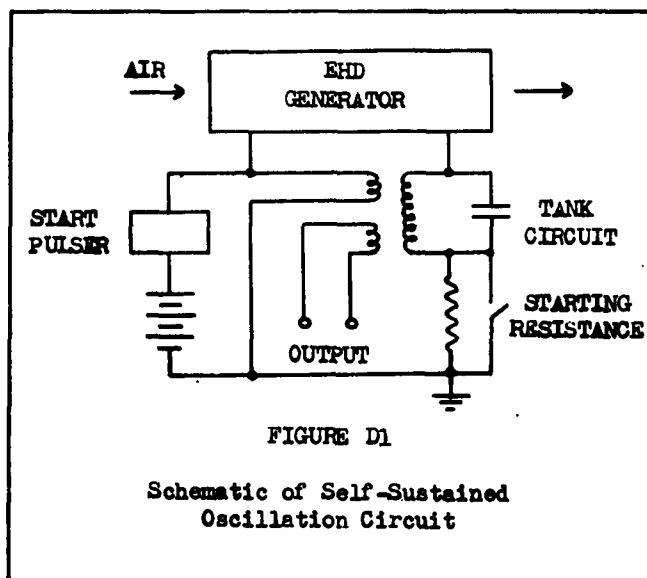
and at saturation  $u = V_f$

so  $V_t = 0$  and  $t_r \rightarrow \infty$

## Appendix D

Generator Self-Sustained Oscillation Calculations

As explained in the text, a wave-shaping tank circuit is required in the output circuit of the generator to attain a suitable feed-back signal for oscillation. The circuit for oscillation is shown in Figure D 1 and operates as follows:



The start pulser applies a 10 cps signal of short duration to the attractor of the generator. The output of the generator sees the start-in load (several megohms) and so an output voltage builds up. The circuit then begins to resonate and the output resistance thus increases and the voltage builds up higher. At this point the starting load is shorted out and the resonant resistance of the tank circuit is the only output load on the generator. Part of the energy in the tank circuit is fed back to the attractor to sustain the oscillations. Any residual

GA/Phys/63-11, 12

energy in the tank circuit is available as output at the terminals of the transformer secondary.

For near maximum voltage and power gain, a load of 100 megohms was found necessary at a frequency of 10 cps. Hence, the resonant resistance of the tank circuit must be 100 megohms.

Then  $R_t = \omega L_t \quad Q = 100 \text{ megohms}$

and, since the resonant frequency = 10 cps,

$$L_t Q = \frac{100 \times 10^6}{6.28 \times 10} = 1.6 \times 10^6$$

If a Q of 100 (high but within reason) is chosen, then

$$L_t = \frac{1.6 \times 10^6}{100} = 16,000 \text{ h.}$$

Now, at resonance,

$$f \approx \frac{1}{2\pi \sqrt{LC}}$$

Hence,

$$C_t = \frac{1}{(6.28)^2 (10)^2 16,000} = 0.0158 \mu\text{f}$$

An alternate calculation would be to find Q knowing the energy available and  $C_t$  :

$$Q = 2\pi \frac{\text{energy stored/cycle}}{\text{energy dissipated/cycle}} = 2\pi \frac{\frac{1}{2} CV^2}{P_L/f}$$
$$= 6.28 \times \frac{1}{2} \left[ \frac{0.0158 (14.1)^2 \times (10^3)^2}{1/10} \right] = 99.2 \approx 100$$

where the power available = 1 watt from Figure 26 and maximum voltage  $V = 14,100$  from Figure 19.

## Appendix B

Sine Wave: Square Wave Power CalculationsInput Power Ratio

To obtain the theoretical value for the ratio of sine wave input power to square wave input power, the square of the voltage is integrated over the ionization region for half a cycle for both wave shapes and the ratio of the two integrals is then the required power ratio.

For a 6.5 kv RMS sine wave input, the input voltage  $V = V_{\max} \sin \theta$   
 where  $V_{\max} = \frac{6.5}{0.707} = 9.2$  kv

Therefore,

$$V = 9.2 \sin \theta \text{ and } V^2 = 84.5 \sin^2 \theta$$

If ionisation occurs at 5.5 kv, then

$$\theta = \sin^{-1} \frac{5.5}{9.2} = 36.75^\circ$$

The limits of the ionization region are therefore  $36.75^\circ$  and  $143.25^\circ$ .

$$\begin{aligned} \text{Then the area under the curve} &= \int_{36.75^\circ}^{143.25^\circ} V^2 d\theta = 84.5 \int_{36.75^\circ}^{143.25^\circ} \sin^2 \theta d\theta \\ &= 84.5 \left[ \frac{1}{2} \theta - \frac{1}{4} \sin 2\theta \right]_{36.75^\circ}^{143.25^\circ} = 119.0 \end{aligned}$$

For a 6.5 kv RMS square wave input,

$$\text{the area under the curve} = \pi \times (6.5)^2 = 132.9$$

$$\text{Then, } \frac{\text{Sine wave input power}}{\text{Square wave input power}} = \frac{119.0}{132.9} = 0.896$$

Output Power Ratio

The theoretical value for the output ratio is found by obtaining instantaneous output currents,  $I_o$ , from the DC characteristics (Figure

GA/Phys/63-11, 12

11), plotting  $(I_o)^2$  against phase angle  $\theta$  and comparing the areas under the curves. The areas under the curves are computed by adding squares. This process is shown on Figure K1. A value of  $I_o = 26 \mu\text{a}$  is chosen for the square wave by considering the spread in the DC characteristic and choosing the highest value. The ratio thus obtained is:

$$\frac{\text{Sine wave output power}}{\text{Square wave output power}} = \frac{1120}{121.5} = 9.22$$

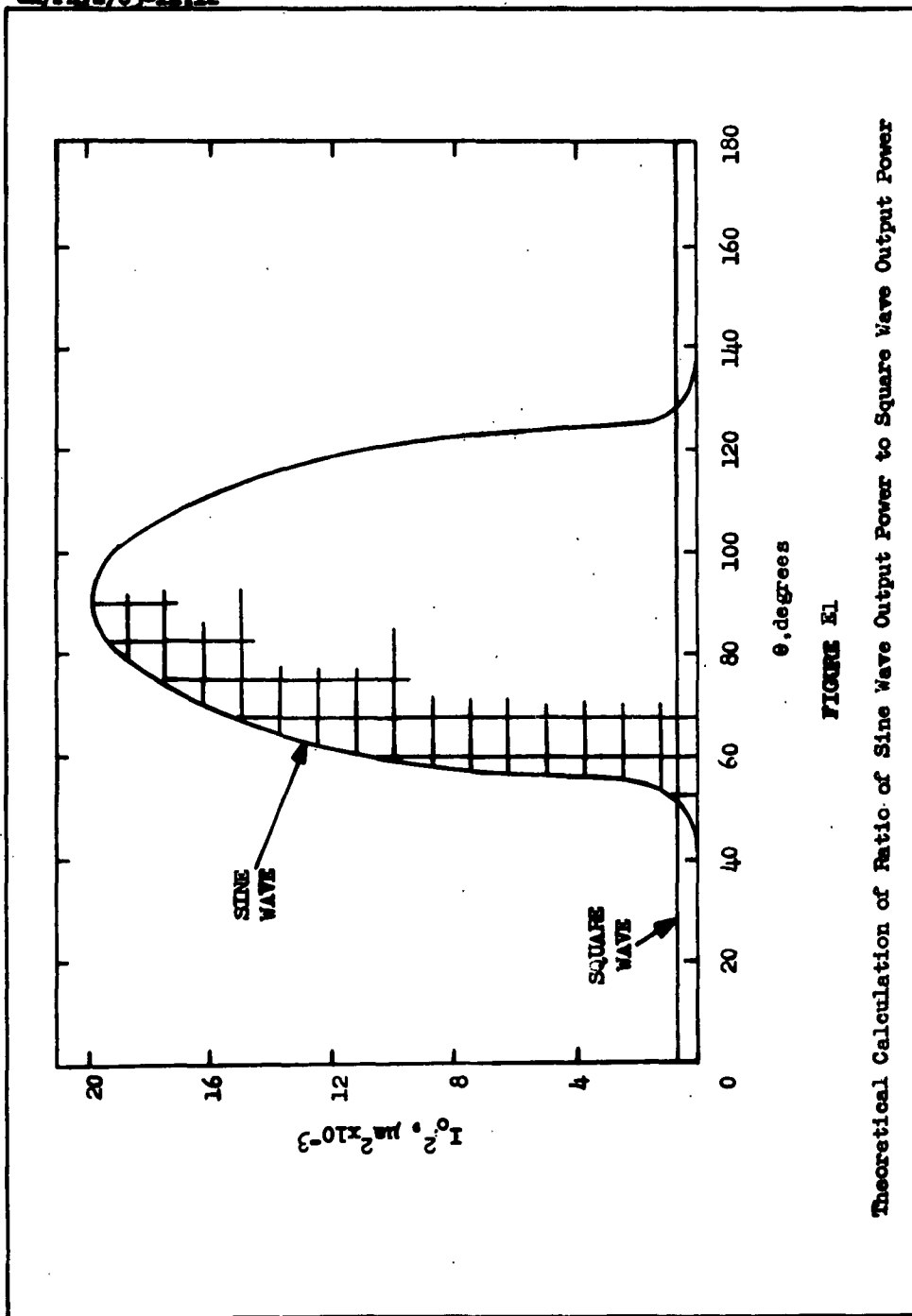


FIGURE E1

Theoretical Calculation of Ratio of Sine Wave Output Power to Square Wave Output Power

Appendix F

Original Experimental Data

The following data is listed by runs which are numbered chronologically in the order in which they were done. Runs numbered 1, 2, 3, 10, 12, 13, 15, and 18 are not listed. The data from these runs were discarded due to inaccurate instrumentation, faulty air supply, or generator failure of one sort or another.

The units and symbols used throughout this appendix are as follows:

- Attractor potential,  $V_a$  . . . . . kv
- Collector potential,  $V_o$  . . . . . kv
- Load Resistance,  $R_L$  . . . . . megohms
- Total temperature,  $T_o$  . . . . . °F
- Output Current,  $I_o$  . . . . .  $\mu$ a
- Frequency,  $f$  . . . . . cps
- Power,  $P_L$  . . . . . watts

The total pressure,  $P_o$ , was maintained constant at 150 psig for all runs.

TABLE V

HUNS #4,5,6, - Peak-to-Peak Output Voltage Data for a Sine Wave Input

HUN # 6		$R_L = 50$ megohms		$T_0 = 40^\circ F$	
$f = 10$ cps		$f = 20$ cps		$f = 30$ cps	
$V_a$	$V_o$	$V_a$	$V_o$	$V_a$	$V_o$
18.5	22.3	18.8	19.8	19.4	18.1
17.6	21.2	17.8	18.4	18.2	16.8
16.2	20.2	16.2	16.3	16.8	14.6
15.4	19.8	14.8	13.4	14.4	7.4
14.3	15.6	14.0	8.0	13.8	5.3
12.7	6.8	13.0	4.5	11.8	2.0
11.2	2.9	11.9	3.3	10.4	0.9
9.6	0.6	9.8	0.1	9.7	0.1
9.1	0.0	8.9	0.0	9.5	0.0

HUN # 4		$R_L = 100$ megohms		$T_0 = 50^\circ F$	
$f = 10$ cps		$f = 20$ cps		$f = 30$ cps	
$V_a$	$V_o$	$V_a$	$V_o$	$V_a$	$V_o$
18.2	29.4	18.6	24.3	19.2	23.2
17.2	27.9	18.4	24.7	18.1	22.1
16.1	26.6	17.4	23.7	16.6	18.6
15.3	25.4	16.5	21.8	15.9	15.4
14.3	21.5	14.9	16.4	14.5	9.6
12.2	8.1	13.2	6.0	13.2	6.1
10.8	2.8	11.2	1.5	18.1	21.2

HUN # 5		$R_L = 200$ megohms		$T_0 = 45^\circ F$	
$f = 10$ cps		$f = 20$ cps		$f = 30$ cps	
$V_a$	$V_o$	$V_a$	$V_o$	$V_a$	$V_o$
18.0	37.2	18.9	28.5	18.3	21.0
17.6	36.4	18.0	28.3	17.9	21.0
17.0	33.8	17.8	27.8	17.2	20.4
16.0	32.0	16.4	24.6	16.2	19.0
15.0	28.7	15.9	23.0	15.4	16.1
13.6	16.4	14.3	13.4	14.4	10.0
11.5	7.2	11.9	4.6	12.9	5.8
9.9	0.6	10.5	0.6	11.0	1.4
7.0	0.0	10.0	0.0	7.1	0.0

GA/Phys/63-11, 12

TABLE VI

RUN # 7, 8, 11 - Direct Current Characteristic Data  
( $R_L = 100$  megohms)

RUN # 7

Negative Ions $T_0 = 25^\circ F$			Positive Ions $T_0 = 38^\circ F$		
$V_a$	$V_0$	$I_0$	$V_a$	$V_0$	$I_0$
5.60	0.0	0.0	4.00	0.0	0.0
6.75	1.50	15.0	5.20	0.60	6.0
7.00	6.25	62.5	5.75	2.50	25.0
7.50	14.25	142.5	6.25	4.05	40.5
8.00	16.20	162.0	6.75	3.50	35.0
8.50	17.10	171.0	7.50	6.00	60.0
6.95	2.35	23.5	8.30	11.25	112.5
			9.00	11.80	118.0

RUN # 8

Positive Ions $T_0 = 18^\circ F$		
$V_a$	$V_0$	$I_0$
5.50	0.0	0.0
6.25	0.75	7.5
7.25	2.25	22.5
7.90	3.50	35.0
8.10	7.10	71.0
8.60	10.25	102.5
9.10	10.50	105.0
10.00	14.10	141.0

RUN # 11 (a)

Negative Ions $T_0 = 40^\circ F$			Positive Ions $T_0 = 38^\circ F$		
$V_a$	$V_0$	$I_0$	$V_a$	$V_0$	$I_0$
6.46	0.0	0.0	4.86	0.8	8.0
7.42	1.9	19.0	4.73	0.0	0.0
7.65	3.1	31.0	5.45	1.1	11.0
8.15	8.3	83.0	8.00	3.9	39.0
8.42	10.9	109.0	8.95	5.4	54.0
9.06	13.9	139.0	9.35	8.1	81.0
9.26	14.1	141.0	9.55	10.1	101.0
9.65	15.2	152.0	10.40	11.3	113.0
			10.80	13.1	131.0

GA/Phys/63-11, 12

TABLE VI (Continued)

RUN # 11 (b)

Negative Ions $T_0 = 48^\circ F$			Positive Ions $T_0 = 40^\circ F$		
$V_a$	$V_0$	$I_0$	$V_a$	$V_0$	$I_0$
5.40	0.0	0.0	6.58	0.0	0.0
6.01	1.3	13.0	7.46	2.2	22.0
6.38	2.1	21.0	8.50	2.6	26.0
6.69	4.9	49.0	8.50	3.4	34.0
7.00	7.7	77.0	8.90	3.7	37.0
7.38	10.3	103.0	8.90	4.4	44.0
7.78	12.0	120.0	9.64	4.9	49.0
8.39	13.5	135.0	9.64	7.8	78.0
9.05	14.4	144.0	10.20	9.9	99.0
9.78	15.3	153.0	10.20	10.6	106.0
			10.40	12.4	124.0
			10.80	12.8	128.0

RUN # 11 (c)

Negative Ions $T_0 = 35^\circ F$			Positive Ions $T_0 = 45^\circ F$		
$V_a$	$V_0$	$I_0$	$V_a$	$V_0$	$I_0$
5.78	0.0	0.0	6.02	0.0	0.0
6.52	0.8	8.0	7.20	1.6	16.0
7.00	3.4	34.0	8.50	2.6	26.0
7.22	4.1	41.0	8.50	3.9	39.0
7.50	6.4	64.0	8.90	4.6	46.0
8.00	10.3	103.0	9.35	6.2	62.0
8.39	12.7	127.0	9.35	9.1	91.0
9.05	14.3	143.3	9.62	7.4	74.0
			9.62	8.3	83.0
			9.62	9.5	95.0
			10.20	7.9	79.0
			10.20	8.9	89.0
			10.70	12.8	128.0

TABLE VII

## RUN # 9 - Output Voltage Data for Step Input

Data taken from Figure 38 (a)

Time (msec)	$V_a \text{ max} - V_a$ (7.95 - $V_a$ )	$V_o \text{ max} - V_o$ (16.2 - $V_o$ )
0.0	7.80	16.2
0.3	7.00	16.2
1.3	3.50	16.2
2.3	1.20	16.2
3.3	0.75	15.9
4.3	0.45	14.1
5.3	0.35	12.3
6.3	0.15	10.5
7.3	0.15	8.6
8.3	0.10	7.3
9.3	0.05	6.1
10.3	0.00	5.3
11.3	0.00	4.1
12.3		3.6
13.3		2.9
14.3		2.5
15.3		2.1
16.3		1.7
17.3		1.5
18.3		1.3
19.3		0.8
20.3		0.6
21.3		0.5
22.3		0.5
23.3		0.4
24.3		0.4
25.3		0.3
26.3		0.3

GA/Phys/63-11, 12

TABLE VIII

RUNS # 14, 17 - Output Voltage for Biased Sine Wave Input

RUN # 14 DC Bias 6.2kv $R_L = 100$ megohms $T_0 = 55^\circ F$		RUN # 17 DC Bias 6.9 kv $R_L = 100$ megohms $T_0 = 60^\circ F$	
Frequency	$V_o$ (P-P)	Frequency	$V_o$ (P-P)
9	17.5	9	18.3
11	17.5	10	17.5
13	17.8	10	13.2
15	17.8	11	13.2
30	14.2	11	15.0
60	8.7	12	15.4
100	6.1	15	14.5
120	4.6	20	13.8
140	4.3	25	13.8
160	3.8	30	11.5
200	2.7	40	10.0
250	3.0	60	7.0
		100	5.2
		300	2.3

TABLE IX

RUN # 16 - RMS Output Voltage Data for a Sine Wave Input

$R_L = 50$ megohms		$T_0 = 55^\circ F$			
$f = 10$ cps		$f = 25$ cps		$f = 40$ cps	
$V_a$	$V_o$	$V_a$	$V_o$	$V_a$	$V_o$
2.87	0.0	2.89	0.0	2.54	0.0
3.62	1.2	4.12	1.7	4.29	1.3
4.18	3.15	4.6	2.6	4.85	2.7
4.67	3.45	4.9	3.1	5.05	3.1
5.1	3.95	5.25	3.18	5.35	3.65
5.4	5.0	5.45	4.4	5.6	4.25
5.75	5.95	5.7	5.1	6.1	5.0
6.0	6.45	6.1	5.7	6.25	5.4
6.65	7.45	6.5	6.55	6.5	6.05

$R_L = 100$ megohms		$T_0 = 55^\circ F$			
$f = 10$ cps		$f = 25$ cps		$f = 40$ cps	
$V_a$	$V_o$	$V_a$	$V_o$	$V_a$	$V_o$
2.78	0.0	2.89	0.0	2.85	0.0
2.08	0.5	3.53	1.55	4.04	1.8
3.42	1.7	3.94	3.6	4.23	3.1
3.74	3.6	4.1	4.3	4.53	4.2
3.87	4.1	5.0	5.2	5.1	5.1
4.06	4.8	5.3	5.8	5.4	5.3
4.27	5.7	5.5	6.5	5.7	6.0
4.7	5.9	5.8	7.25	6.2	7.1
4.95	6.3	6.16	7.95	6.6	8.15
5.2	7.05	6.44	8.65		
5.34	7.8				
5.54	8.4				
5.75	8.9				
6.22	9.9				
6.70	10.35				

$R_L = 200$ megohms		$T_0 = 55^\circ F$			
$f = 10$ cps		$f = 25$ cps		$f = 40$ cps	
$V_a$	$V_o$	$V_a$	$V_o$	$V_a$	$V_o$
2.95	0.0	2.98	0.0	3.17	0.0
3.63	1.4	3.56	1.6	4.09	1.6
4.27	3.0	4.25	2.95	4.45	4.2
4.6	4.7	4.55	3.95	5.1	5.4
4.9	6.2	4.75	4.70	5.82	6.2
5.5	7.3	5.14	5.70	6.23	7.25
5.95	8.8	5.50	6.2	6.48	8.25
6.15	9.7	6.05	7.55		
6.45	10.6	6.32	8.55		
		6.58	9.60		

GA/Phys/63-11,12

TABLE X

HUN # 19 - RMS Output Voltage Data For a Square Wave Input

$R_L = 100$ megohms				$T_o = 63^\circ F$			
$f = 10$ cps		$f = 25$ cps		$f = 40$ cps			
$V_a$	$V_o$	$V_a$	$V_o$	$V_a$	$V_o$		
4.94	0.0	5.25	0.0	5.15	0.0		
5.25	1.4	5.80	2.05	5.75	2.5		
5.6	3.1	6.30	2.5	6.05	3.9		
5.7	4.35	6.35	4.5	6.25	4.4		
6.25	5.3	6.48	5.4	7.35	5.6		
6.65	6.25	7.6	6.7				
7.60	8.45	7.7	7.6				
7.95	9.80						

$R_L = 50$ megohms				$T_o = 63^\circ F$			
$f = 10$ cps		$f = 25$ cps		$f = 40$ cps			
$V_a$	$V_o$	$V_a$	$V_o$	$V_a$	$V_o$		
5.35	0.0	5.75	0.0	5.3	0.0		
6.6	2.85	6.9	2.5	6.25	2.05		
7.3	4.15	7.25	3.9	6.75	3.4		
7.55	5.25	7.65	4.35	7.25	3.65		
7.95	6.2	7.75	4.85	7.5	4.0		
8.3	7.2						

$R_L = 200$ megohms				$T_o = 63^\circ F$			
$f = 10$ cps		$f = 25$ cps		$f = 40$ cps			
$V_a$	$V_o$	$V_a$	$V_o$	$V_a$	$V_o$		
4.75	0.0	5.05	0.0	5.4	0.0		
5.15	1.9	5.25	1.2	5.55	1.6		
5.25	2.7	6.15	3.25	6.1	3.5		
5.3	4.1	6.3	4.9	6.5	4.9		
5.65	4.6	6.55	5.5	6.8	5.9		
5.95	5.95	6.9	7.5	7.5	6.8		
6.25	7.9	7.55	8.5				
7.45	9.4	7.75	8.9				

TABLE XI

Power Calculations  
( $f=10$  cps)

Square Wave			Sine Wave		
$R_L = 100$ megohms					
$V_a$	$V_o$	$P_o$	$V_a$	$V_o$	$P_o$
4.94	0.0	0.0	2.75	0.0	0.0
5.20	1.0	0.01	3.20	1.0	0.01
5.35	2.0	0.04	3.50	2.0	0.04
5.55	3.0	0.09	3.70	3.0	0.09
5.80	4.0	0.16	3.80	4.0	0.16
6.15	5.0	0.25	4.05	5.0	0.25
6.50	6.0	0.36	4.65	6.0	0.36
6.85	7.0	0.49	5.20	7.0	0.49
7.30	8.0	0.64	5.40	8.0	0.64
7.70	9.0	0.81	5.80	9.0	0.81
			6.35	10.0	1.00
$R_L = 50$ megohms					
5.40	0.0	0.00	2.90	0.0	0.00
6.10	1.0	0.02	3.50	1.0	0.02
6.40	2.0	0.08	4.00	2.0	0.08
6.75	3.0	0.18	4.30	3.0	0.18
7.10	4.0	0.32	5.00	4.0	0.32
7.40	5.0	0.50	5.40	5.0	0.50
7.80	6.0	0.72	5.80	6.0	0.72
8.30	7.0	0.98	6.35	7.0	0.98
$R_L = 200$ megohms					
4.70	0.0	0.00	2.90	0.0	0.00
5.10	1.0	0.01	3.50	1.0	0.01
5.20	2.0	0.02	3.90	2.0	0.02
5.25	3.0	0.05	4.30	3.0	0.05
5.35	4.0	0.08	4.55	4.0	0.08
5.60	5.0	0.13	4.65	5.0	0.13
5.75	6.0	0.18	4.80	6.0	0.18
6.10	7.0	0.25	5.35	7.0	0.25
6.40	8.0	0.32	5.80	8.0	0.32
7.10	9.0	0.41	5.95	9.0	0.41
			6.20	10.0	0.50
			6.50	10.7	0.57
			6.70	11.0	0.61

TABLE XI(Continued)

Square Wave ( $V_a = 7.5$ kv)								
$f = 25$ cps			$f = 40$ cps			$f = 10$ cps		
$R_L$	$V_o$	$P_o$	$R_L$	$V_o$	$P_o$	$R_L$	$V_o$	$P_o$
50	4.25	0.362	50	4.00	0.320	50	5.20	0.541
100	7.10	0.504	100	5.70	0.325	100	8.50	0.722
200	8.60	0.369	200	6.80	0.231	200	9.50	0.451

Sine Wave ( $V_a = 6.5$ kv)								
50	6.55	0.858	50	6.05	0.733	50	7.20	1.037
100	8.80	0.774	100	7.83	0.614	100	10.15	1.030
200	9.25	0.428	200	8.30	0.345	200	10.70	0.573

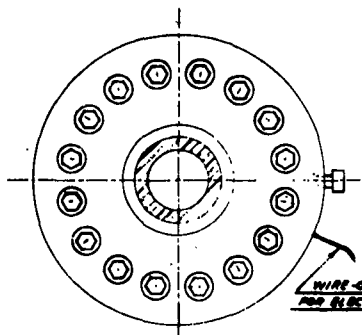
GA/Phys/63-11, 12

Appendix G

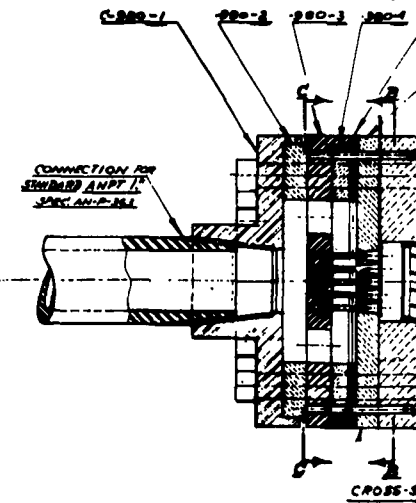
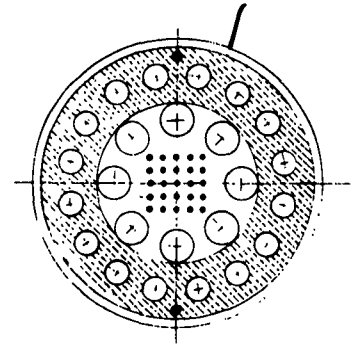
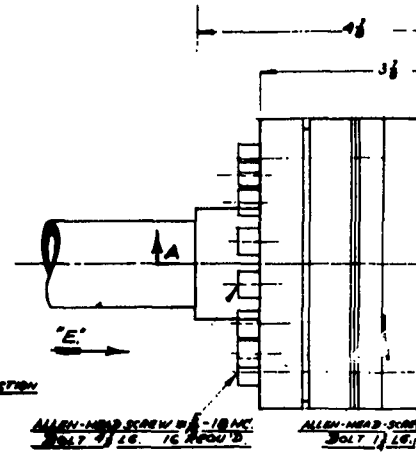
Complete Engineering Drawings of the HED Generator

- |                   |                           |
|-------------------|---------------------------|
| 1. RN-61-D-979    | The Generator Assembly    |
| 2. RN-61-C980     | Generator Body Detail     |
| 3. RN-61-A-980-6A | Nozzle Plate Assembly     |
| 4. RN-61-B-981    | Collector Assembly        |
| 5. RN-62-C-1094   | Alterations and Additions |

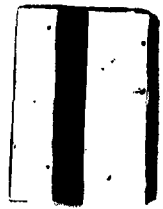
**CONFIDENTIAL**



WIRE-OUTLET  
FOR ELECTR. CONNECTION

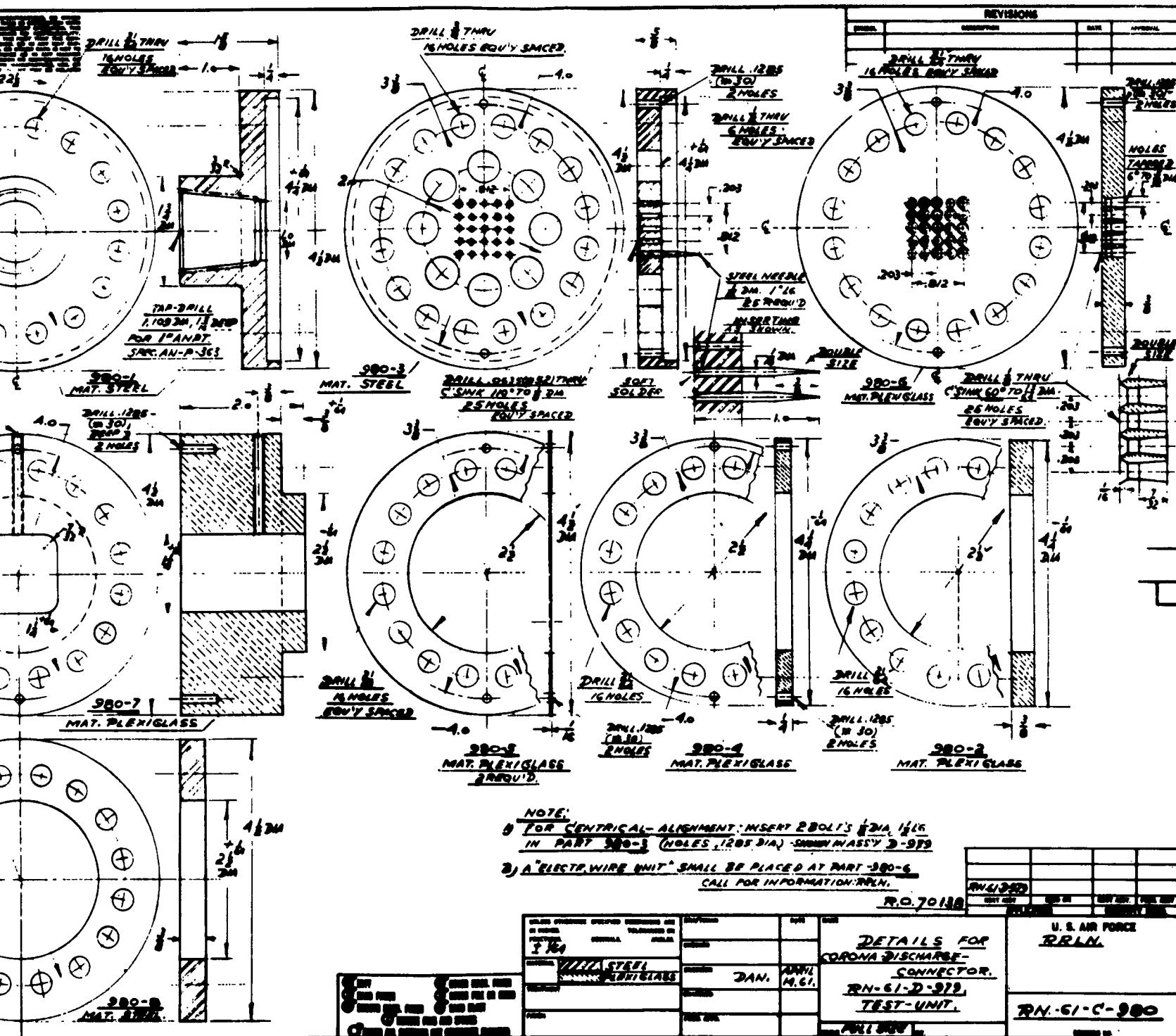


FOR OTHER TEST-POSSIBILITIES:  
FABRICATE A SECOND "NOZZLE-PLATE"  
900-5 TO SPILT IN 2-DIRCS  
EACH 1/2 THICKNESS  
AS SHOWN IN 1-900-CA

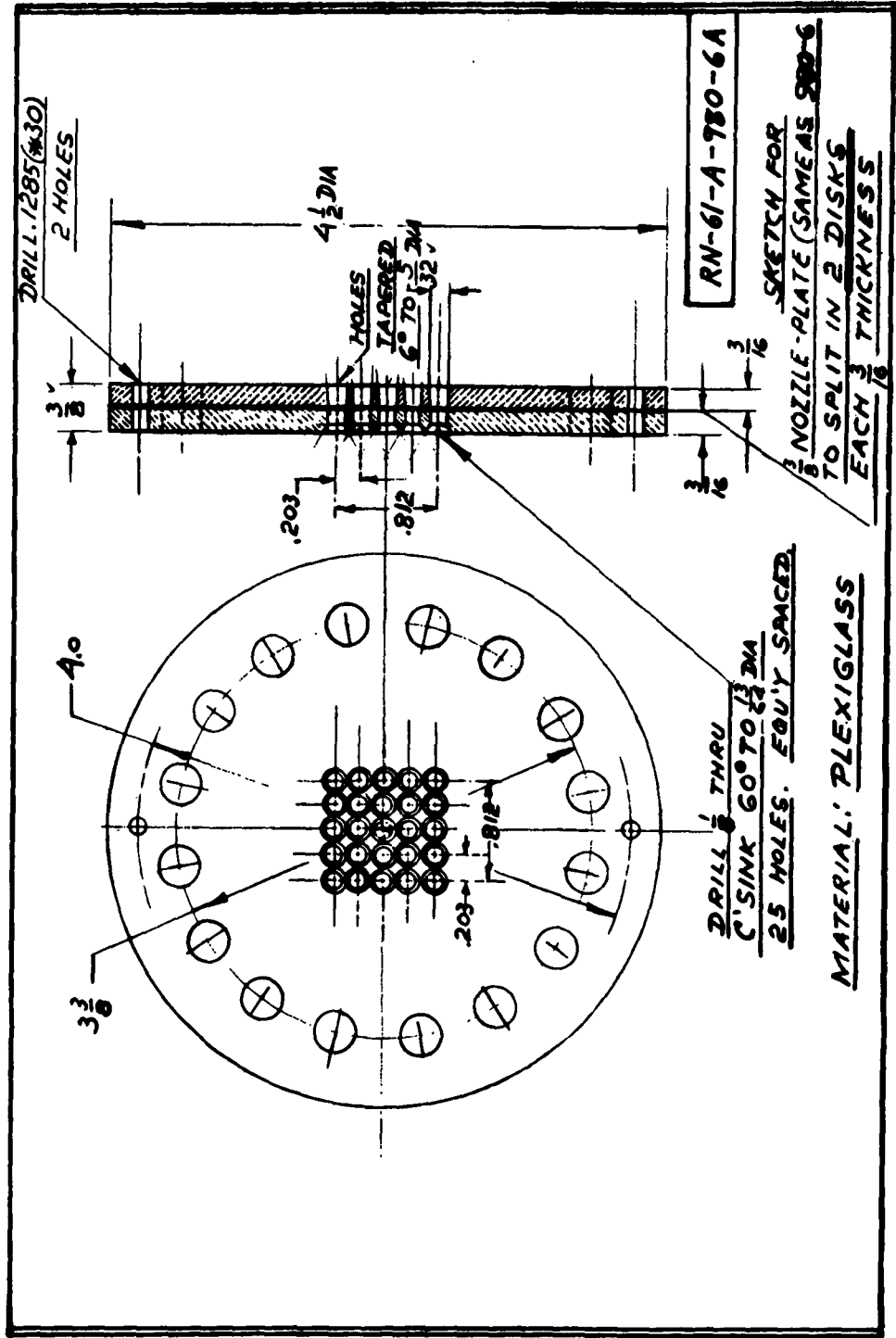








**2**



**RN-61-A-780-6A**

SKETCH FOR  
NOZZLE PLATE (SAME AS 980-6  
TO SPLIT IN 2 DISKS  
EACH 3/16 THICKNESS

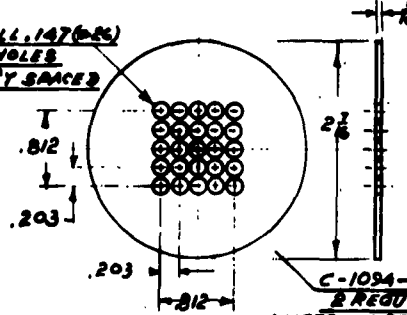
DRILL 1/8 THRU  
C'SINK 60° TO 1/32 DIA  
25 HOLES. EQU'Y SPACED.

MATERIAL: PLEXIGLASS



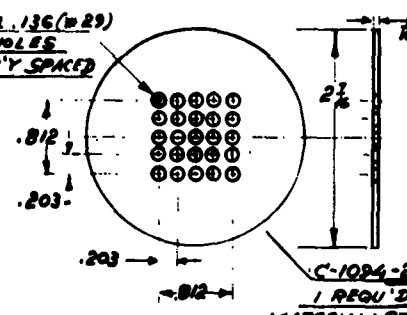
C-1094-1 TO -7 NEW PARTS REQU'D.

DRILL .147 (#45)  
25 HOLES  
EQU'Y SPACED



C-1094-1  
2 REQU'D.  
MATERIAL: STAINLESS-STEEL

DRILL .136 (#29)  
25 HOLES  
EQU'Y SPACED



C-1094-2  
1 REQU'D.  
MATERIAL: STAINLESS-STEEL

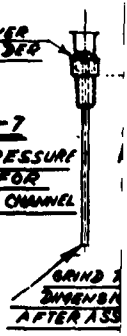
STANDARD  
HYPODERMIC  
NEEDLE 22G



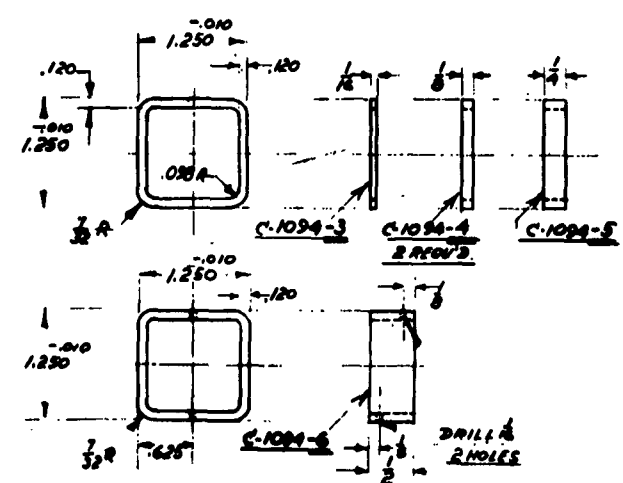
STANDARD  
ALLEN-HEAD-S  
2-70-32 N/A  
2 REQU'D.

SILVER  
SOLDED

C-1094-7  
STATIC PRESSURE  
PROOF FOR  
ION FLOW CHANNEL



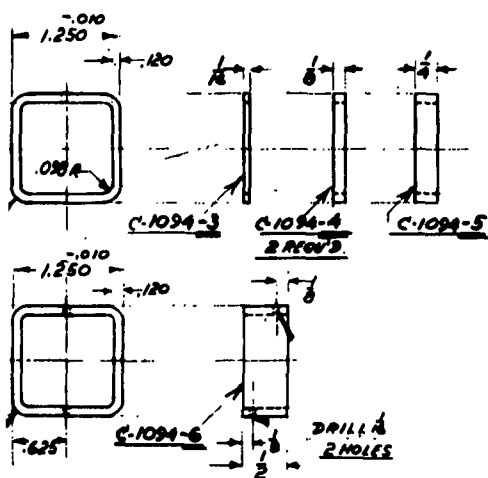
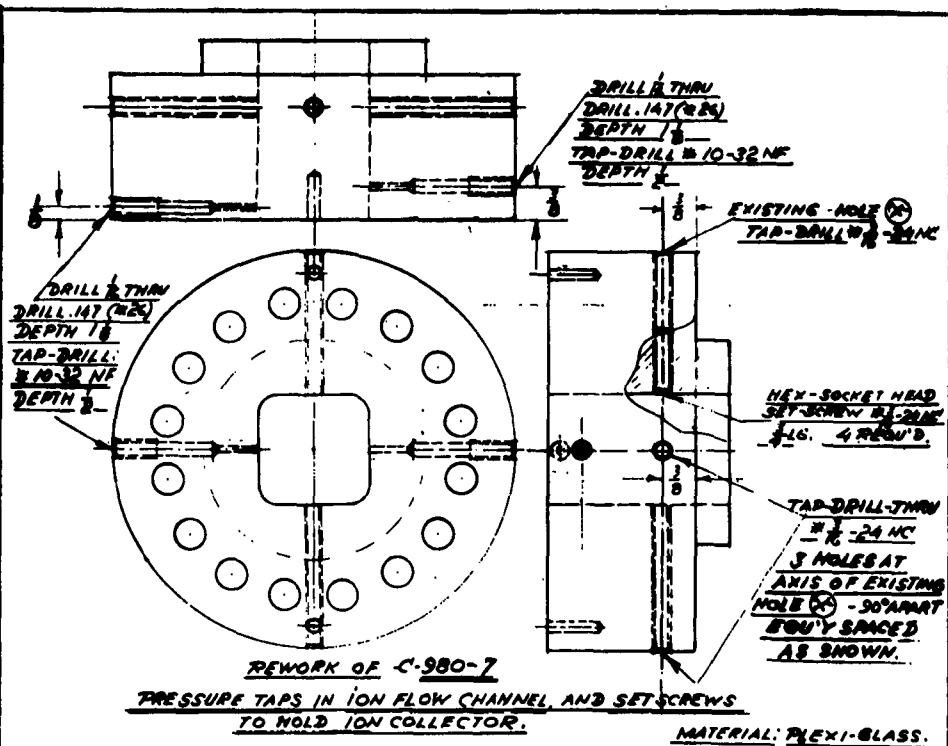
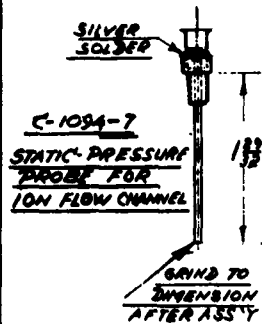
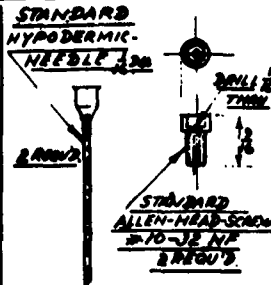
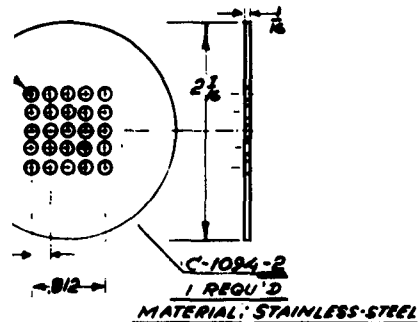
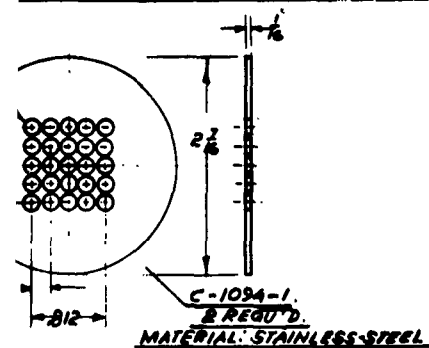
GRIND &  
FINISH  
AFTER ASS



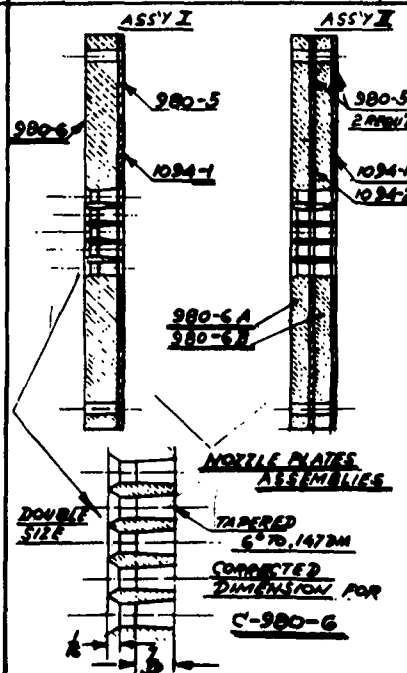
C-1094-3 TO -6: SPACERS TO ESTABLISH LENGTH  
OF ION FLOW CHANNEL.  
MATERIAL: PLEXI-GLASS.



**C-1094-1 TO -7 NEW PARTS REQU'D**



3 TO -6: SPACERS TO ESTABLISH LENGTH  
OF ION FLOW CHANNEL.  
MATERIAL: PLEXI-GLASS.



**NOTES FOR REVISIONS REQUIRED**

1. AT DRAWING **RN-61-C-980**:  
PART 980-5 SHOULD READ 6 REQU'D.  
ALSO A PART 980-5A SHOULD BE  
SPECIFIED-SIMILAR TO 980-5 BUT  
ONLY 1/2 THICK INSTEAD OF 1/4
2. AT DRAWING **RN-61-C-981**:  
THE ION COLLECTOR HAD TO BE BUILT.  
CHANGES:  
A. THE GRID (981-3) NOW RUNS THE FULL  
LENGTH OF THE OUTER SHELL (981-1)  
BUTTING AGAINST THE SCREEN (981-4)
- B. ALL INTERNAL GRID JOINTS ARE  
FURNACE BRAZED AND THE GRID IS  
BRAZED INTO THE OUTER SHELL.
- C. THE SCREEN (981-4) MUST BE STAINLESS-  
STEEL TO PREVENT ITS WIRES FROM  
SHEARING THROUGH EACH OTHER

THIS CHANGES WERE ACCOMPLISHED BY CAPTAIN  
WHEELER AND LT. LAURITSEN DURING THE COURSE  
OF THEIR WORK WITH THE APPARATUS.

TITLE: ADDENDA TO ORIGINAL: U.S. AIR FORCE  
DRAWINGS: RNC-2-975; C-980-7; RNC-2-980 MAR. 28, 1942  
OF THE ELECTRO-HYDRODYNAMIC- WAFB  
GENERATOR (COMMON DISCHARGE TEST UNIT) 3474  
RNC-2-C-1094

